U-Pb Geochronology of the Acasta Gneiss Complex in Northwest Canada

by

Roxana G. Safipour

Submitted to the Department of Earth, Atmospheric and Planetary Sciences

in Partial Fulfillment of the Requirements for the Degree of

Bachelor of Science in Earth, Atmospheric and Planetary Sciences

at the Massachusetts Institute of Technology

May 8, 2009 [June 2009]

Author Signature redacted
Department of Earth, Atmospheric and Planetary Sciences
May 8, 2009

Certified by Signature redacted
Samuel Bowring
Thesis Supervisor

Accepted by Signature redacted
Samuel Bowring
Chair, Committee on Undergraduate Program

Acknowledgements

I would like to thank the following people, whose help on this project was invaluable:

Prof. Samuel Bowring at MIT, my thesis advisor.

Prof. George Gehrels at the University of Arizona, under whose direction I obtained the LA-ICPMS data.

Dr. Nilanjan Chatterjee, for help with using the microprobe to obtain images of my grains.

Dr. Matthew Rioux, who was a constant source of advice.

Linnea Koons and Caitlin Tems, for training me in laboratory procedures.

Jane Connor, for help with the writing process.

The faculty, researchers, graduate students, and staff of the 11^{th} and 12^{th} floors, for sharing their lab space with me and answering my many questions.

Table of Contents

Abstract

The Acasta Gneiss Complex in Northwest Canada contains the oldest dated rocks in the world. The gneisses range in age from 4.03-3.6 Ga, as determined by U-Pb dating of zircons (Bowring and Williams 1999). U-Pb dating of xenocrystic cores in these zircons indicates a cryptic record of continental crust older than 4.0 Ga. In this study, zircons were selected and characterized from thirteen samples of Acasta Gneisses. Many of the zircons contain xenocrystic cores mantled by younger domains. U-Pb geochronological data were collected using laser ablation inductively coupled plasma mass spectrometery (LA-ICPMS). Twelve of the samples show evidence for two distinct crystallization events, one which formed the cores and another in which the mantle domain overgrew the cores. The oldest cores were dated at >4.0 Ga. This provides additional evidence for pre-4.0 Ga crust formation in the late Hadean.

Introduction

Less than 15% of the Earth's continental area is made up of Archean crust, and Hadean crust (older than 3.8 Ga) has a total area of only a few hundred kilometers (Figure 1). One of the most important unresolved questions is whether this small volume of Archean and Hadean continental crust reflects the actual amount of continental crust formed in those eons, or whether a large volume of early crust was destroyed by tectonic recycling processes which return crust to the mantle (Bowring and Williams 1999). Understanding the early history of continental crustal growth is important because it has ramifications on our understanding of both the preservation of the geologic record and the development of life on land (Harrison 2009). Studying the oldest rocks available provides direct evidence of early crustal formation and planetary differentiation processes and can help to resolve this issue (Bowring and Williams 1999).

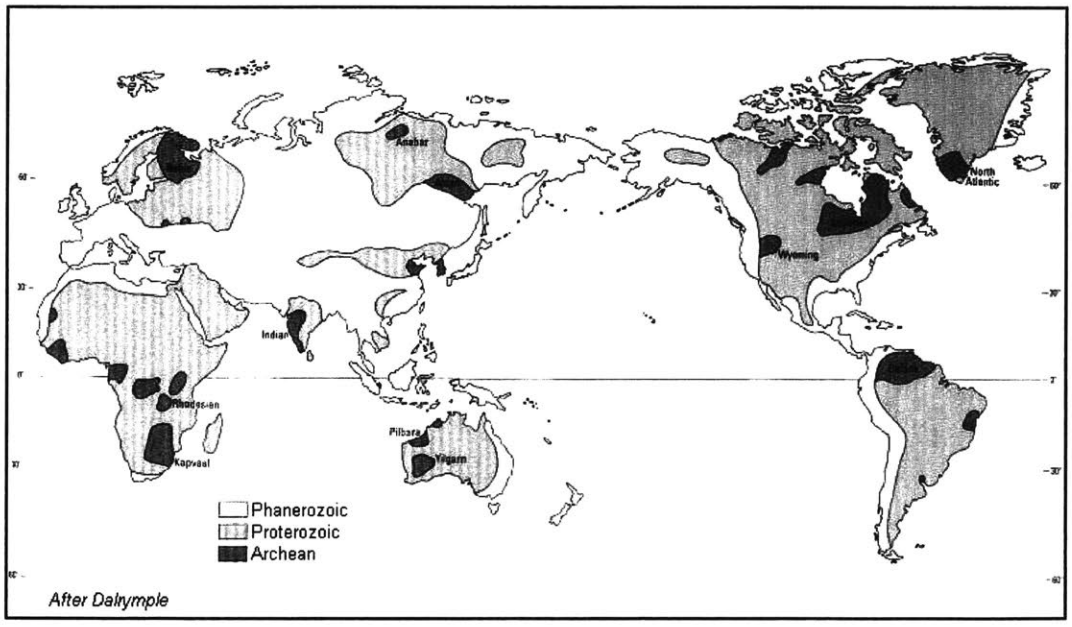

Figure 1: Distribution of the world's crust. Archean crust (dark gray) accounts for less than 15% of the continental surface area.

A traditionally accepted theory is that crust began to grow in the Hadean and has since grown continuously in an approximately linear fashion. This theory is supported by an absence of a rock record older than 4 Ga and by evolution of depleted mantle in the post-Archean according to $^{143}Nd/^{144}Nd$ and $^{176}Hf/^{177}Hf$ analysis (Harrison, 2009). However, in recent years an increasing body of evidence has developed which argues for rapid formation early in Earth's history of a volume of crust comparable to present day volume. In his classic paper, Armstrong (1991) calls slow crustal growth a "myth" and states that there is no process which would lead to rapid differentiation of the core and volatiles but slow differentiation of silicates. The theory of rapid crustal formation holds that a large amount of continental crust had already formed by 4 Ga and that the present day crust reflects an approximate steady state between newly formed crust and crust that recycled into the mantle.

Various proposed models of crustal volume as a function of time are shown in Figure 2 below. One can see that the curves differ greatly, with some studies advocating late, slow formation and others advocating early, rapid formation. Fyfe (1978) even argues that the crustal volume in the past may have been greater (Curve F, Figure 2).

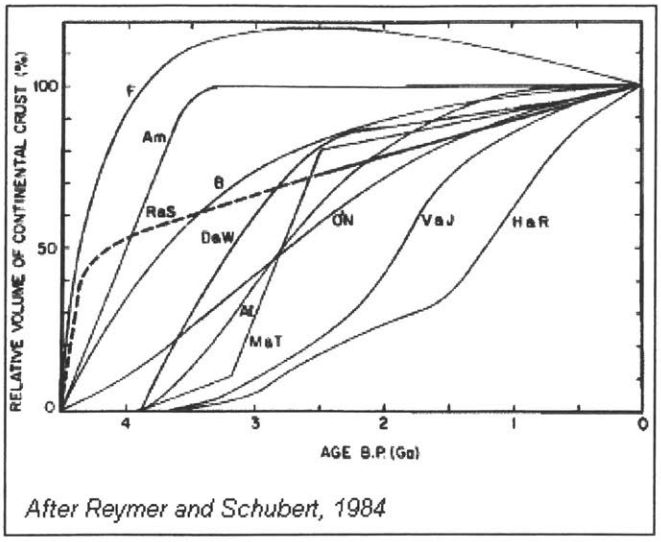

Figure 2: Proposed crustal growth curves from various studies.

There are several proposed explanations for the exact process by which Hadean crust could have been destroyed, from plate tectonics (Hopkins, 2008) to the late heavy meteorite bombardment (LHMB) which is postulated to have occurred on earth between 4.0 and 3.85 Ga (Kranendonk, 2007). A third theory proposes that the Hadean crust formation consisted of the "eruption and horizontal growth of a basaltic shell on a hot mantle" which lead to ineffective cooling of the mantle through this crust and an eventual destructive melting event (Kamber, 2007). Still others propose that only a small volume of crust was created during the Hadean, and no large scale recycling event occurred.

One way to try to resolve this controversy is to study the physical and chemical conditions of Earth's early history. The only direct evidence available of these conditions is provided by the oldest rocks which still survive today. Many Archean rocks contain the mineral zircon ($ZrSiO_4$). Zircon is a very resistant mineral; it can survive the mechanical, chemical, and thermal breakdown of the original host rock and be incorporated into new

rocks that are formed. Thus many of the zircons found in Archean rocks contain trace element and isotopic signatures that provide information on the conditions under which the older original host rock formed (Harrison 2009). In this way zircons can provide information regarding the conditions of crustal formation that occurred earlier than the current rock record.

What makes zircon a useful mineral for studying the early Archean is the relative ease with which zircon grains can be dated. When zircon forms, some uranium atoms substitute for zirconium in the crystal lattice. Over time this uranium decays to lead. Lead atoms are excluded from zircon when it initially forms, but the sample retains lead that is subsequently formed by radioactive decay. The ratio of U/Pb in a zircon crystal is thus an indication of the sample's age. Two different isotopes of uranium can be used: ^{238}U decays to ^{206}Pb with a half-life of 4.5 billion years. ^{235}U decays to ^{207}Pb with a half-life of 700 million years. This method can be used to date samples younger than one million years or as old as the Earth.

In order to study the trace element and isotopic signatures of pre-Archean zircons, zircons of this age must first be identified. The purpose of this project is to date zircons from Archean rocks found in the Acasta Gneiss complex in northwestern Canada. These gneisses range in age from 3.6 Ga to 4.0 Ga, and some of the zircons found in the gneisses contain xenocryst cores from earlier Hadean-age host rocks (Figure 3). Xenocrysts as old as 4.2 Ga have already been identified in some zircons from Acasta samples (Iisuka, 2006).

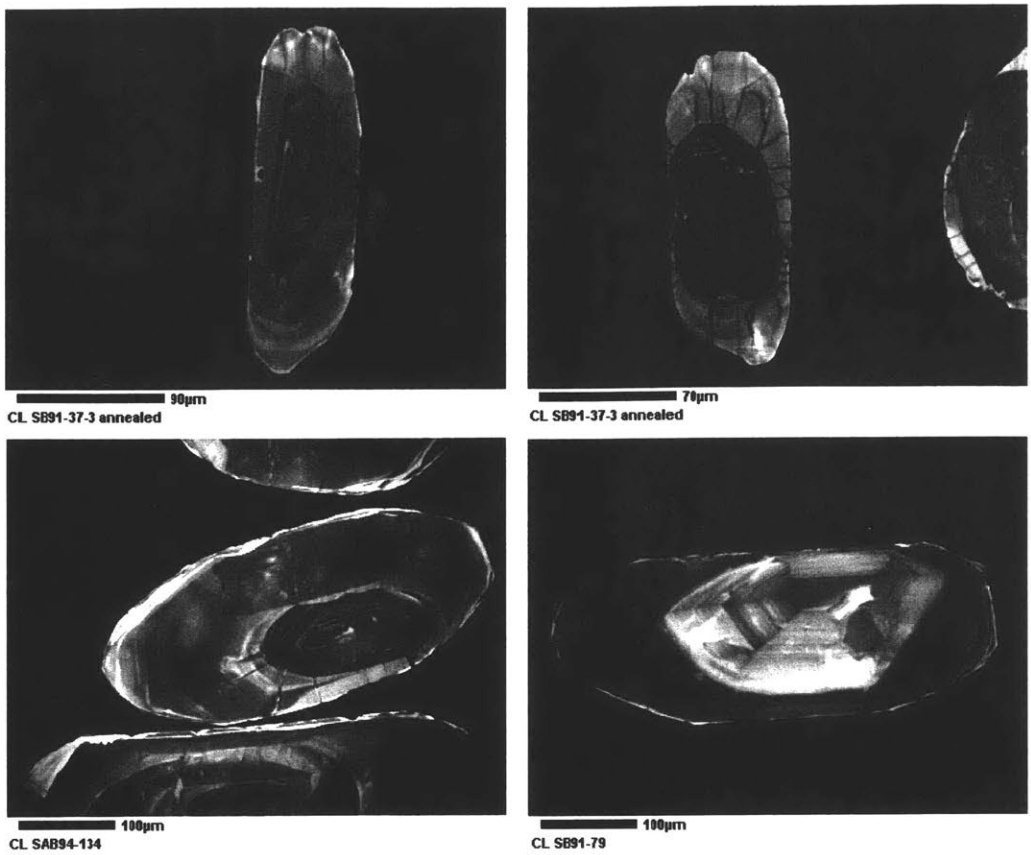

Figure 3: Images of zircons with cores.

Identifying and characterizing zircons that are older than 4 Ga is an important first step in the process of collecting data on the early conditions of crustal formation. Relatively few samples of Acasta gneiss have been dated, and it is possible that the oldest of these rocks is yet to be discovered. This study characterizes and dates new samples, and some previously analyzed samples, from the Acasta Gneiss complex. Our analyses add to the total body of data available on these rocks. In this study, zircons from thirteen Acasta gneiss samples were isolated in a search for pre-4.0 Ga components, and both the cores and outer bodies of these zircons were dated. Several zircon cores yielded dates of

over 4.0 Ga. Future studies on the trace element and isotopic signatures of these cores would add to the total body of data on Hadean-age zircons and perhaps shed new light on the controversy over the processes that formed Earth's earliest continents.

Background Information

Wetherill concordia diagrams

In this study, U-Pb data are plotted on Wetherill concordia diagrams. The Concordia curve is derived by solving the two U decay equations for values of t and the curve is derived by plotting the radiogenic ratios of $^{207}Pb/^{235}U$ vs. the ratio of $^{206}Pb/^{238}U$. (Figure 4a). Analyses that plot along this curve are said to be concordant; the age calculated for the $^{207}Pb/^{235}U$ system agrees with the age calculated for the $^{206}Pb/^{238}U$ system.

Analyses that plot off the concordia are said to be discordant. A common cause of discordance is the loss of radiogenic lead from the zircon. ^{207}Pb and ^{206}Pb are lost in proportion to their relative composition in the grain, thus as a grain loses lead over time its measured ratios would move diagonally away from the concordia towards the origin. Pb is not lost by thermally activated volume diffusion but more likely by fast pathway diffusion through linked sites of radiation damage and defects. Thus, damaged crystals are susceptible to younger thermal events that can enhance diffusivity. Analyses from grains that underwent a lead-loss event thus plot along a tie-line between the original crystallization age on the concordia and the age on the concordia at which the lead-loss occurred. This tie-line is known as the "discordia" (Figure 4b). The discordia can be used to project analyses back to their original crystallization age.

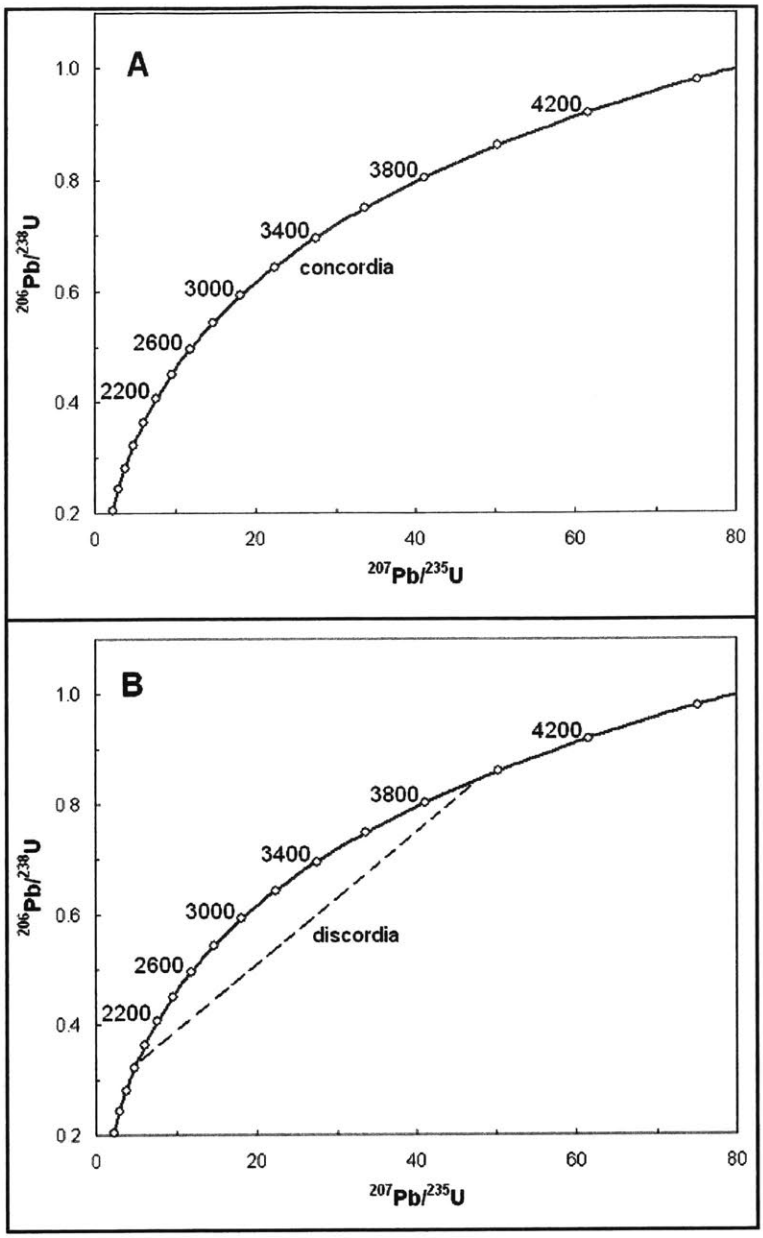

Figure 4: (a) A Wetherill concordia diagram. The concordia curve represents ratios of equal age for the $^{207}Pb/^{235}U$ and $^{206}Pb/^{238}U$ systems. (b) Lead loss causes analyses to plot below the concordia on a tie-line between the original crystallization age and the age of the lead-loss event.

Metamictization

The term "metamictization" refers to the process by which the crystal lattice of a mineral is damaged by radiation. In zircon, this damage is often caused by α-decay events as U and Th decay to Pb. A single α-decay event can cause 700-2000 displacements of atoms in the crystal lattice. In contrast, β-decay events cause an average of only 0.1 displacements per event, so it is the α-decay events that are considered primarily responsible for metamictization. The decay chain for ^{238}U has eight α-decay events, ^{235}U has seven α-decay events, and ^{232}Th has six α-decay events (Ewing et all 2003).

In general, zircons that have higher initial concentrations of U and Th will incur more radiation damage. Older zircons, which have experienced more α-decay events over time, will also tend to have higher levels of damage (Ewing et all 2003). Since the zircons analyzed in this study are among the oldest found on Earth, metamictization is an important consideration.

Radiation damage is accumulated in three stages. In stage I, isolated point defects accumulate in the lattice, causing distortion and expansion of the unit-cell and a decrease in density. In stage II, amorphous domains begin to develop in the grain. In stage III, the grain is already entirely amorphous, but further distortion occurs leading to a second decrease in density (Murakami et all 1991).

Effects of this damage on the properties of zircon include decreased density, decreased birefringence, decreased elastic moduli, decreased hardness, increased fracture toughness, increased dissolution rate, and decreased thermal conductivity. X-ray diffraction experiments show decreased long-range periodicity in the crystal structure with increasing α-decay events, eventually culminating in the complete loss of long-range

order as the grain becomes amorphous. The short-range order is also affected. Mean Zr-O bond length decreases, and the coordination number of some Zr atoms decreases from 8 to 7. The SiO_4 tetrahedra, which are isolated in undamaged zircon, begin to polymerize. In metamict zircon the number of O atoms shared by the tetrahedra ranges from 0-4 (Ewing et all 2003).

Radiation damage may allow for increased Pb loss from the lattice. Discordance or open system behavior is found to correlate with higher concentrations of U. Discordance is often caused by lead loss, and higher U concentrations allow for greater accumulated radiation damage. In a now classic study of Precambrian zircons from Johnny Lyon granodiorite in Arizona, Silver and Deutsch (1963) proposed that "the coupling of the trend of increasing discordance with increasing radioactivity strongly suggests that the greater the total radiation flux in the history of these zircons, the greater their vulnerability to disturbance".

The zircon lattice can recover from radiation damage through thermally driven recrystalization. Two stages of recrystalization have been identified. In the first stage point defects heal and short-range order is recovered. In the second stage the amorphous fraction of the grain decreases, until the grain is fully healed at temperatures above 900 °C. It has been proposed that on geologic timescales this recrystalization process could occur at much lower temperatures (Ewing et all 2003).

Dating methods

Three primary methods exist for obtaining U/Pb dates of zircons: ID-TIMS, SIMS, and LA-ICPMS.

Isotope dilution thermal ionization mass spectrometry (ID-TIMS) is the most precise method to obtain U-Pb data. Zircons selected for analysis are first air abraded to remove the outer portion of the grains, where lead loss is assumed to be the most abundant. The zircons are then annealed and leached with HF and HNO_3 acids to dissolve the more soluble portions of the grains which have experienced greater radiation damage. These preparation steps greatly improve concordance of the analyses. The selected zircons are dissolved with HF or HNO_3 and an isotope tracer is added to the dissolved sample. Isotopic compositions are measured using a thermal ionization mass spectrometer (Parrish and Noble 2003). Although high precision and concordance is obtained by this method, the main drawback to ID-TIMS is that sample preparation is labor intensive, making it less efficient for obtaining large amounts of data.

In secondary ion mass spectrometry (SIMS), zircons are mounted and polished in epoxy pucks. A high-energy beam is focused on the polished grain surface, which ablates and ionizes a small portion of the sample. The composition of the ionized matter is measured with a mass spectrometer. A very small volume of sample can be analyzed with SIMS: the analyzed portion can be as small as 10 μm in diameter and 5 μm in depth. This makes SIMS advantageous for analyzing complex zircons with multiple domains of different crystallization ages. The small volume analyzed leads to a trade off in precision, however, and SIMS is therefore not as precise as ID-TIMS (Ireland and Williams 2003). It is typically more precise than LA-ICPMS (Parrish and Noble 2003).

In laser ablation ionically coupled plasma mass spectrometry (LA-ICPMS) the zircon grain is ablated using a laser, causing a small portion of the sample to vaporize. The released atoms are then run through a plasma of argon gas at temperatures of 8000 to

10,000K and atomic species are ionized by the high energy plasma. The ions are then accelerated through a mass spectrometer and the concentrations of all isotopes of U, Th, and Pb are measured (Kosler and Sylvester 2003). LA-ICPMS is less precise than ID-TIMS or SIMS. However, large amounts of data can be obtained very quickly. It is possible to obtain several hundred analyses per day.

Geologic Setting

The zircons dated in this study are from rocks collected in the Acasta Gneiss Complex. The Acasta Gneiss Complex is located on the Slave craton in the northwest corner of the Canadian shield (Figure 5). Earth's oldest rocks are generally found in the central area of cratons, and the Slave craton contains the oldest rocks identified anywhere on Earth so far (Bowring and Housh 1995).

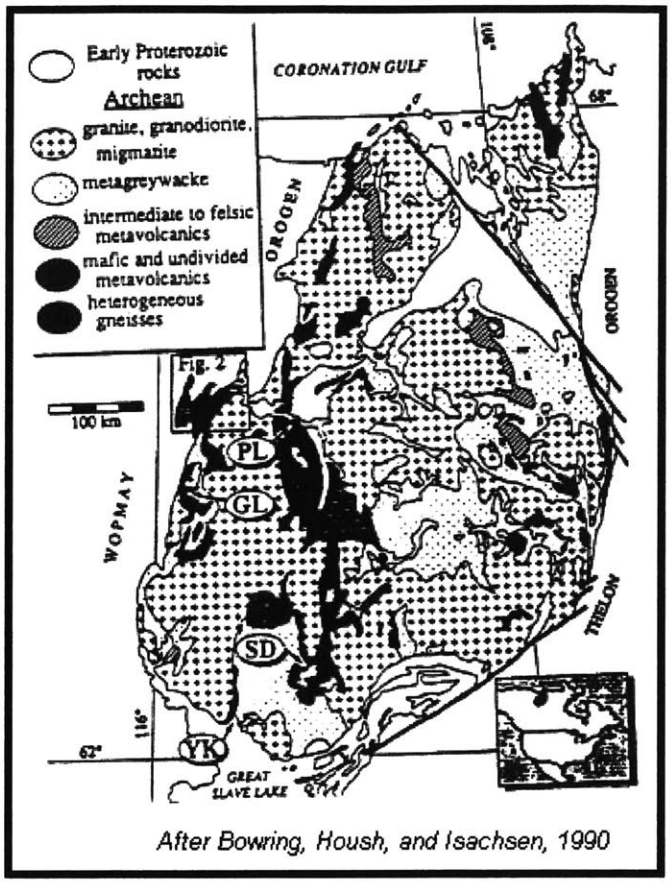

Figure 5: A geologic map of the Slave craton in Northwestern Canada.

Much of the Slave craton is a classical Archean granite-greenstone terrane where structural remnants of mafic volcanics and associated turbiditc sedimentary rocks are

intruded by a range of granitoids. It has a total area of approximately 190,000 km^2. The Thelon orogen (2.0–1.9 Ga) bounds the craton to the east, and Wopmay orogen (2.02–1.84 Ga) bounds it to the west. Fourty percent of the outcrop in the Slave craton consists of a group of supracrustal rocks called the Yellowknife Supergroup. These supracrustal rocks contain a higher proportion of metaturbidites and a lower proportion of metavolcanic rocks than is typically found in other cratons (Bowring et. all 1990). Uranium-lead zircon ages indicate that the majority of the metavolcanics erupted between 2.66 and 2.72 Ga, and granitic to dioritic plutons intruded the metavolcanics between 2.58 to 2.70 Ga (Isachsen and Bowring 1994). The remaining 60 percent of the Slave craton consists of granitoids and gneisses. Rocks in the Slave craton that are older than the Yellowknife Supergroup occur only in the westernmost part of the craton (Bowring et. all 1990).

The Acasta Gneiss Complex is a heterogenous assemblage of Hadean and Archean rocks found in the westernmost part of the craton (Figure 6). The complex contains the oldest dated rocks found on earth. The complex includes foliated gneissic tonalites, granites, and granodiorites ranging from 3.6 to >4.0 Ga. The complex also includes amphibolites and ultramafic rocks of undetermined age (Bowring and Williams 1999). The gneisses are commonly interlayered on a centimeter scale with the amphibolites, but large areas composed almost entirely of amphibolites also occur. The area has a complex history of intrusions and deformation. All the rocks contain intrusions of weakly foliated, gabbroic to dioritic dikes and pods as well as weakly to strongly foliated to mylonitic granites. The gneisses are intruded by diabase dikes which trend north and are possibly correlated with the Mackenzie dike swarm at ca. 1.267 Ga

(Bowring et all 1990). In high-strain localities the gneisses are finely banded and layers of different age and composition are juxtaposed. In low-strain zones, contacts between rock types are sharp and cross-cutting relationships between primary igneous precursors can be identified (Bowring and Williams 1999).

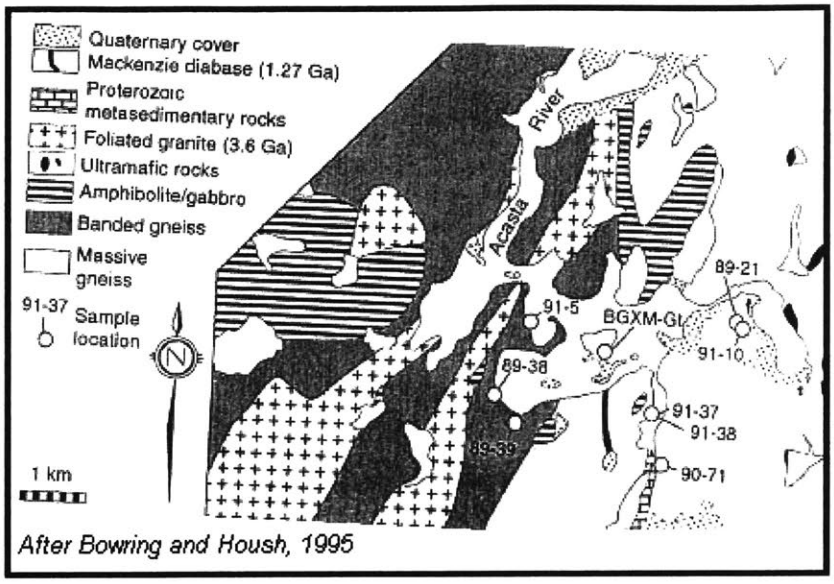

Figure 6: Geologic map of the Acasta Gneiss complex in the Slave craton.

Supracrustal rocks of Wopmay orogen were thrust eastward over the western 100 kilometers of the Slave craton during the Calderian Orogeny at around 1.9 Ga, covering the Acasta gneisses with Proterozoic rocks. Metamorphic conditions in the Proterozoic cover have been estimated to have reached up to 9.5 kbar and 620°C (Bowring et. all 1990). The Acasta gneisses were exposed from beneath this Proterozoic cover as a result of deformation that occurred between 1.89 and 1.84 Ga. Interference between two thick-skinned, basement-involved fold sets exposed the Acasta Gneiss complex. The first set of folds trend north with a wavelength of approximately 35 km and an amplitude of approximately 6 km. The second set of folds trend northeast with 80-140 km wavelengths

and amplitudes of up to 15km. The Acasta gneisses exhibit a Proterozoic fabric near the basement-cover interface. This fabric is defined by a schistosity of aligned retrograde chlorite grains and a lineation of recrystalized quartz, hornblende, and feldspar grains (Bowring et all 1990).

Sample Descriptions

The samples analyzed in this study were collected from the Acasta Gneiss Complex. Figure 7 is a map of sample collection locations.

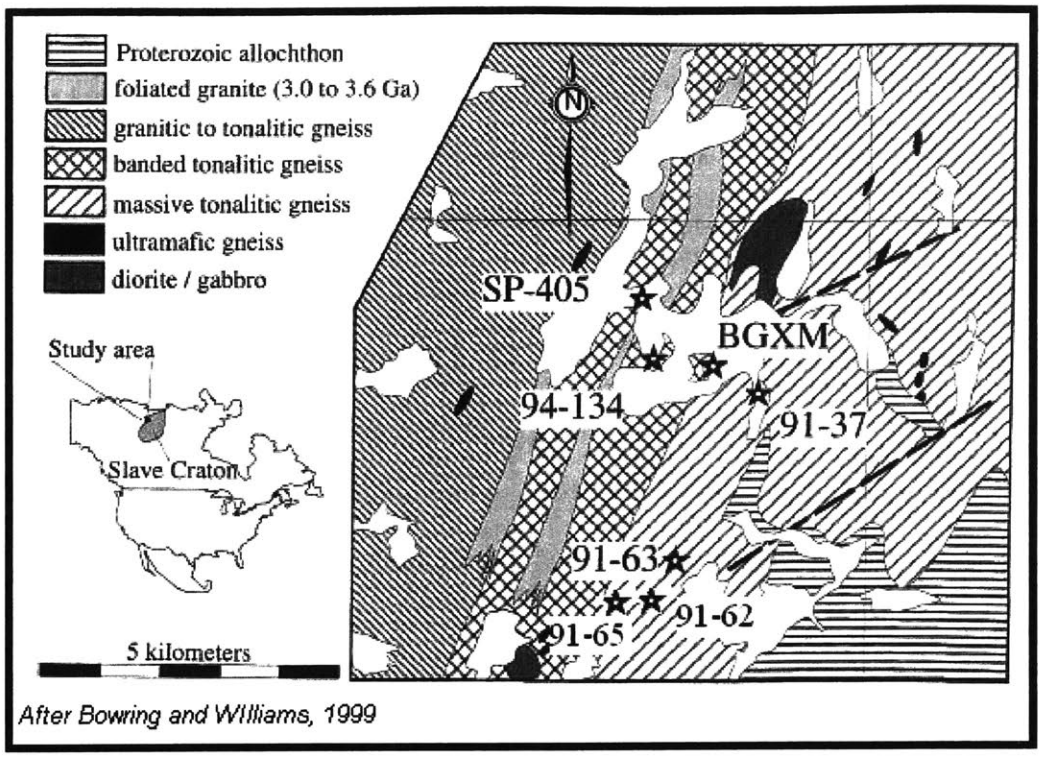

Figure 7: Geologic map of the Acasta Gneiss Complex with sample collection locations marked. White areas are lakes.

Hand samples were acquired and examined for six samples, and thin sections were made of these samples. Additionally, thin sections were available for samples SAB94-77 and SAB94-134. These hand samples and thin sections are described below. The other seven samples were obtained as mineral separates. The zircon grains selected are described for all samples. When a range of sizes of zircons existed in a sample only the largest zircons were selected for this study.

SAB89-28

SAB89-28 is a dark gray rock with a slight greenish tint and a small percentage (<10%) leucocratic layers. The rock is medium to coarse grained and no foliation is apparent. In thin section the sample consists of approximately 70% biotite, 20% plagioclase, 10% quartz, 1% apatite, and <1% zircon.

The zircons from sample SAB89-28 are typically 80-150 μm. Most grains have an aspect ratio of about 1.5, although a few are as high as 3; most grains do not have sharp terminations and have rounded edges. Most grains are clear, but a few are turbid. Many of the grains exhibit radial and/or concentric fracturing around the outer part of the grain and most have strong compositional zoning. A few have patchy textures which may indicate recrystalization (Figure 8). Some grains have a thin rim that exhibits a high CL response, most likely formed by metamorphic overgrowth. About half of the grains appear to contain xenocrystic cores.

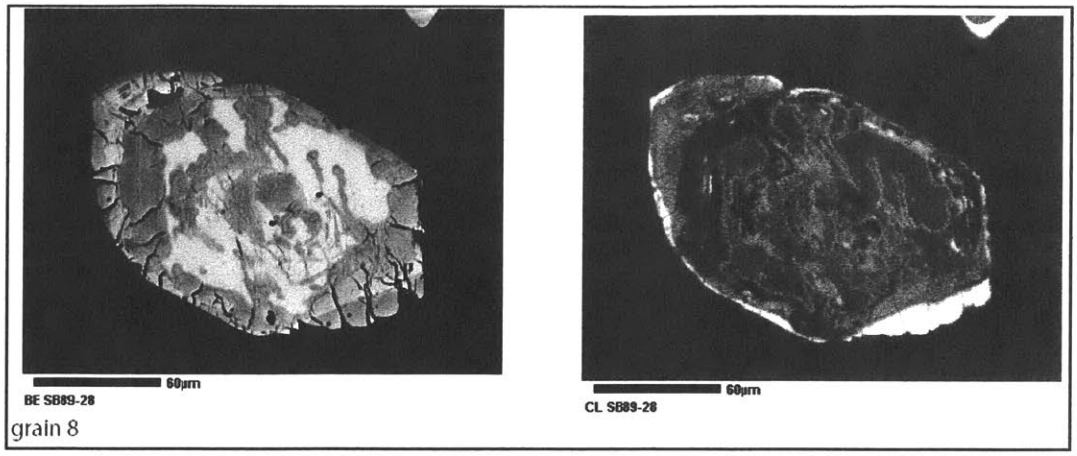

Figure 8: A E image (left) and CL image (right) of a zircon from sample SAB89-28. A patchy texture is observed in this and many other grains. This texture may result from partial recrystalization of the grain.

SAB91-35

SAB91-35 is a lower-medium to upper-coarse grained gneiss. The rock is compositionally banded with about 75% dark layers and 25% leucocratic layers. The rock is strongly foliated with folds of foliation (Figure 9). A thin section was made of a white band in the rock, which comprises approximately 40% plagioclase, 40% quartz, 15-20% biotite, 1-2% apatite and 1-2% zircon.

The zircons selected from sample SAB91-35 range from 150-400 µm. The grains are prismatic, with aspect ratios of 2-3. They are subrounded to rounded. Most of the grains are slightly turbid, but a few are clear. All of the grains exhibit radial fractures and a few exhibit concentric fractures bounding an inner core. About half of the grains are concentrically zoned. The other half exhibit a patchy recrystalization texture. Most of the zoned grains appear to contain a xenocrystic core. Often the core has a patchy texture

while the outer body is zoned and fractured. The grains have a very low CL response, but a few of the grains have a very thin rim with a higher CL response.

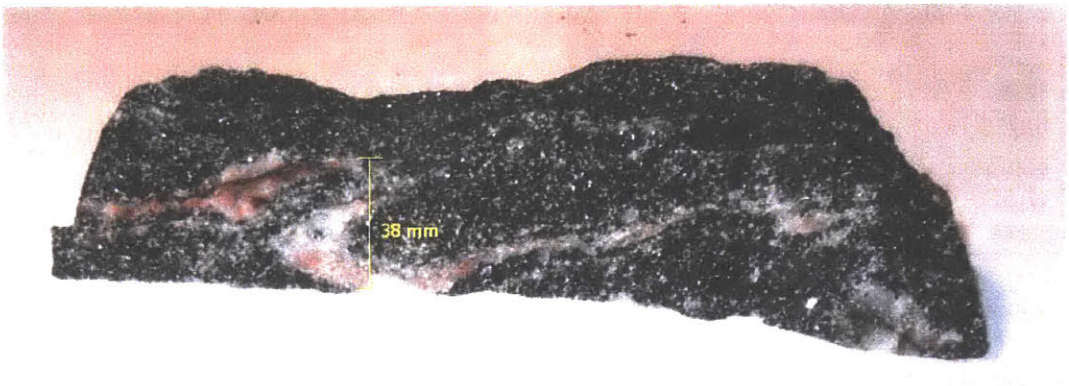

Figure 9: Fold in a piece of sample SAB91-35.

SAB91-37-3

Sample SAB91-37-3 is a lower-medium to lower-coarse grained gneiss. It contains about 40% light-colored bands and 60% dark bands. The rock is highly foliated.

The zircons selected from SAB91-37-3 are mostly approximately 100-300 μm, but a few grains of up to 300 μm were also found. The grains are prismatic and elongated, most with an aspect ratio of 3 or higher, and are rounded. The grains are clear but highly fractured. All have radial fractures, and a few have linear fractures that cut across the entire grain as well. A few grains have concentric fractures, but most do not. All of the grains are zoned, and most appear to contain a xenocrystic core. The cores are usually concentrically zoned, but in a few cases exhibit a patchy texture. In some cases the cores are unfractured and only the outer part of the zircon exhibits radial fracture. About half of the grains have a rim with a high CL response.

SAB91-52

SAB91-52 was obtained in the form of mineral separates. The sample contained very few zircons. The grains selected are approximately 100-200 μm. The grains are prismatic, most with aspect ratios of 2-3. However, a few very elongated grains are broken in half and only half the grain was obtained. Most of the grains are slightly turbid, but a few are clear. Most of the grains exhibit radial fractures around the cores. Some concentric zoning is apparent in most of the grains, although many are highly recrystalized and exhibit entire regions of patchy texture. All of the grains also exhibit a high CL-response metamorphic rim.

SAB91-53

SAB91-53 is a medium to coarse grained gneiss, with some quartz grains up to several millimeters in diameter. The rock is approximately 30% light colored layers and 70% dark layers and well foliated. In thin section, the sample consists of approximately 35% plagioclase, 35% quartz, 30% biotite, and 1-2% apatite. Zircon was not found in the thin section.

The zircons selected from SAB91-53 range from 100-150 μm. The grains are rounded to well rounded. Some are elongated with aspect ratios of 1.5-3, while others are entirely round and may have had an equant habit. The grains are clear. All have radial fractures in the outer part of the grain, and a few have concentric fractures bounding an inner core. All of the grains are concentrically zoned. A few grains clearly contain xenocrystic cores, however in many of the grains it is difficult to distinguish a xenocrystic core from concentric zoning. All of the grains have a high CL-response

metamorphic rim. A few grains appear to contain inclusions of other minerals (Figure 10).

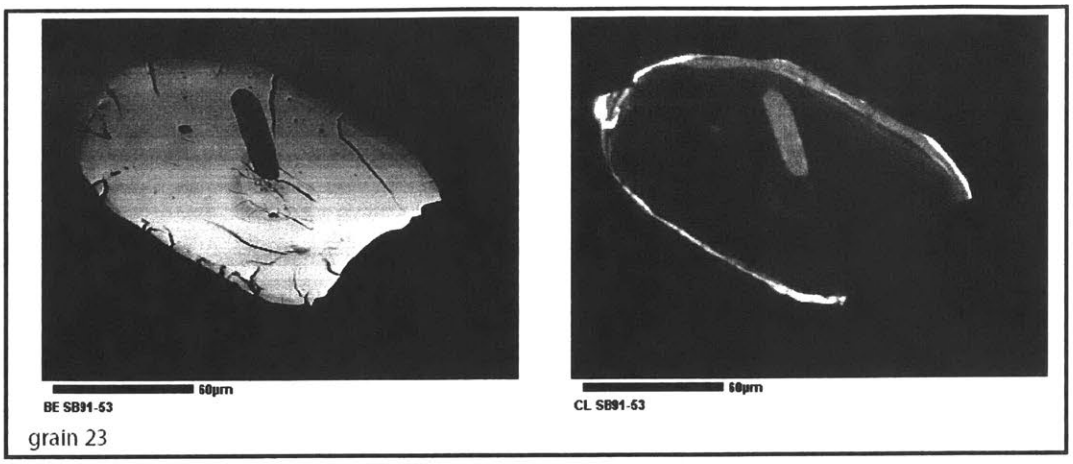

Figure 10: A BE image (left) and CL image (right) of a zircon from sample SAB91-53. A large inclusion can be seen in the upper part of the grain. Other important features of this grain are concentric zoning, radial fractures, and a thin rim with a high CL response that is most likely the result of metamorphic overgrowth.

SAB91-54

SAB91-54 is a lower-medium to lower-coarse grained rock. It contains approximately 40% white grains and 60% black grains, with a very small percentage (<1%) of red feldspars. No foliation is apparent. In thin section the sample consists of approximately 45% quartz, 40% plagioclase, 15% biotite, <1% apatite and <1% zircon.

The zircons selected from SAB91-54 are 100-200 µm in size. They are prismatic and rounded, with aspect ratios of 2-4. The grains are clear and highly fractured. Most have both radial and linear fractures, and a few have concentric fractures bounding an inner core. Concentric zoning is apparent in most of the grains. Some grains have

xenocrystic cores that exhibit a patchy recrystalization texture. Others have zoned xenocrystic cores that appear to be partly resorbed. A few grains appear to have multiple generations of cores, each with a different texture and level of CL response (Figure 11). Very thin rims with a high CL response are observed in most of the grains.

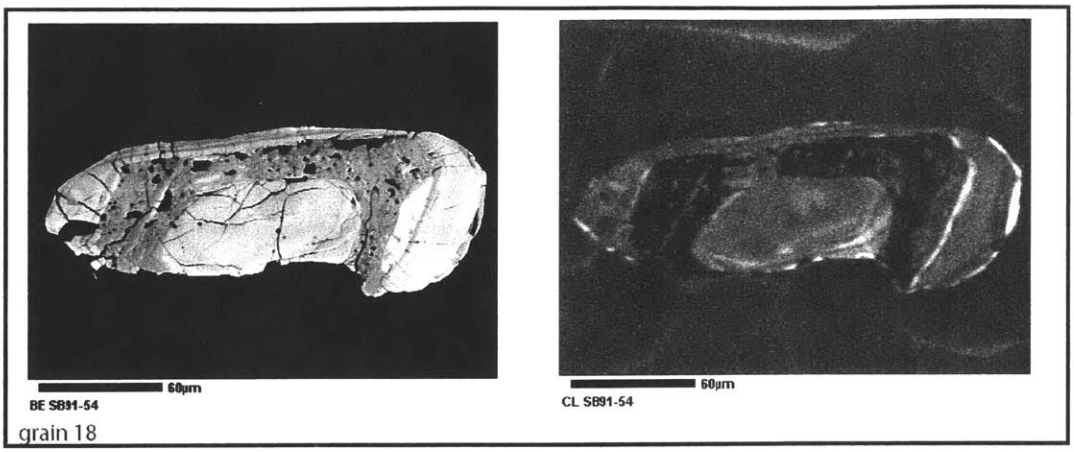

Figure 11: A BE image (left) and CL image (right) of a zircon from sample SAB91-54. The grain appears to contain two generations of xenocrystic cores. The outer core exhibits a patchy recystalization texture, while the inner core is concentrically zoned.

SAB91-62

Sample SAB91-62 was obtained as mineral separates. The zircons selected are approximately 50-150 µm. The grains are prismatic, with aspect ratios of 2-3, and are subrounded to rounded. The grains are slightly turbid. Most have both radial and concentric fractures, and a few have linear fractures as well. All of the grains exhibit concentric zoning, but some are dominated by regions of patchy recrystalization texture. Xenocrystic cores are present in most of the grains, and some of the cores appear to be slightly resorbed. The cores often have a higher CL response than the outer part of the

grain. A few grains have multiple generations of cores. Most grains have a thin rim with a high CL response.

SAB91-65

SAB91-65 was obtained as mineral separates. The zircons selected are 60-300 μm in size. The grains are rounded. Some are elongated, with aspect ratios up to 4. Others are round and may have been equant. Approximately 50% of the grains are clear and 50% are slightly turbid. Some grains exhibit radial and linear fractures. A few have concentric and radial fracturing around a core. The grains are concentrically zoned, and a few have regions of patchy recrystalization texture. Most of the grains appear to contain a xenocrystic core that is partly resorbed. Most of the grains also have a thin rim with a high CL response.

SAB91-79

SAB91-79 is a foliated medium to coarse grained gneiss with light and dark colored layering. In thin section the sample consists of approximately 40% plagioclase, 40% quartz, 15% biotite, 1-2% apatite, and 1% zircon.

The zircons from sample SAB91-79 are approximately 100-400 μm. They are prismatic and elongated, with aspect ratios of 3-4, and are subrounded to rounded. Approximately 50% of the grains are clear and 50% are slightly to very turbid. Most of the grains exhibit radial and concentric fractures. The grains are concentrically zoned, and most appear to contain a xenocrystic core. Some of these cores are partly resorbed. The grains also exhibit rims with a high CL response.

SAB94-77

SAB94-77 was obtained as mineral separates, but a thin section was also available. In thin section the sample consists of approximately 65% biotite, 20% plagioclase, 10% quartz, and 5% zircon.

The grains selected range from 200-400 μm and range from rounded to elongate with aspect ratios up to 3 while others have irregular shapes. About 30% of the grains are clear and 70% slightly turbid. A few grains have radial fractures, but most have only randomly oriented linear fractures. None of the grains in this sample exhibited any CL response, and therefore only BE images were successfully obtained. Concentric zoning is visible in most of the grains, and a few appear to contain cores.

SAB94-134

Sample SAB94-134 was obtained as mineral separates, but a thin section was also available. In thin section the sample consists of approximately 40-45% quartz, 40-45% plagioclase, 10% biotite, 2-3% zircon, and 1% apatite.

The zircons selected are approximately 150-300 μm and most are rounded. Some are elongated, with aspect ratios of 2-3, and probably had a prismatic habit. Approximately 50% of the grains are clear and 50% are slightly turbid. Most of the grains have radial fractures in the outer part and a few have cores bounded by concentric fractures. Other grains are simply cut by randomly oriented linear fractures. The grains are concentrically zoned. About half of the grains clearly contain a xenocrystic core, some of which appear partially resorbed. Other grains may contain xenocrystic cores, but they are difficult to distinguish from the concentric zoning. The grains have rims with a high CL response.

SAB96-60

Sample SAB96-60 was obtained as mineral separates. The zircons selected are approximately 100-300 μm in size. They are prismatic and rounded, with aspect ratios ranging from 2-4; most of the grains are clear. Most of the grains have randomly oriented linear fractures, but a few have radial fractures in the outer part, bounding a core. Most of the grains are concentrically zoned, but two grains have a linearly banded pattern. About half of the grains have a xenocrystic core and most grains have rims with a high CL response.

SAB96-76

Sample SAB96-76 was obtained as mineral separates. The zircons selected are approximately 150-200 μm in size. Some are rounded and slightly elongated. Other grains are irregular and jagged and appear to be broken fragments. The grains are clear, and have randomly oriented linear fractures. About half of the grains appear to have concentric zoning. Four grains appear to have xenocrystic cores. Only two grains have what appear to be remnants of a thin rim with high CL response.

Methods

Rock Crushing

Five of the thirteen samples analyzed in this study were obtained as whole rocks. These rocks were crushed into sand-sized particles, and the densest minerals were then separated from the sand.

The rocks were first broken with a hammer. A large piece of the rock was saved as a hand sample. The rest was broken into small fragments with dimensions on the order of one or two inches. These fragments were then fed through a jaw crusher machine, which crushed them into pea-sized gravel. The gravel was then ground into sand with a disc mill. The sand was run through a 500μm sieve, and any sand with a grain size >500μm was run through the disc mill a second time. After a second run through the disc mill only a small number of grains >500μm remained. These grains were stored and were not used in the mineral separation phase of sample preparation.

The hammer, jaw crusher, disc mill, and all other tools and surfaces that came in contact with the rocks were cleaned thoroughly between the processing of samples.

Mineral Separation

Wilfley Table

The sand obtained from the crushing phase was run across a Wilfley table. Sand was gently washed down the ridges of the table while it agitated. The sand was then collected in twelve buckets around the edge of the table. The densest minerals move all the way to the left-hand edge of the table and collected in buckets and subsequently placed under heating lamps to dry. The Wilfley table was cleaned thoroughly between processing samples.

Franz Magnetic separation

The sand obtained from the Wilfley table was then run through a Franz magnetic separator. The grains were run along a chute under an electromagnet. The chute was tilted at 20°, and the magnetic field was concentrated along the top edge of the chute. Magnetic grains ran along the top of the chute and collected into one cup, while non-magnetic grains slid down to the bottom of the chute and collected in a different cup. The separation was performed twice at currents of 0.3 and 0.6 amps. If a large amount of non-magnetic material remained, the sample was run through once more at 0.9 amps. The magnetic grains were saved and stored. Only the non-magnetic grains were subjected to heavy liquid separation. The Franz magnetic separator was cleaned with compressed air and wiped down with ethanol between the processing of each sample.

Heavy Liquids

The non-magnetic separates were then poured into a funnel containing methyl iodide (MeI), which has a density of 2.28 g/cm^3. The densest grains were allowed to settle at the bottom of a funnel and then released through a stopcock and collected. The grains were washed thoroughly with acetone and subjected to a final Franz separation. The floats were washed and stored. All glassware used was washed thoroughly with acetone between the processing of each sample.

Final Franz Separation

The grains obtained from the heavy liquid separation were run through the Franz magnetic separator at 1.2 and 1.4 amps. The machine's tilt was then adjusted from 20° to 15°, 10°, and smaller angles as needed until <1 cc of non-magnetic grains remained.

Grain Mounting

Zircon grains were picked from the non-magnetic grains obtained in the final phase of Franz separation. The eight samples that were not obtained as whole rocks were obtained as magnetic separates, so all thirteen samples underwent the procedures described from this point onwards.

Picking Zircon Grains

The remaining grains were placed in a petri dish filled with ethanol and examined under a microscope. Zircon grains were selected and moved to a separate dish. Whenever zircons were abundant in the sample, the larger grains were selected preferentially.

Annealing

Samples SB91-62, SB91-65, and a portion of SB91-37-3 were annealed before mounting. The grains were placed in quartz beakers and cooked in a furnace at 900°C for 60 hours. The annealing process caused radiation damage in the crystal lattice to heal and allowed for clearer CL imaging.

Mounting the Grains

Only grains of a similar size can be placed on the same mount or else it is not possible to polish the mount to a single correct depth. Two samples, SB91-54 and SB91-37-1, had grains of varying sizes selected and thus two separate mounts were made of each of these samples.

The selected grains were arranged on double sided tape along with chips of SL standard. A plastic circular mold with 1" diameter was placed over the grains. Grease was spread on the inside edges of the mold for easier removal. The mold was then filled with 3.0 grams of epoxy and allowed to set for a minimum of six hours. A label with the

sample number was then applied to the top of the hardened epoxy, and a second layer of 3.0 grams of epoxy was poured over the label and allowed to set. After the epoxy was fully hardened the epoxy mount was removed from the mold. The zircon grains remained trapped in the bottom surface of the mount.

Polishing

The mounts containing the zircon grains were polished with 1200 grit sandpaper until the grains were approximately half-way polished through, exposing the middle of the grains. The mounts were then polished with increasingly fine grits, culminating in a final polish with AlO_2 at 0.3μm grit.

Imaging

The grain mounts were coated with carbon. They were then imaged with a scanning electron microprobe. Both cathode luminescence (CL) and backscatter electron (BE) images were taken of each individual grain.

Laser Ablation ICPMS

Laser ablation inductively coupled plasma mass spectrometry (LA-ICPMS) was carried out at the University of Arizona under the direction of Professor George Gehrels. Measurements were taken of approximately 200 zircon grains in total from the 13 samples. Two analyses were taken of grains that appeared to contain a core in the CL and BE images: one analysis of the core and one analysis of the outer part of the zircon. In a few cases grains showed multiple zoned realms. Whenever possible, each zoned layer was analyzed, so several grains have three or four analyses. Tables of the data collected for each sample are contained in Appendix B.

After LA-ICPMS, new BE images were taken of the zircon grains to determine the exact locations of the analyses. These BE images were overlaid with the old CL images and the analysis sites were marked and labeled. These labeled images are contained in Appendix A.

Sources of Error and Corrections

Elemental fractionation occurs during LA-ICPMS. The fractionation is caused by the preferential condensation of U on the edges of the crater in the sample produced by the laser. As the analysis continues and the crater grows deeper, more U is lost (Kosler and Sylvester 2003). Measurements of the SL standard included on the mount were used to correct for elemental fractionation. One analysis of the SL standard was taken after every five unknown analyses. In addition, some grain mounts contained a secondary standard: zircons from sample EKCO2-51. These zircons were previously dated at 3226.1 ± 0.7 Ma using ID-TIMS (Schoene and Bowring 2007). Although not used in correction, the measurements taken of this secondary standard provide a comparison by which the accuracy of our measurements can be judged. When available, the measurements of EKCO2-51 are displayed at the bottom of the data table.

Initial common Pb contained in the zircon is another source of error, as we wish only to measure radiogenically produced Pb. To correct for initial common Pb, the concentration of the non-radiogenic isotope ^{204}Pb in the sample is measured. Measured Pb is then corrected using the assumed ratios of $^{206}Pb/^{204}Pb$, $^{207}Pb/^{204}Pb$, and $^{208}Pb/^{204}Pb$ in common-Pb (Kosler and Sylvester 2003). The source of the common Pb is likely Pb introduced along fractures or from inclusions in zircon.

Data were plotted on concordia diagrams using Isoplot software. These concordia plots are contained in Apendix C. Plots of U concentration vs. concordance were also created, and are contained in Appendix D.

Results and Analysis

Zircons from these samples generally appear to have three distinct domains: an thin rim, a mantle, and a core. In a few cases there appear to be two generations of cores, which are referred to as "inner core" and "outer core". The rims are too thin to collect LA-ICPMS data, but whenever possible an analyses was taken of both the mantle and core of each grain.

SAB89-28

In total, 17 analyses were obtained from 8 grains for sample SAB89-28. The U-Pb isotopic data for the mantles are clustered slightly below concordia between 3.35-3.2 Ga, with the exception of analysis 14-1 from grain 14, which is 2.839 ± 0.0525 Ga and highly discordant. The core data are clustered on concordia between 3.45-3.25 Ga. Grain 14 has both an inner and outer core, which are dated at 3.412 ± 0.0894 and 3.284 ± 0.0588 Ga respectively (Figure 12).

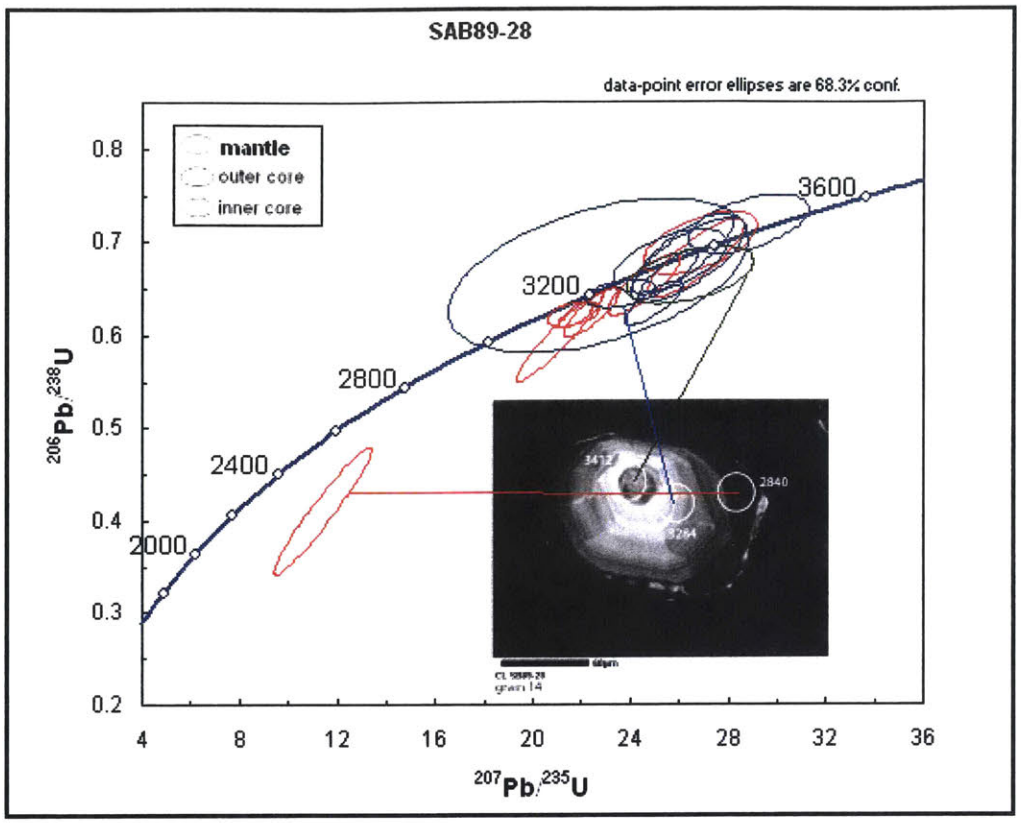

Figure 12: Grain 14 contains three domains which were analyzed separately: a mantle (red), outer core (blue), and inner core (green).

U concentrations in the cores are quite low, ranging from 6 to 104 ppm. U concentrations in the mantles are variable and range from 57-520 ppm. In many of the grains the cores are bounded by concentric fractures, indicating a structural boundary between the core and mantle. The higher U concentrations observed in many of the mantles may have allowed for differential metamictization leading to volume expansion of the mantles and producing the fractures around the core-mantle boundary.

The structural boundary and different U concentrations between the cores and mantles suggest that two separate crystallization events occurred, one between ca 3.45-

3.25 and one between ca 3.35-3.2. Many of the grains also have a thin rim with a high CL response, indicating either metamorphic overgrowth or late-stage igneous overgrowth. The data are consistent with a best estimnate for the age of this rock as 3.4 Ma with slightly older inheritance and some younger metamorphic overgrowths.

SAB91-35

In total, 17 analyses were obtained for sample SAB91-35 over 10 grains. Most U-Pb isotopic data for grain mantles and cores are clustered on concordia between ca 3.6-3.5 Ga, with the exception of a few that plot below concordia indicative of lead loss.

In general, the cores do not have higher uranium concentrations than the mantles, with a typical range from 300-1000 ppm. Most grains exhibit radial fractures in the mantle which truncate at the core, interpreted to reflect volume expansion. Patchy textures (Figure 13) are seen in many of the cores. This texture is not observed in the mantles, which are concentrically zoned. This texture may be the result of either metamictization or recrystalization. However, since the U concentrations are not found to be higher in the cores than the mantles, it is unlikely that differential metamictization has occurred. Recrystalization of the cores before the overgrowth of the mantles would require that the cores are xenocrystic and are older than the mantles.

In most grains the date calculated for the core is not significantly older than the mantle. In a few cases the core date is younger than the mantle date, which indicates lead loss. However, as most dates are concordant, large amounts of lead loss have not occurred. The cores are therefore not interpreted to be significantly older than the mantles. If these two domains are the result of separate crystallization events, they must have occurred close together in time.

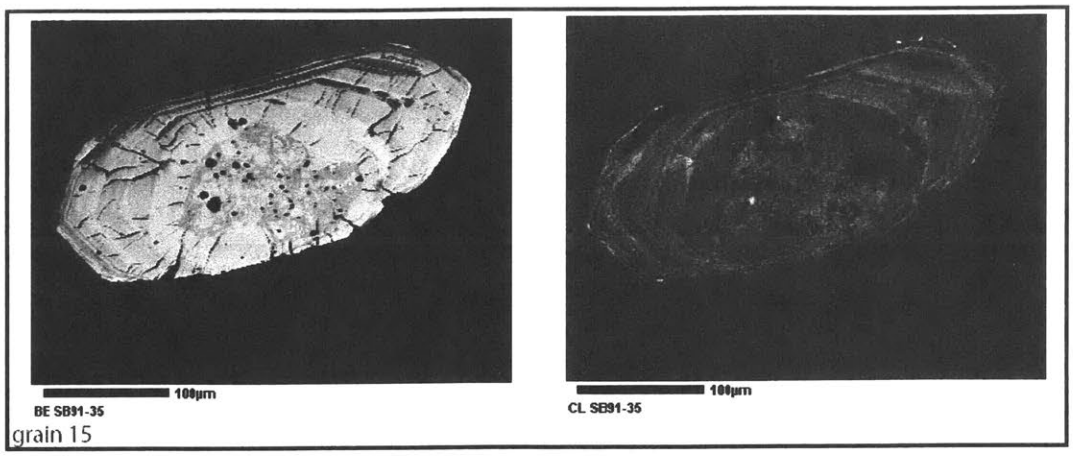

Figure 13: A BE image (left) and CL image (right) of a grain from SB91-35. The core exhibits a patchy texture. The mantle is concentrically zoned and exhibits radial fractures which truncate at the core boundary.

Although the dates are roughly the same and the cores do not appear resorbed, the differences in texture and the termination of radial fractures at the core indicate a structural boundary between the core and mantle domains. This suggests that the cores are xenocrysts. Thus we infer two separate crystallization events that occurred very close together in time. As the data are clustered between ca 3.6 - 3.5 Ga, we interpret that the two crystallization events both occurred between ca 3.6-3.5 Ga. Some of the grains appear to have a very thin rim with a high CL response, which may be either a metamorphic overgrowth or a late stage magmatic overgrowth. The age of the rock is inferred to be approximately 3.6 Ga.

SAB91-37-3

A total of 66 analyses were obtained from 40 grains in sample SAB91-37-3. Most of the U-Pb data for both cores and mantles is clustered on concordia at ca 3.55 Ga. However, some data for both the cores and mantles are discordant and define a linear

array anchored by the several concordant analyses at ca 3.9 Ga and projecting towards a lower intercept of ca 1.2 Ga. This is consistent with a lead loss event occurring at ca 1.2 Ga which affected some of the grains.

U concentrations are variable, with most ranging from 0 to 1000 ppm in both the mantles and cores. In general analyses with higher U concentrations are more discordant, indicating that lead loss has occurred preferentially in grains with high U concentrations. This is not surprising, as susceptibility to lead loss is linked to metamictization (Silver and Deutsch 1963).

In some of the grains, radial fractures are present in the mantle and terminate at the core, indicating a structural boundary between the core and mantle. This suggests that the cores and mantles are the result of separate crystallization events. In other grains no structural boundary is present.

We interpret two crystallization events. The first event occurred at ca 3.9 Ga, the upper intercept of the linear array of data. This is consistent with a more precise age of 4.012 Ga determined by Bowring and Williams (1999). The second event occurred at ca 3.55 Ga indiacted by a cluster of concordant data. Both the cluster and the array contain analyses from cores and mantles, indicating that the cores and mantles are not easily divided into separate crystallization events. It is possible that some zircons are entirely the result of the first crystallization event, some were entirely formed by the second event, and some consist of a xenocrystic core from the first event with mantle overgrowth from the second event. About half of the grains also exhibit a thin rim with a high CL response, which indicates either metamorphic overgrowth or late-stage igneous overgrowth.

This data is consistent with data obtained by Bowring and Williams (1999) using SIMS. The data was collected with a sensitive high resolution ion microprobe (SHRIMP). In their study, two concordant clusters were identified at 4.0 and 3.6 Ga, along with discordant analyses indicating lead loss. The older cluster consisted of analyses of unzoned or weakly zoned centers, and the younger cluster of overgrowths, intermediated layers, and recrystallized domains. Bowring and Williams' interpretation is that the zircons initially crystallized at about 4.0 Ga, and overgrowth and recrystalization occurred at about 3.6 Ga. A sampling of data collected from both Bowring and Williams and this study is displayed on a Tera-Wasserburg plot (Figure 14). This is a concordia plot which compares the measured $^{206}Pb/^{207}Pb$ ratio with the $^{238}U/^{206}Pb$ ratio.

The SIMS data collected by Bowring and Williams is more precise than the data collected in this study. Errors in the $^{206}Pb/^{207}Pb$ ages from ca 3.5 Ga zircons are typically less than ±10 Ma, whereas the data presented in this study have typical errors on the order of ± 20-100 Ma.

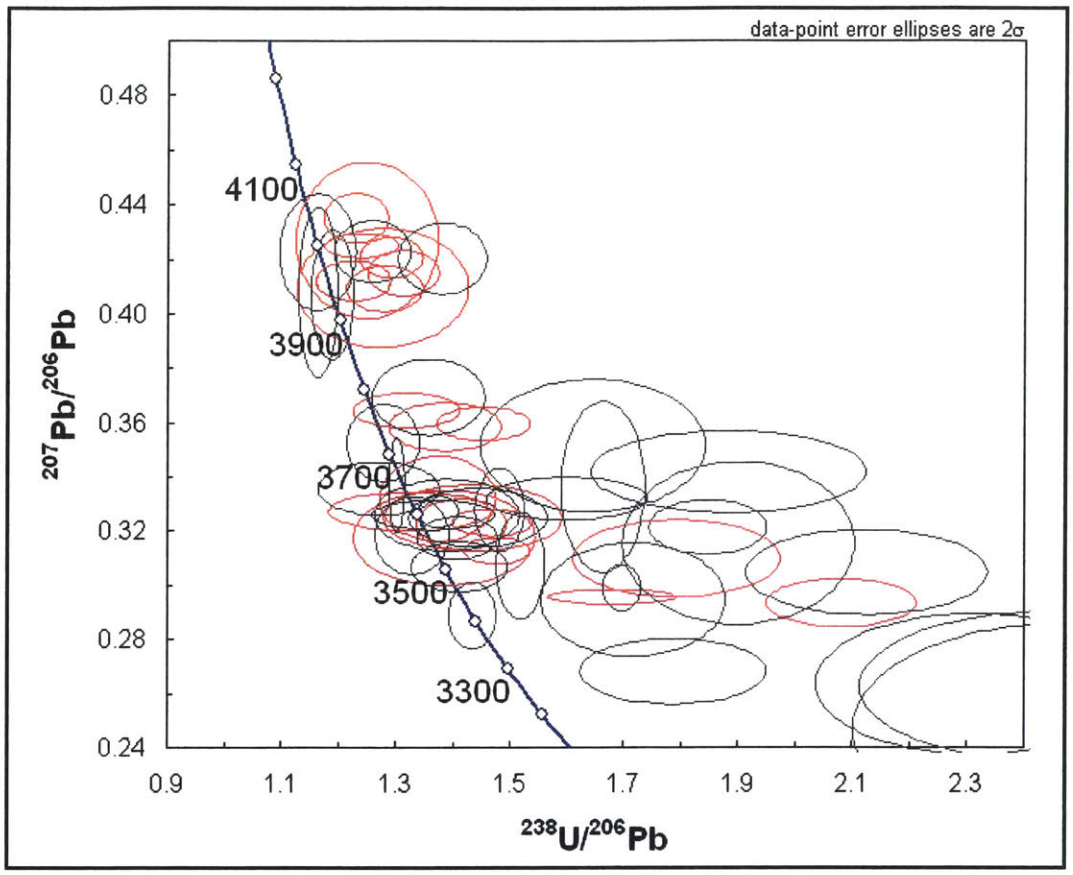

Figure 14: U-Pb data for sample SAB91-37-3, plotted on a Tera-Wasserburg diagram. Red: from Bowring and Williams 1999. Gray: this study.

SAB91-52

A total of 13 analyses were obtained from 7 grains. Some of the U-Pb data are clustered on concordia at ca 3.6 Ga. Other data define a linear array with an upper intercept anchored by the concordant analyses at 3.6 Ga and trending toward a lower intercept of ca 1.0 Ga.

Most of the grains have U concentrations ranging from 100-1500 ppm. There is a clear trend of high U concentration with discordance, indicating that lead loss has occurred preferentially in grains with higher U concentration.

Many of the grains exhibit radial fractures in the mantles which terminate at the core, indicating a structural boundary between mantle and core. The grains have domains of concentric zoning and domains of a patchy texture. This patchy texture may be the result of metamictization.

The existence of a structural boundary between the cores and mantles suggests two separate crystallization events, but the U-Pb data is consistent with only a single event at ca 3.6 Ga. It is possible that two events occurred very close together in time at ca 3.6 Ga. Many of the grains have a thin rim with a high CL response, which is likely the result of metamorphic overgrowth or late-stage igneous overgrowth.

SAB91-53

A total of 15 analyses were obtained from 8 grains from sample SAB91-53. Most of the U-Pb data is clustered on concordia at ca 3.8 Ga. Some data trend in a linear array below concordia whose upper intercept is anchored by the concordant analyses at 3.8 Ga, consistent with lead loss. Further evidence for lead loss are reversals in which younger dates were obtained for cores than for mantles in some grains. U concentrations range from 200-700 ppm for both cores and mantles.

Some of the grains contain cores bounded by concentric and radial fractures. These cores appear xenocrystic, as concentric zoning is truncated at the boundary with the mantle. Other grains do not appear to contain cores. The U-Pb data is consistent with a single crystallization event at ca 3.8 Ga, which does not support the interpretation of the cores as xenocrystic. It is possible that two separate crystallization events occurred very close together in time at ca 3.8 Ga. The cores were formed by the first event and were overgrown by the mantles in the second event. Those zircons without cores were formed

entirely by the second crystallization event. The thin rims around the grains are the result of later metamorphic overgrowth or late-stage igneous overgrowth.

SAB91-54

18 analyses were obtained from 8 grains from sample SAB91-54. Some data are clustered on concordia between 3.75-3.65 Ga. The rest of the data trends in a linear array below concordia whose upper intercept is anchored by the cluster of concordant analyses. This indicates lead loss in some of the grains. Most U concentrations for both cores and rims range from 100-600 ppm.

Some of the grains appear to contain cores. In a few grains the core is bounded by radial and concentric fractures, indicating a structural boundary. In some cases the cores also appear partly resorbed. This suggests that at least some of the cores present are xenocrystic. Two grains, grain 15 and grain 17, appear to contain both an inner and outer core. However, in both cases, the dates measured for the three domains of the grain are not significantly different. In the case of grain 15 it is possible that the core is not xenocrystic. In the case of grain 17, the zoning of the inner and outer cores is cut off by the core-mantle boundary, indicating a xenocrystic core (Figure 15). The inner core analysis is quite discordant (72.2%) indicating that the actual age of the core is likely older.

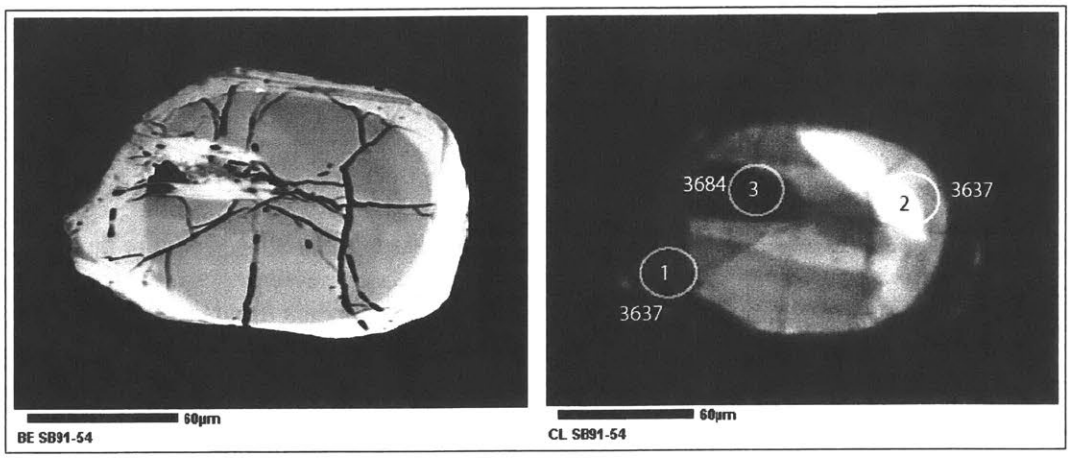

Figure 15: A BE image (left) and CL image with dates (right) of grain 17. The inn and outer cores appear xenocrystic because their concentric zoning pattern is cut off at the boundary with the mantle.

The grains without cores may be the result of a single crystallization event. Other grains with xenocrystic cores may be the result of two crystallization events which occurred between 3.75-3.65 Ga. A few grains have thin rims which are either metamorphic overgrowth or late-stage igneous overgrowth.

SAB91-62

A total of 23 analyses were obtained from 11 grains. Most of the U-Pb data for the cores are clustered on concordia at ca 3.6 Ga. The data for the mantles define a linear array below concordia with an upper intercept of ca 3.4 Ga and a lower intercept of < 2.0 Ga. This indicates that lead loss has occurred in the mantles. Three outer core analyses fall along this linear array as well. Two grains also contain inner cores, both of which plot along this array.

The U concentration data for sample SAB91-62 is striking in that analyses are quite distinct for cores and mantles (Figure 16). Data from outer cores range from 87-335 ppm. Data from mantles range from 521-1876 ppm. The two inner core analyses are 929

and 2069 ppm. The much higher U concentrations in the mantles explains the lead loss observed in the mantles but not the outer cores. Metamictization is linked to lead loss susceptibility (Silver and Deutsch 1963). Higher U concentrations in the mantles allowed for greater metamictization and higher lead loss susceptibility.

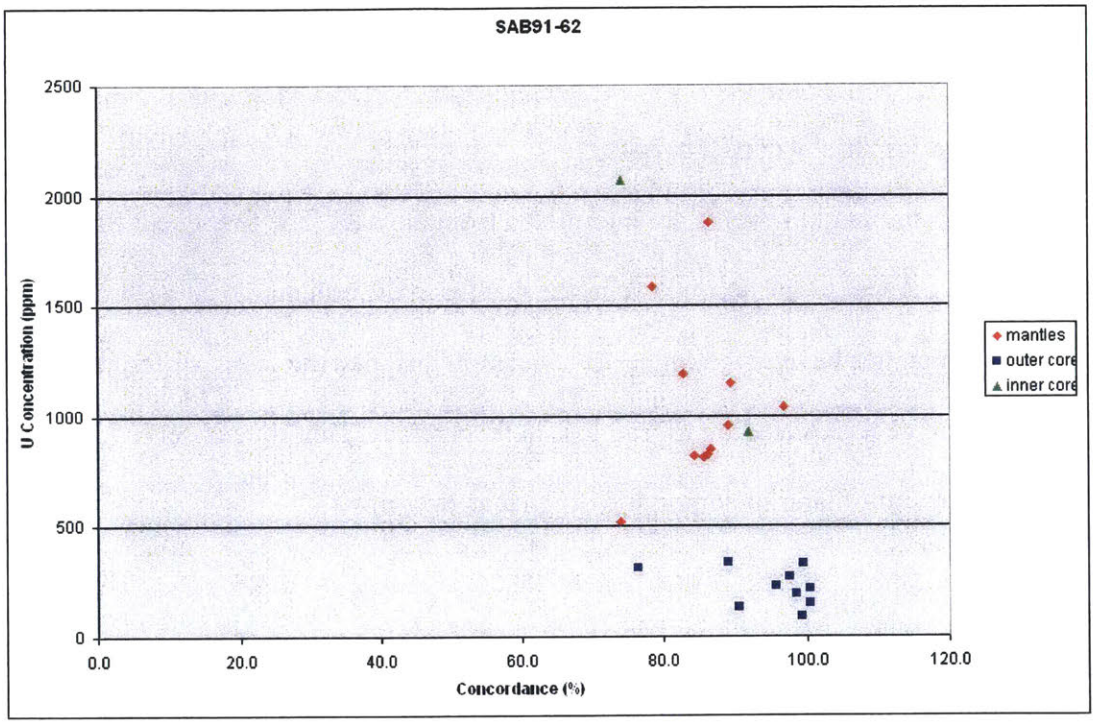

Figure 16: U concentration vs. concordance in sample SAB91-62. Mantles (red diamonds) have much higher concentrations than outer cores (blue squares). Inner cores (green triangles) also have high concentrations.

In CL images some of the cores appear slightly resorbed, and other cores have zoning patterns that are cut off at the boundary with the mantle. Radial fractures in the mantles terminate at the core, indicating a structural boundary. This evidence and the distinct U concentrations observed in cores and mantles indicate that the cores are xenocrystic.

The two grains which contain both an inner core and outer core, grains 30 and 37, are a bit more difficult to interpret. The outer cores have lower U concentrations, 217 and 335 ppm, while the inner cores have higher U concentrations, 2069 and 929 ppm. In grain 30 the outer core has a concordant date of 3.921 ± 0.0448 Ga and the inner core has a discordant date of 3.272 ± 0.2522 Ga. This indicates lead loss has occurred in the inner core but not the outer core. In grain 37 the outer core and inner core are both discordant, suggesting lead loss has occurred in both.

Two crystallization events are interpreted from the data. The first event formed the cores at ca 3.6 Ga. In the second event, the mantles grew around the cores at ca 3.4 Ga. Since the mantles have much higher U concentrations than the cores, differential metamictization occurred leading to lead loss in the mantles. Thin rims observed on the grains are the result of later metamorphic or igneous overgrowth.

SAB91-65

Tewnty-six analyses were obtained from 12 grains. U-Pb data for mantles and outer cores are clustered on concordia at ca 3.6 Ga. A few analyses plot below the concordia on two linear arrays, the first with an upper intercept at ca 3.6 Ga and a lower intercept at ca 1.5 Ga and the second with an upper intercept at ca 4.0 Ga and a lower intercept at ca 1.5 Ga. This is consistent with a lead loss event occurring at ca 1.5 Ga. One core plots on concordia at 4.046 Ga. Two grains, grain 0 and grain 32, have inner cores which plot on concordia at 4.051 and 3.976 Ga respectively. Although relatively imprecise (±79.2 Ma, ±66.2 Ma) the cores suggest this sample may contain more zircons in excess of 4.0 Ga.

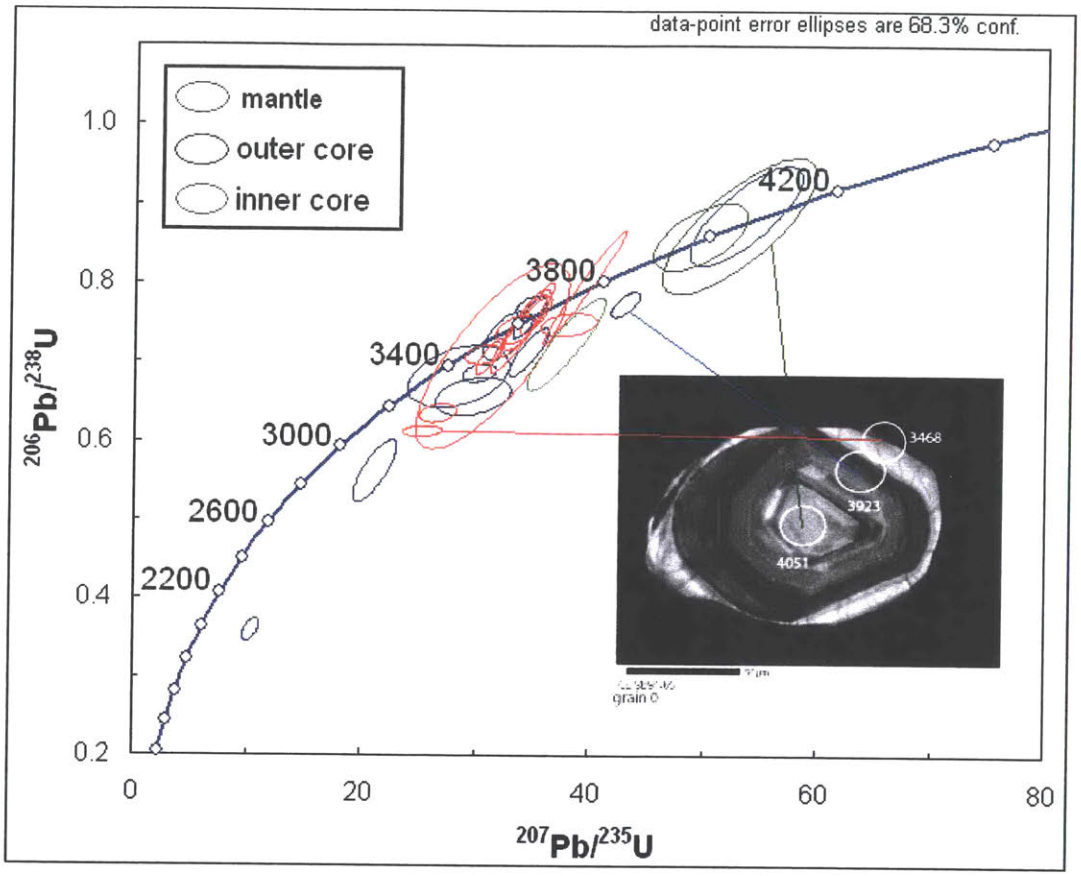

Figure 17: A concordia diagram for sample SAB91-65. Grain 0 is pictured with analyses of mantle, outer core, and inner core domains. The outer core and mantle plot below concordia, indicating lead loss.

Most U concentrations for the mantles range from approximately 100-300 ppm. U concentrations for the cores are much more spread out and range from 100-1000 ppm. About half of the cores have U concentrations of over 500 ppm.

Many of the cores appear slightly resorbed in CL images, suggesting that they are xenocrystic. Two crystallization events can be inferred: the first at ca 4.0 Ga and the second at ca 3.6 Ga. A lead loss event at 1.5 Ga affected some of the grains. Thin rims on most of the grains resulted from later metamorphic or igneous overgrowth.

SAB91-79

Twenty-eight analyses were collected from 13 grains. Most U-Pb data for mantles and cores are clustered on concordia between 3.7-3.6 Ga. A few analyses are on concordia between 3.55-3.35 Ga. The data are almost all concordant, with only two analyses < 97% concordant. This indicates that very little or no lead loss has occurred in this sample.

U concentrations for the mantles range from 71-236 ppm. The cores generally have lower U concentrations, ranging from 53-95 ppm.

Many of the grains have mantles with a low CL response and cores with a high CL response. Radial fractures in the mantles terminate at the core, indicating a structural boundary. The cores appear partly resorbed, indicating they are xenocrystic (Figure 18).

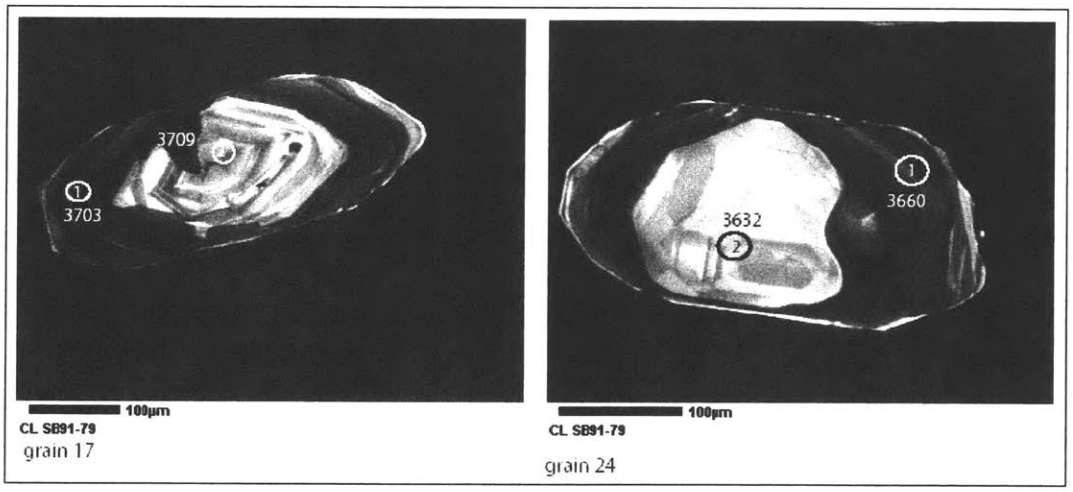

Figure 18: Many cores in grains from sample SAB91-79 appear partly resorbed, indicating they are xenocrystic.

The presence of xenocrystic cores requires two separate crystallization events. Since only a single cluster is present on concordia, these two events must have occurred very close together in time, between 3.7-3.6 Ga. A few of the mantle analyses are

concordant and date as late as 3.35 Ga, suggesting that either the second crystallization event which formed the mantles was very slow, or a third event occurred at ca 3.35 Ga in which further overgrowth occurred. Thin rims observed on some of the grains are the result of later metamorphic or late-stage igneous overgrowth.

SAB94-77

Fifteen analyses were collected from 11 grains from sample SAB94-77. All of the data plot along concordia, indicating that no or very little lead loss has occurred. The majority plot in two clusters: one at ca 3.75 Ga and one at ca 3.6 Ga. There are also two outliers: one analysis plots at ca 3.3 Ga and another at ca 3.35 Ga. The U-Pb data suggests two separate crystallization events at ca 3.75 and ca 3.6 Ga. The majority of the grains have U concentrations ranging from 50-200 ppm. These low U concentrations may account for low rates of lead loss, as it is likely that very little metamictization has occurred.

Analysis of this sample is somewhat limited by the fact that the grains had no CL response, and only BE images were successfully obtained. This makes the identification of cores difficult. A few grains appear to have cores, but fractures do not indicate any obvious structural boundary between the cores and mantle. Without CL images it is difficult to determine whether the grains are xenocrystic.

SAB94-134

A total of 24 analyses were obtained from 12 grains from sample SAB94-134. U-Pb data from the grain mantles are clustered on concordia at ca 3.7 Ga. Two core analyses are > 4.0 Ga and concordant: analysis 09-2 is 4.032 ± 0.0219 Ga and analysis 20-2 is 4.085 ± 0.0326 Ga. All other data from the cores define a linear array anchored by

the two concordant analyses at ca 4.0 Ga and projecting towards a lower intercept of <2.0 Ga. This is consistent with lead loss in the cores. Lead loss explains the reversals seen in a few grains in which cores were dated as younger than the outer interior (Figure 19).

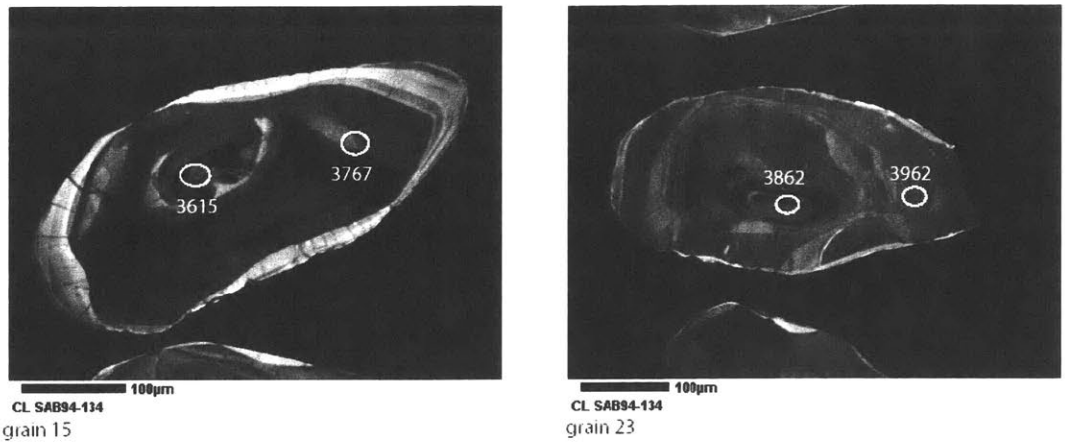

Figure 19: Two "reversed" grains from sample SB94-134. The cores appear to be younger that the outer interior because lead loss has occurred in the cores. This loss of daughter product causes the calculated date to be younger than the real age.

The cores of the grains also in general have higher U concentrations than the interiors. The mantles have U concentrations of 100-300 ppm, while more than half of the cores were measured at 600-900 ppm. Higher U concentrations in the cores explain the fracture patterns observed in the grains. Volume expansion often occurs in U-rich domains of the zircon due to differential metamictization (Corfu, 2003). This volume expansion of the cores causes the outer interior realms to fracture. The radial and concentric fractures that bound the cores in many of these grains are likely a result of volume expansion of the cores.

Some of the cores observed in these grains appear slightly resorbed around the edges. This, combined with the higher uranium concentrations observed, is convincing

evidence that the cores are xenocrysts. It is possible that the higher U concentrations in the cores lead to metamictization, which is responsible for the lead loss observed in the cores.

The xenocrystic cores were first crystallized at approximately 4.0 Ga. The original host rock was later reincorporated into a new melt, and the mantle domain crystallized around the cores at ca 3.7 Ga. The thin rims with high CL response observed on the grains are likely the result of later metamorphic or igneous overgrowth.

The data obtained here is consistent with data obtained by Bowring and Williams (1999). In their study, 32 grains were analyzed. Analyses from the grain mantles were found to cluster at 3.75 Ga, which is consistent with the cluster found in this study at ca 3.7 Ga. Cores from Bowring and Williams' study were found to cluster at ca 4.0 Ga, consistent with the core age interpreted in this study. Data from both Bowring and Williams' study and this study are displayed below on a Tera-Wasserburg plot (Figure 20).

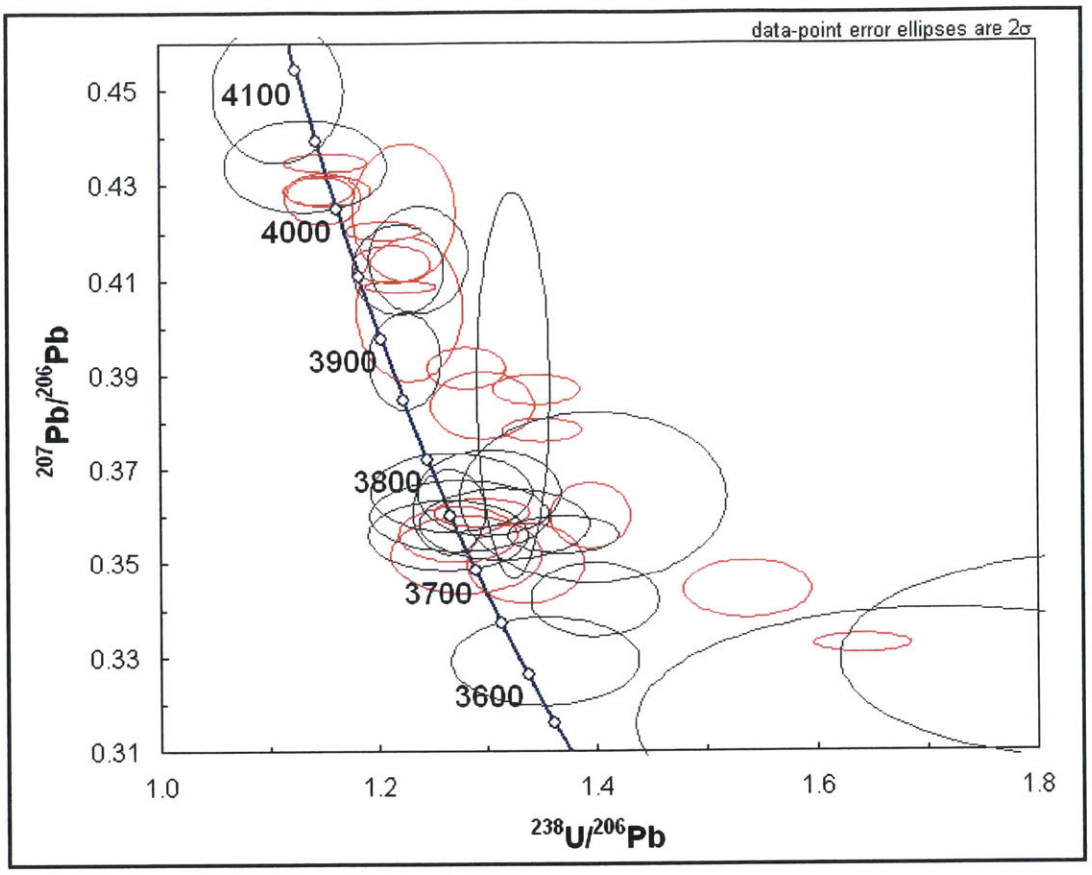

Figure 20: U-Pb data from sample SAB94-134 plotted on a Tera-Wasserburg concordia diagram. Red: Bowring and Williams 1999. Gray: this study.

SAB96-60

Eleven analyses were collected from eight grains. Eight of these analyses were of cores and only three analyses were obtained of mantles. Four of the analyses for cores are clustered on concordia between at ca 3.6 Ga. Two analyses are slightly below concordia, but more analyses would be needed to conclude if this represents a general lead loss trend in the sample. The three mantle analyses are ca 3.45 Ga. One is on concordia and two are

slightly below it. However, three analyses are not sufficient to draw conclusions about the relative ages of the mantles vs. the cores. U concentrations range from 100-450 ppm.

Most of the grains contain cores, and several of these cores appear to be slightly resorbed, indicating they are xenocrystic. This implies two separate crystallization events which occurred between 3.6-3.45 Ga. The first event, in which the cores were formed, is interpreted to have occurred at ca 3.6 Ga. The three mantle analyses imply that the second crystallization event occurred at ca 3.45 Ga. More data is needed from this sample to further constrain the crystallization history.

SAB96-76

Nine analyses were collected from seven grains. Seven of the analyses are clustered on concordia at ca 3.5 Ga. Two analyses plot slightly below concordia at ca 3.3 Ga, indicating some lead loss has occurred. More analyses are needed to determine if this represents a general lead loss trend in the sample. U concentrations are very low: most range from 3-33 ppm, with the exception of a single analyses at 111 ppm.

About half of the grains have cores, one of which appears to show slight resorbtion. However, it is not possible to conclude from the images whether the cores are xenocrystic. The data support a single crystallization event at ca 3.5 Ga, but more than nine analyses are needed to confirm this conclusion.

Discussion

Twelve of the thirteen samples analyzed show evidence of at least two crystallization events in the zircons' history. The xenocrystic cores found in these samples is strong evidence that older crust played a role in generating the granitoid rocks of all ages. The oldest dates obtained for cores in this study are ca >4.0 Ga, expanding the number of samples from previous studies with histories extending before 4.0 Ga. Further analysis is needed to refine the results of this study. The LA-ICPMS method is effective at quickly obtaining large amounts of data, but higher precision data could be obtained by ID-TIMS and SIMS.

SIMS analysis permits even smaller volumes of zircon to be analyzed than were analyzed using LA-ICPMS in this study. The data presented in this study was obtained with a 15 μm diameter laser spot, and analyses were approximately 12 μm deep. In a few cases the laser ablated entirely through the grain, and in many of the analyses of core regions it may have ablated through the core to the mantle domain on the other side of the grain. This leads to analyses that contain a mixture of both the core and the mantle regimes, which leads to a calculated core age that is younger than the true age. Smaller volumes could be analyzed with SIMS, allowing for core measurements that are not contaminated with matter from the mantle domain.

Likewise it is also possible to extract the polished grains from a mount and do ID-TIMS analyses, which should be even more precise. In this approach one could microsample the old cores. However, the small size of the cores, and the fact that many cores are not perfectly centered in the grain, would make their isolation quite difficult. Thus SIMS may be the preferred method with these grains.

SIMS data could be used to place more precise constraints on the ages of the crystallization events that formed these zircons. This data, combined with trace element geochemistry analysis, could lead to better interpretations of continental crustal formation processes in the late Hadean. Nearly all of the zircons isolated in this study have structural cores, indicating a complex history involving interaction of mantle derived melts with older crust. Further study of these and other ca 4.0 Ga rocks could provide more evidence to constrain problems such as the timing of early crustal differentiation and the controversy over the volume of crust produced in the Hadean and Archean. It is possible that rocks even older than those analyzed so far are waiting to be discovered. Continued characterization and dating of the Acasta gneisses and other Archean-aged rocks is the only way to find them.

Works Cited

Armstrong RL (1991) The persistent myth of crustal growth. *Australian Journal of Earth Sciences* **38** 613-630.

Bowring SA, Housh TB, Isachsen CE (1990) The Acasta Gneisses: Remnant of Earth's Early Crust. *Origin of the Earth.* Eds. H.E. Newson and J.H. Jones. Oxford University Press.

Bowring SA and Housh TB (1995) The Earth's Early Evolution. *Science* **269** 1535-1540.

Bowring SA and Williams IS (1999) Priscoan (4.00-4.03 Ga) orthogneisses from northwestern Canada. *Contrib. Mineral Petrol* **134** 3-16.

Corfu F, Hanchar JM, Hoskin PWO, Kinney P (2003) Atlas of Zircon Textures. *Reviews in Mineralogy and Geochemistry* **53:** Zircon. pp 469-500. Eds. J.M. Hanchar and P.W.O. Hoskin. Mineralogical Society of America.

Dalrymple GB (1991) *The Age of the Earth.* Stanford University Press. Stanford, CA.

Ewing RC, Alkiviathes M, Wang L, Weber WJ, Corrales LR (2003) Radiation Effect in Zircon. *Reviews in Mineralogy and Geochemistry* **53:** Zircon. pp 387-425. Eds. J.M. Hanchar and P.W.O. Hoskin. Mineralogical Society of America.

Fyfe WS (1978) The evolution of Earth's crust: modern plate tectonics to aincient hot spot tectonics? *Chemical Geology* **23** 89-114.

Harrison TM (2009) The Hadean Crust: Evidence from >4 Ga Zircons. *Annu. Rev. Earth Planet. Sci.* **37** (Unpublished at the time of writing this).

Hopkins M, Harrison TM, Manning CE (2008) Low heat flow inferred from >4 Gyr zircons suggests Hadean plate boundary interactions. *Nature* **456** 493-496.

Iizuka T, Horie K, Komiya T, Maruyama S, Hirata T, Hidaka H, Windley BF (2006) 4.2 Ga zircon xenocryst in an Acasta gneiss from northwestern Canada: Evidence for early continental crust. *Geology* **34** 245-248.

Ireland TR and Williams IS (2003) Considerations in Zircon Geochronology by SIMS. *Reviews in Mineralogy and Geochemistry* **53:** Zircon. pp 215-241. Eds. J.M. Hanchar and P.W.O. Hoskin. Mineralogical Society of America.

Isachsen CE and Bowring SA (1994) Evolution of the Slave craton. *Geology* **22** 917-920.

Kamber BS (2007) The Enigma of the Terrestrial Protocrust: Evidence for its Former Existence and the Importance of its Complete Disappearance. *Developments in*

Precambrian Geology 15: Earth's Oldest Rocks. pp75-90. Eds. Martin J van Kranendonk et all. Elsevier.

Kosler J and Sylvester PJ (2003) Present Trends and the Future of Zircon in Geochronology: Laser Ablation ICPMS. *Reviews in Mineralogy and Geochemistry* **53:** Zircon. pp 243-276. Eds. J.M. Hanchar and P.W.O. Hoskin. Mineralogical Society of America.

Murakami T, Chakoumakos BC, Ewing RC, Lumpkin GR, Weber WJ (1991) Alpha-decay event damage in zircon. *American Mineralogist* **71** 1510-1532.

Parrish RR and Noble SR (2003) Zircon U-Th-Pb Geochronology by Isotope Dilution—Thermal Ionization Mass Spectrometry (ID-TIMS). *Reviews in Mineralogy and Geochemistry* **53:** Zircon. pp 183-213. Eds. J.M. Hanchar and P.W.O. Hoskin. Mineralogical Society of America.

Reymer A and Schubert G (1984) Phanerozoic addition rates to the continental crust and crustal growth. *Tectonics* **3** 63-77.

Schoene B and Bowring SA (2007) Determining accurate temperature-time paths from U-Pb thermochronology: An example from the Kaapvaal craton, southern Africa. *Geochimica et Cosmochimica Acta* **71** 165-185.

Silver LT and Deutsch S (1963) Uranium-Lead Isotopic Variations in Zircon: A Case Study. *The Journal of Geology* **71** 721-758.

Van Kranendonk MJ (2007) Tectonics of Early Earth. *Developments in Precambrian Geology 15: Earth's Oldest Rocks.* pp1105-1116. Eds. Martin J van Kranendonk et all. Elsevier.

Appendix A

CL images of zircon grains, with analyses marked and labelled.

SAB89-28 zircons

0 1 2 3 4
12 11 10 9 8 7 6 5
STDS s p p s
STDS s p p s
13 14 15 16 17 18 19 20
23 22 21

R.Safipour

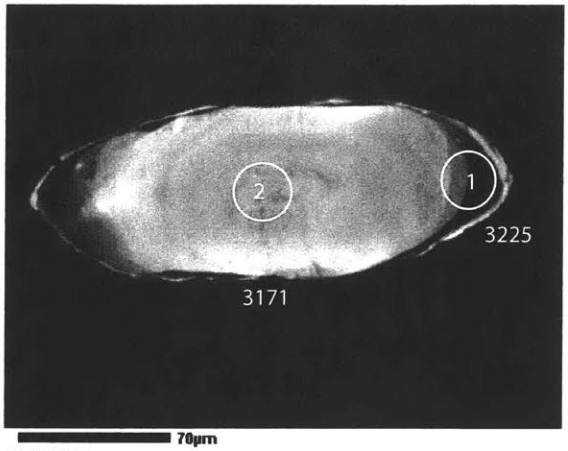

grain 5

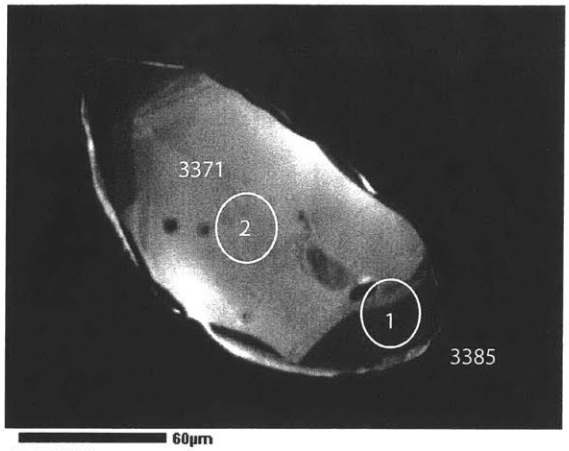

grain 12

grain 9

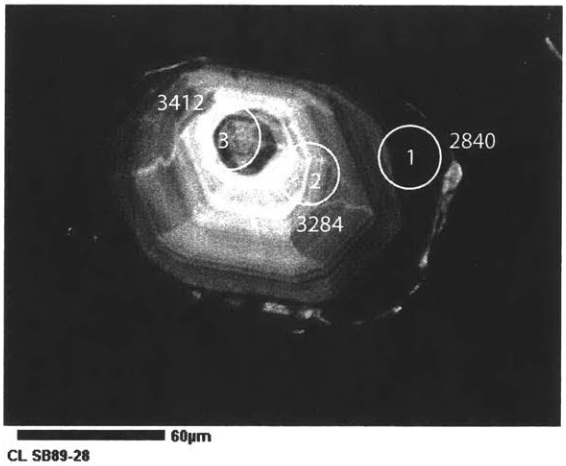

grain 14

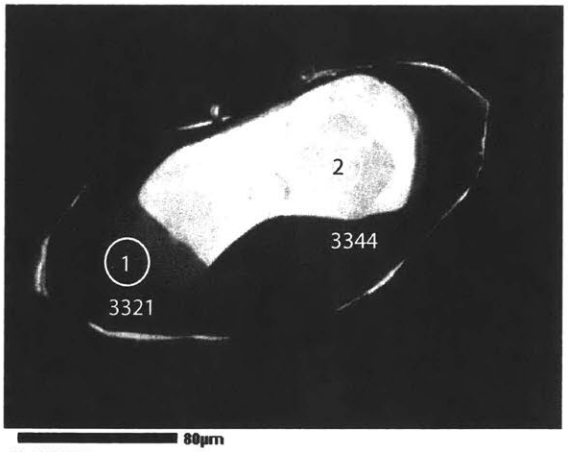

grain 10

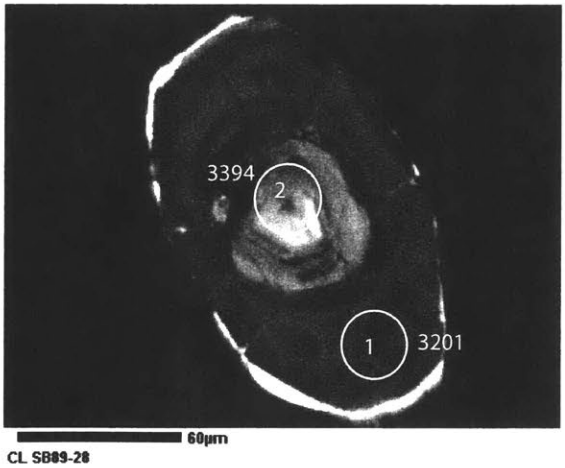

grain 18

SAB89-28 zircons

0 1 2 3 4
12 11 10 9 8 7 6 5
STDS s p p s
STDS s p p s
13 14 15 16 17 18 19 20
23 22 21

R.Safipour

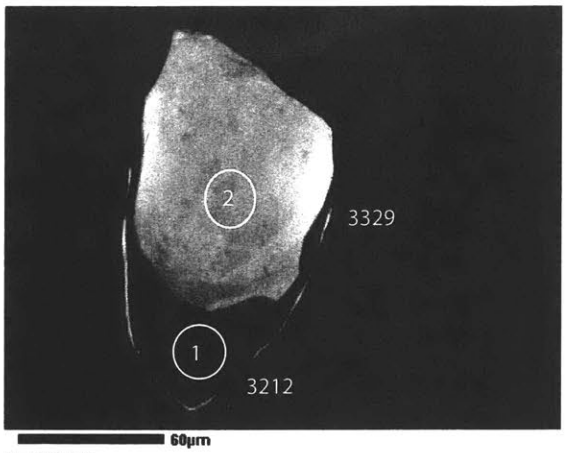

grain 21

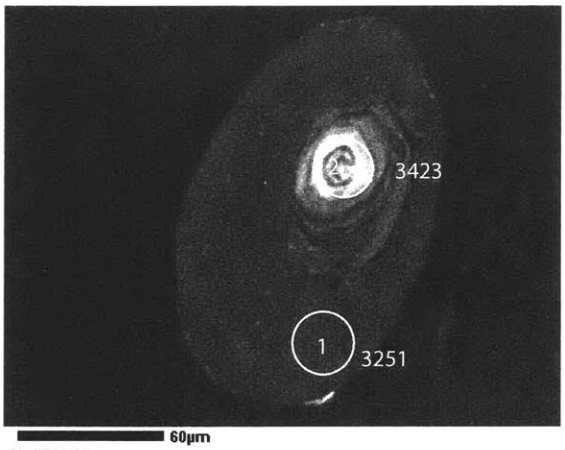

grain 22

SAB91-35 zircons

0 1 2 3 4 5 6
15 14 13 12 11 10 9 8 7
STDS s p p s
STDS s p p s
16 17 18 19 20 21 22 23 24
29 28 27 26 25

R.Safipour

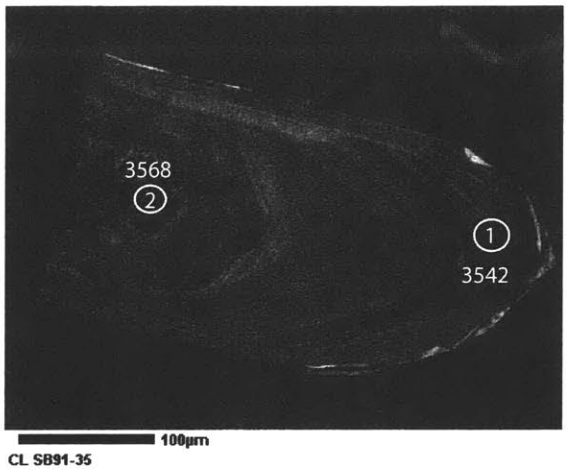

grain 4

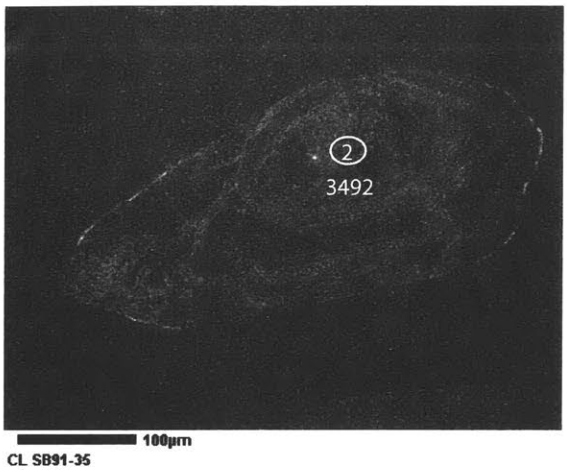

grain 10

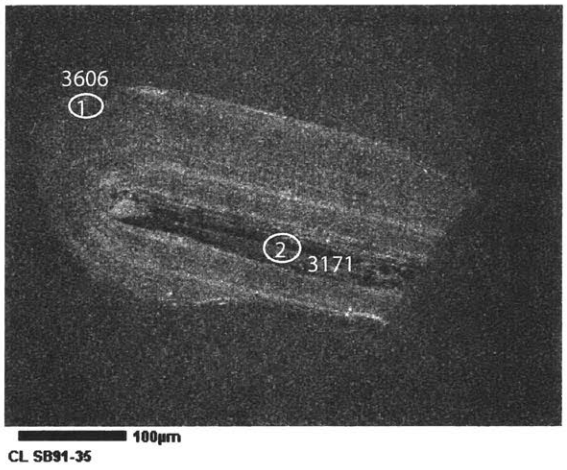

grain 5

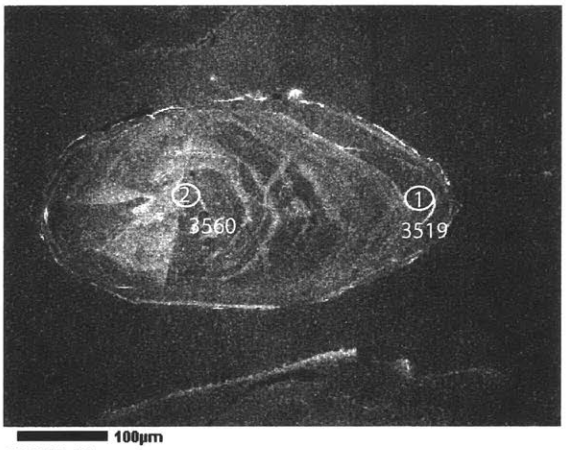

grain 12

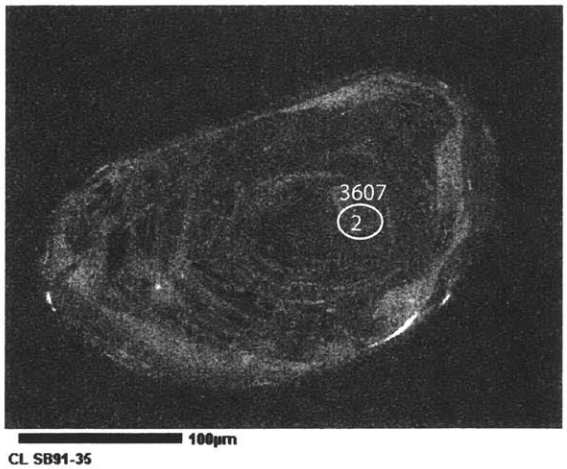

grain 6

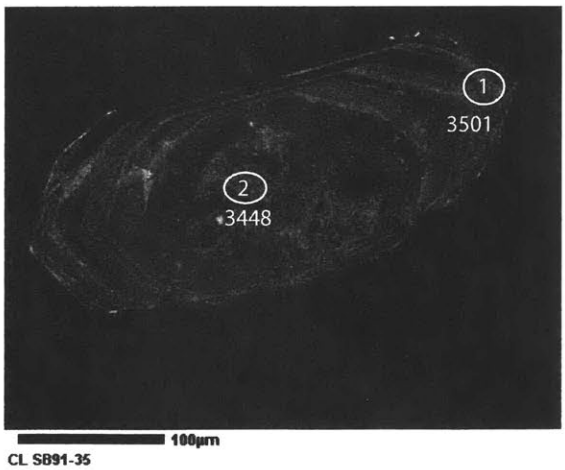

grain 15

SAB91-35 zircons

0	1	2	3	4	5	6		
15	14	13	12	11	10	9	8	7
STDS		s	p	p	s			
STDS		s	p	p	s			
16	17	18	19	20	21	22	23	24
29	28	27	26	25				

R.Safipour

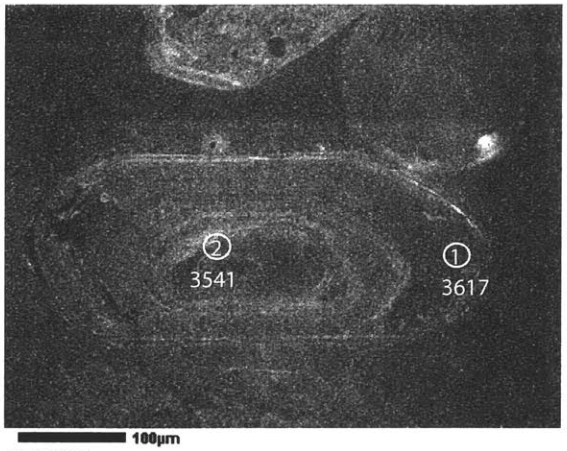

grain 17

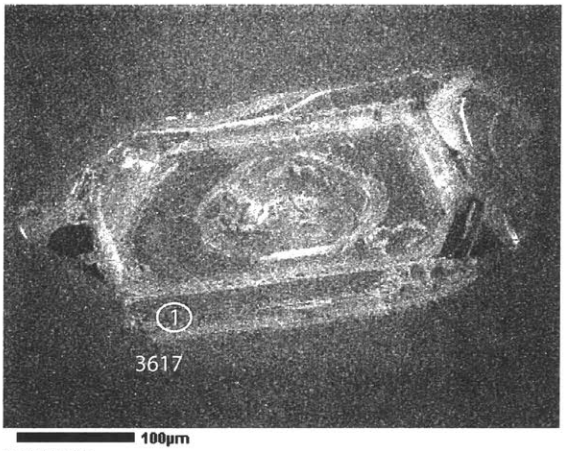

grain 29

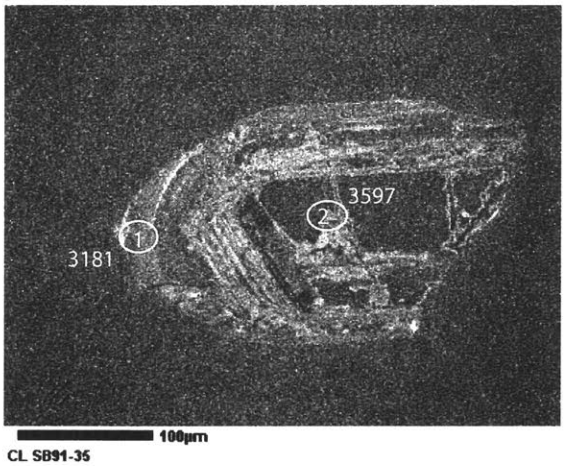

grain 19

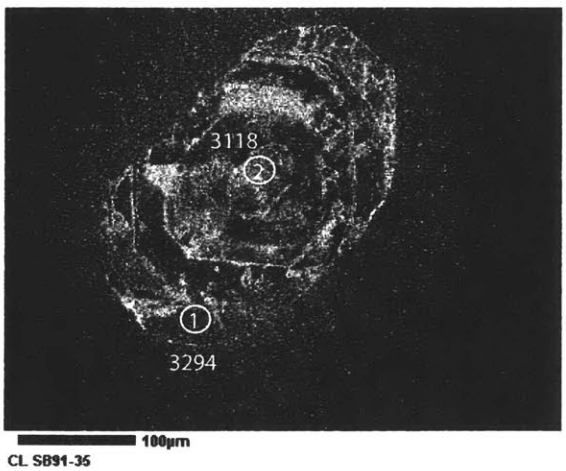

grain 25

SAB91-37-3 large zircons (non-annealed)

Grain Map

0 1 2 3
6 5 4

R.Safipour

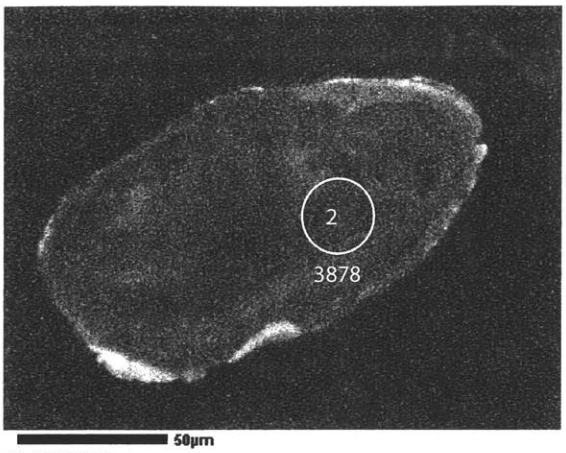

grain 0

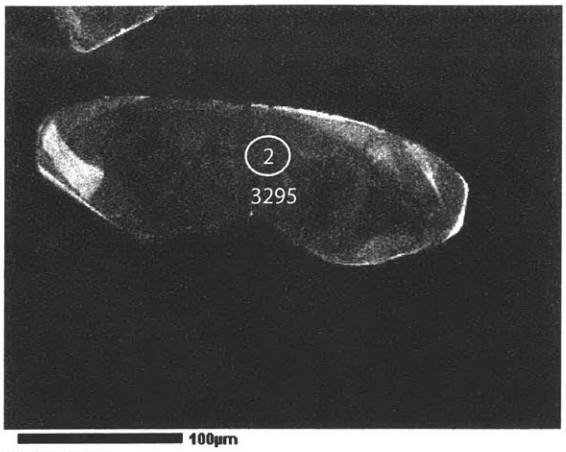

grain 4

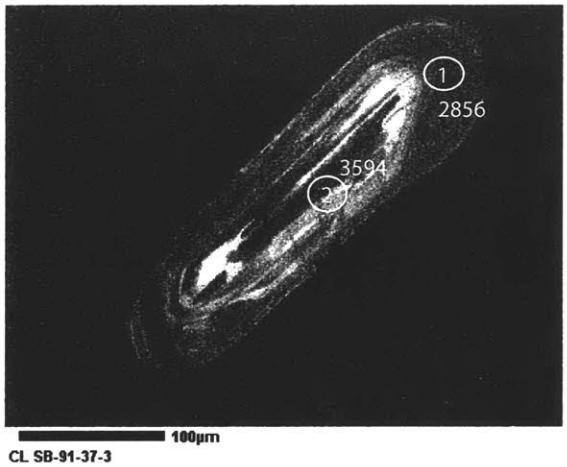

grain 1

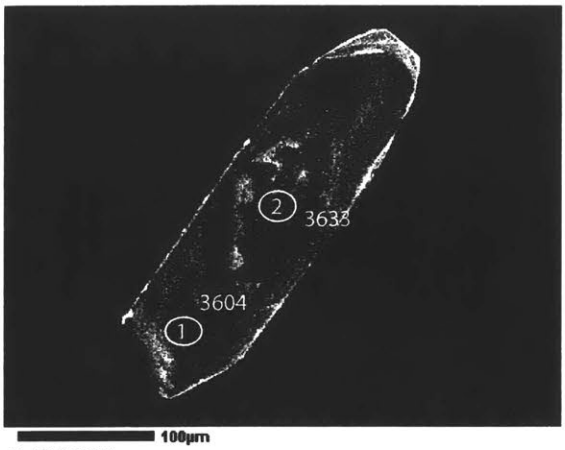

grain 5

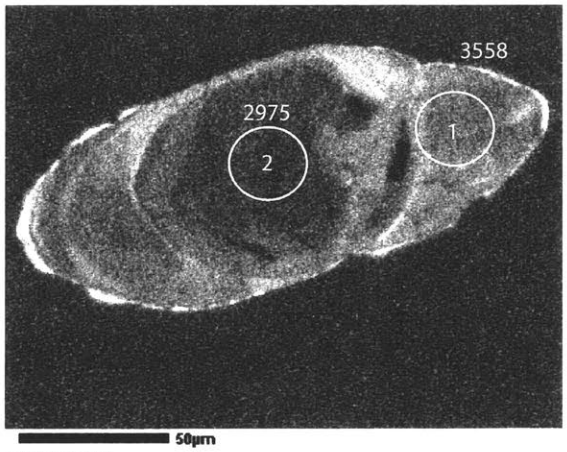

grain 2

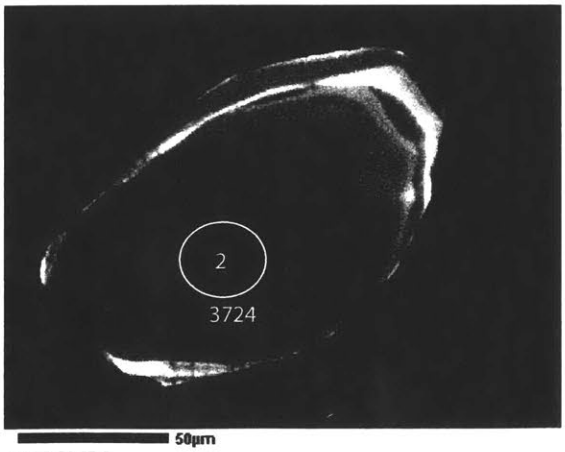

grain 6

SAB91-37-3 supersize zircons (non-annealed)

Grain Map

7 8 9
11 10

R.Safipour

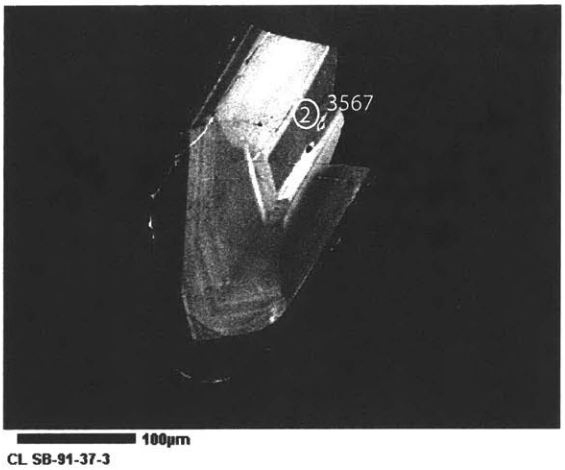

grain 7

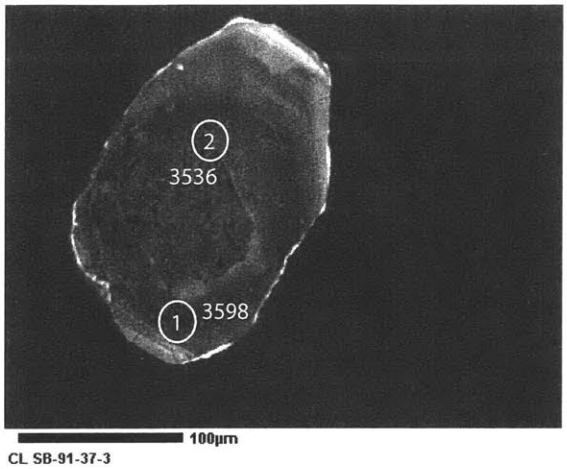

grain 10

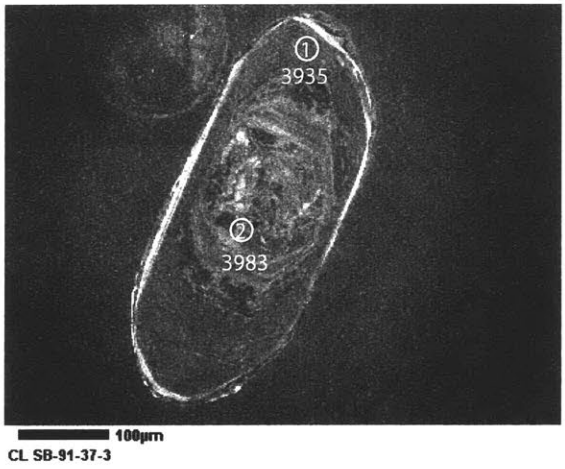

grain 8

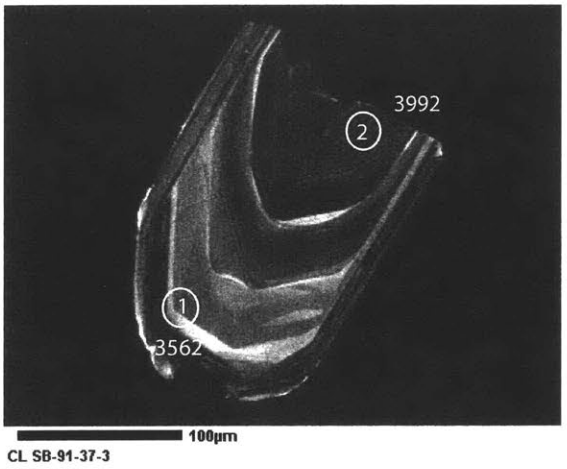

grain 11

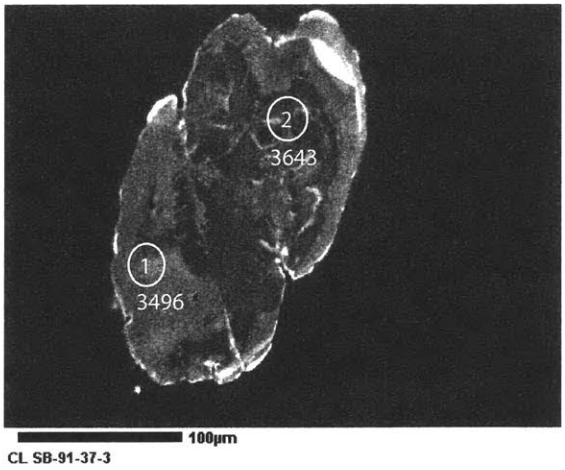

grain 9

SAB91-37-3 annealed zircons 0 1 2 3 4 5 6 R.Safipour
16 15 14 13 12 11 10 9 8 7
STDS
STDS
17 18 19 20 21 22 23 24 25 26
31 30 29 28 27

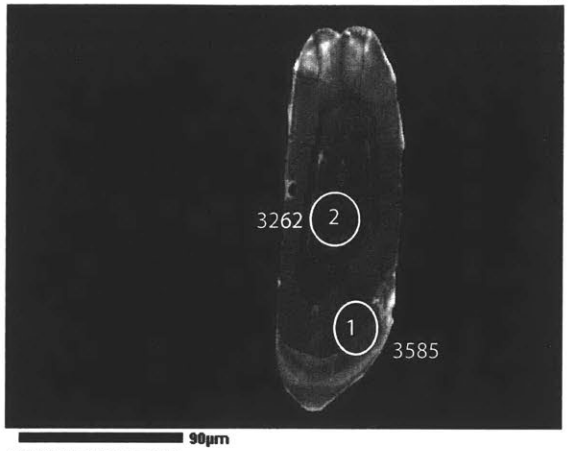

grain 0

grain 3

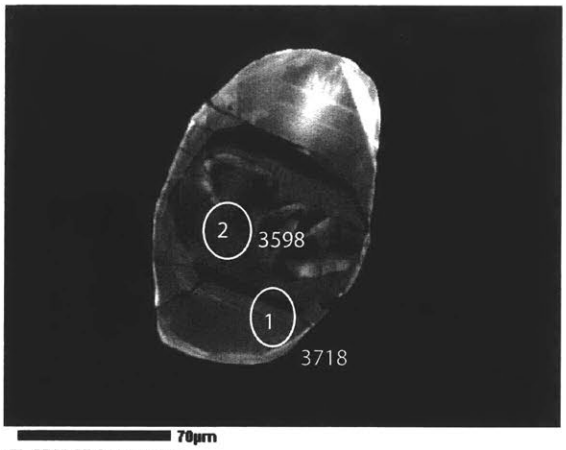

grain 1

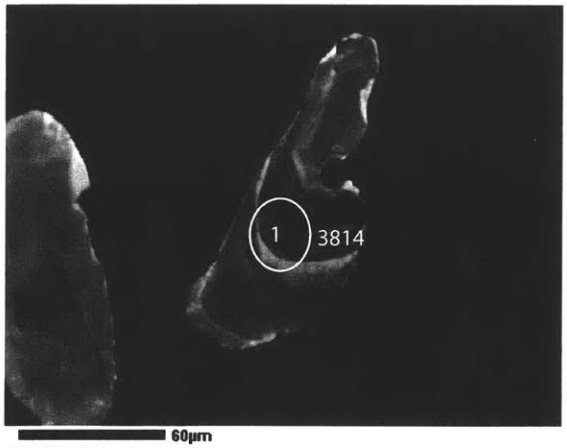

grain 5

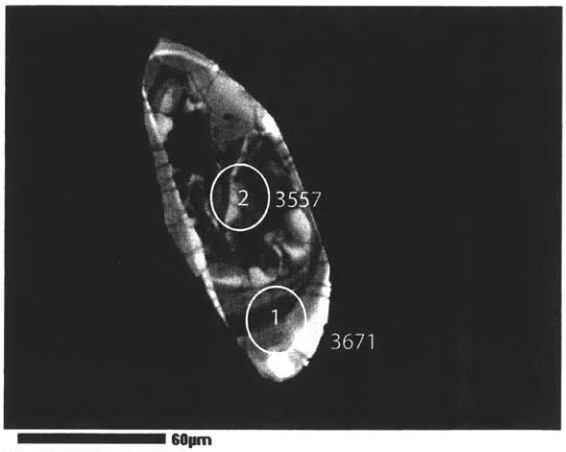

grain 2

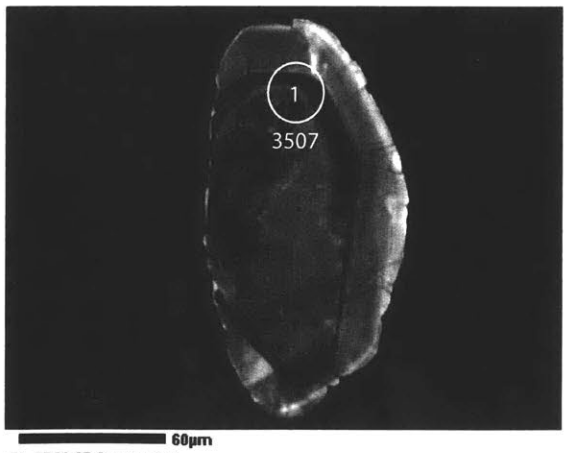

grain 7

SAB91-37-3 annealed zircons 0 1 2 3 4 5 6

16 15 14 13 12 11 10 9 8 7

STDS

STDS

17 18 19 20 21 22 23 24 25 26

31 30 29 28 27

R.Safipour

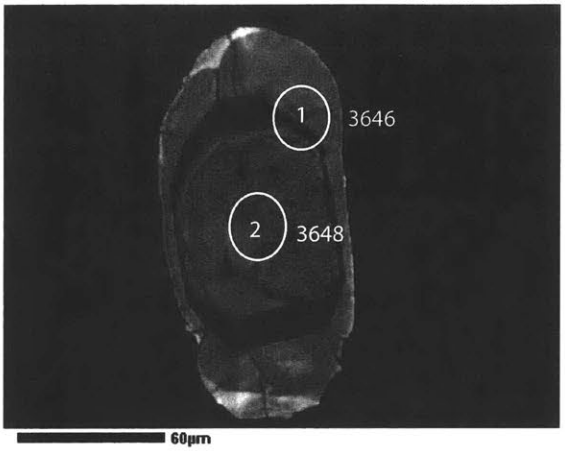

grain 8

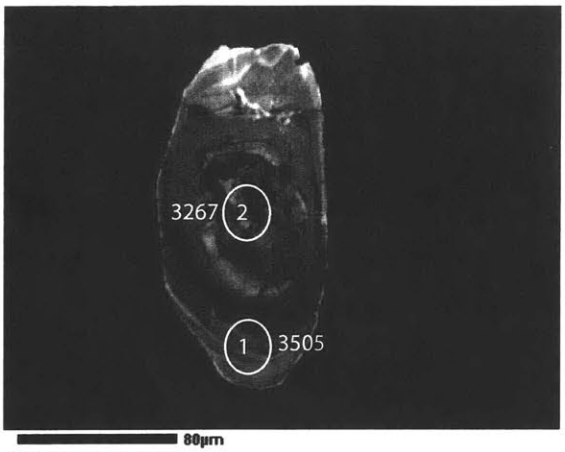

grain 12

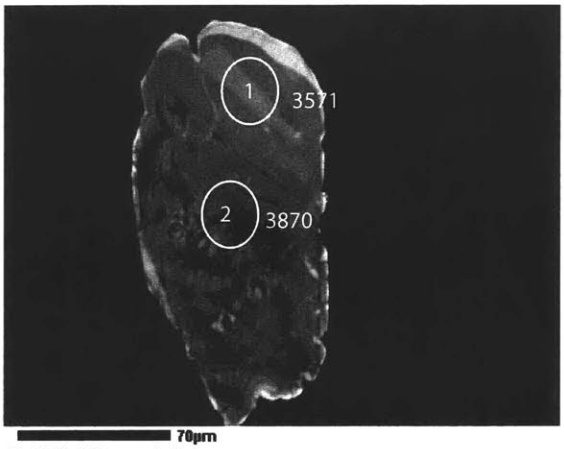

grain 10

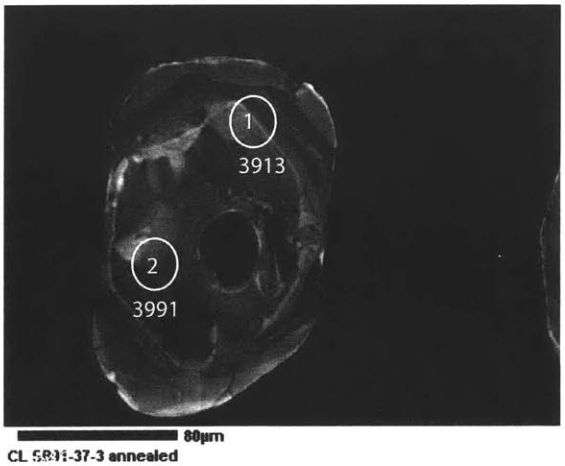

grain 13

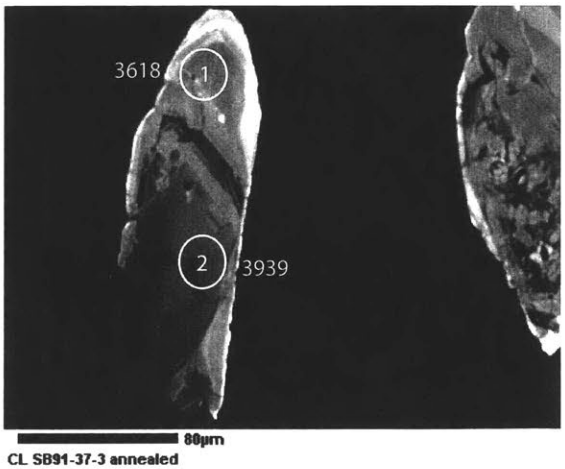

grain 11

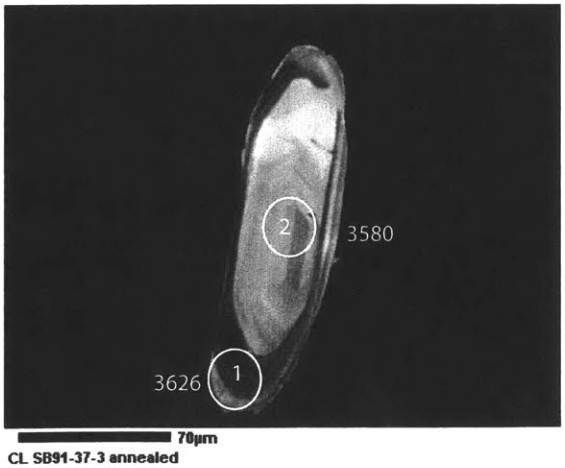

grain 14

SAB91-37-3 annealed zircons 0 1 2 3 4 5 6
16 15 14 13 12 11 10 9 8 7
STDS
STDS
17 18 19 20 21 22 23 24 25 26
31 30 29 28 27

R.Safipour

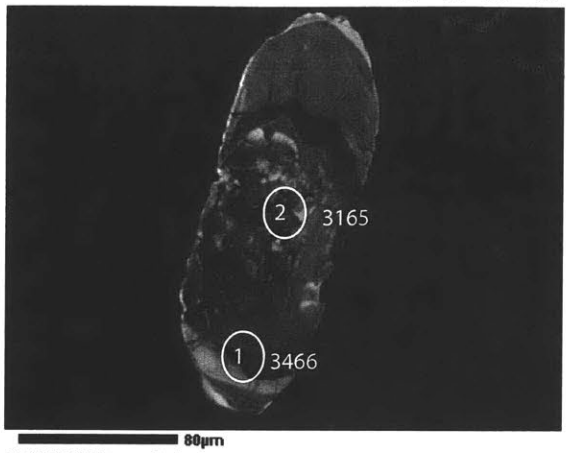

grain 15

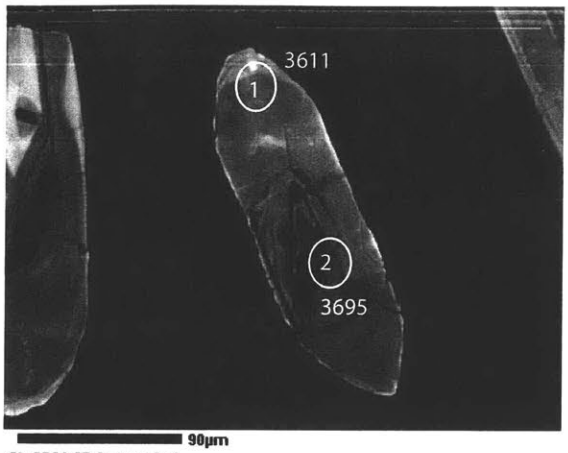

grain 18

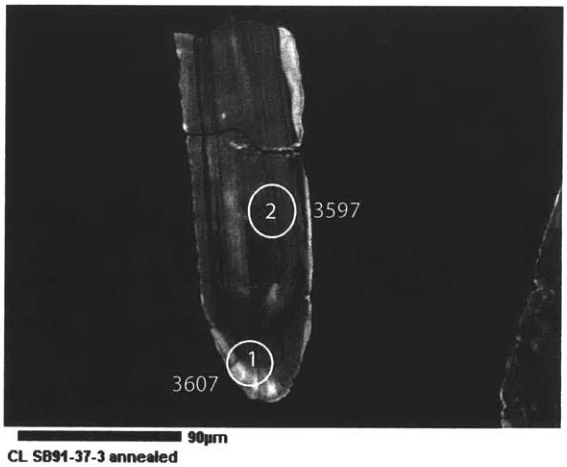

grain 16

grain 19

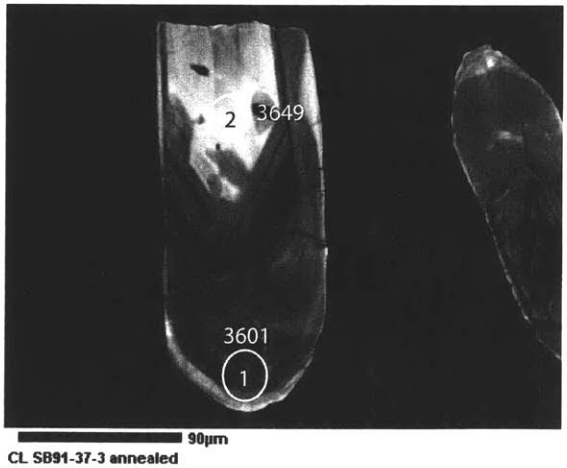

grain 17

grain 20

SAB91-37-3 annealed zircons 0 1 2 3 4 5 6 R.Safipour
16 15 14 13 12 11 10 9 8 7
STDS
STDS
17 18 19 20 21 22 23 24 25 26
31 30 29 28 27

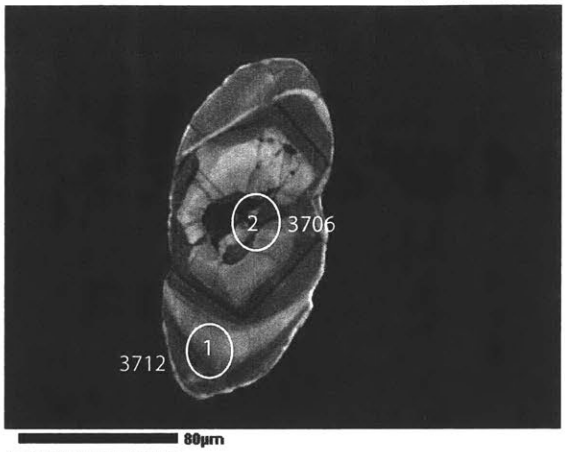

grain 21

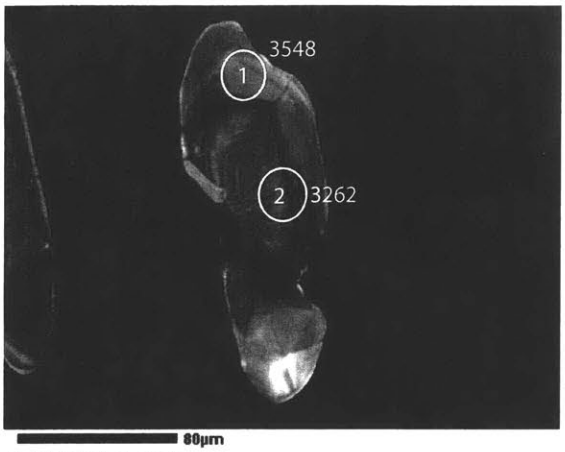

grain 24

grain 22

grain 25

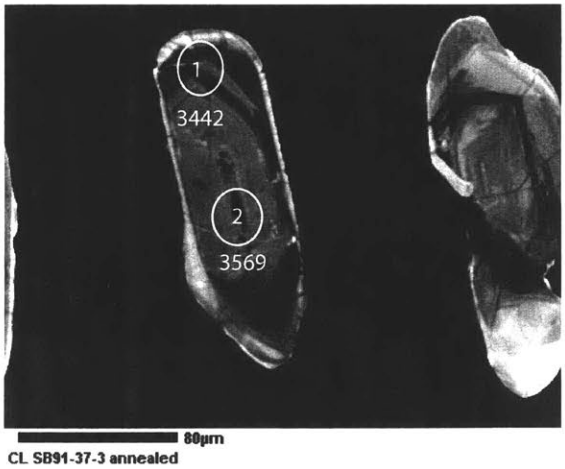

grain 23

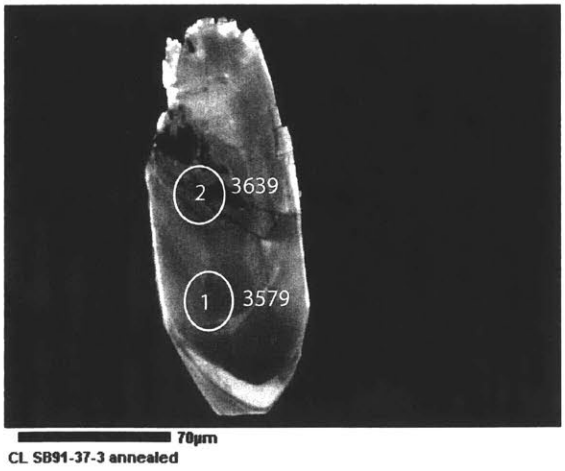

grain 26

SAB91-37-3 annealed zircons 0 1 2 3 4 5 6 R.Safipour
16 15 14 13 12 11 10 9 8 7
STDS
STDS
17 18 19 20 21 22 23 24 25 26
31 30 29 28 27

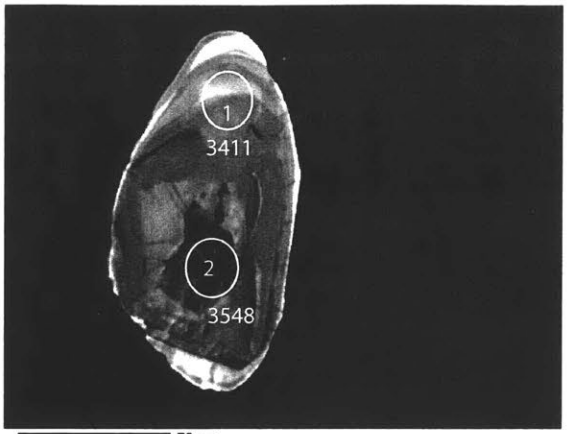

grain 27

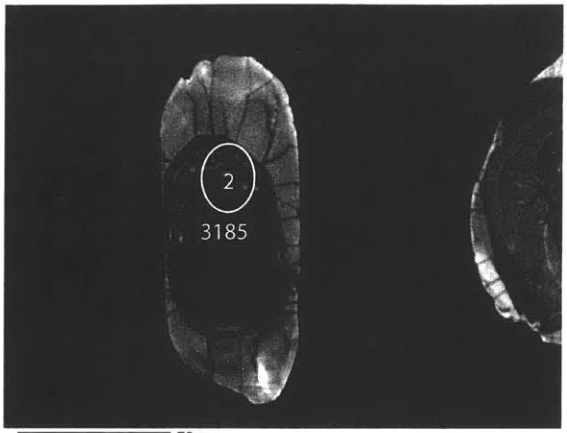

grain 30

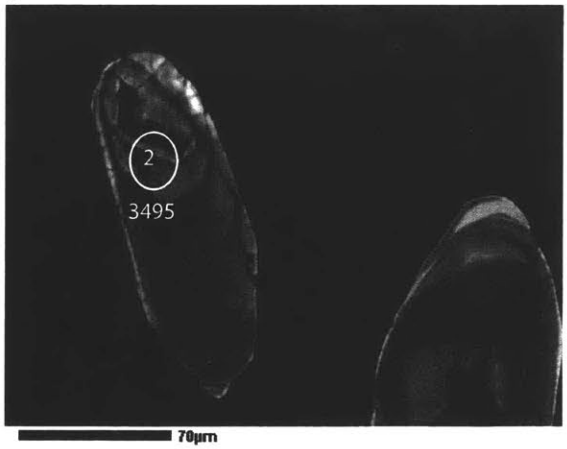

grain 28

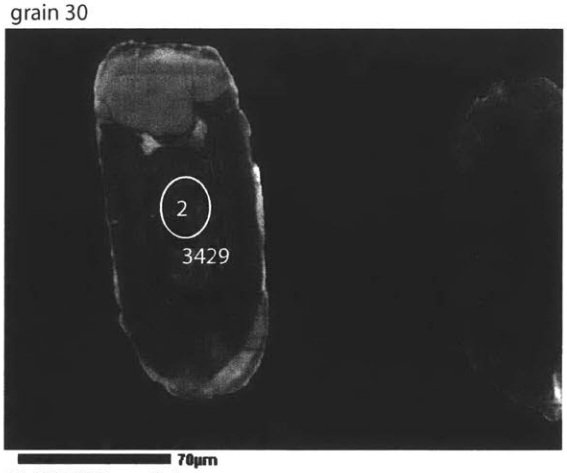

grain 31

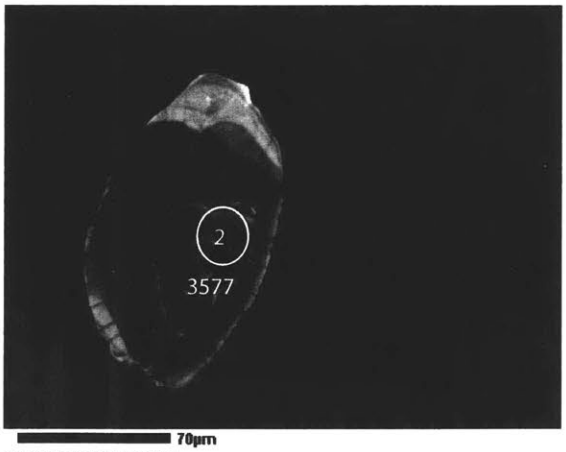

grain 29

SAB91-52 zircons

0	1	2	3	4	5			
STDS		s	s	p	p	s	s	
STDS				p	p			
14	13	12	11	10	9	8	7	6

R.Safipour

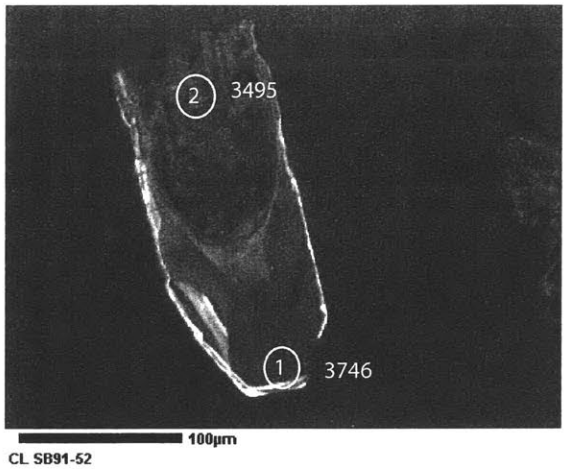

grain 1

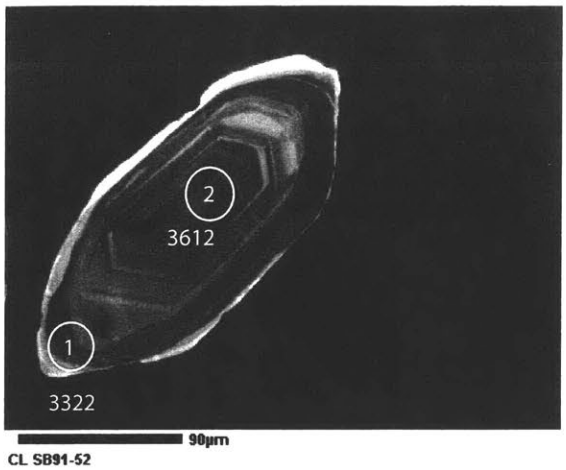

grain 8

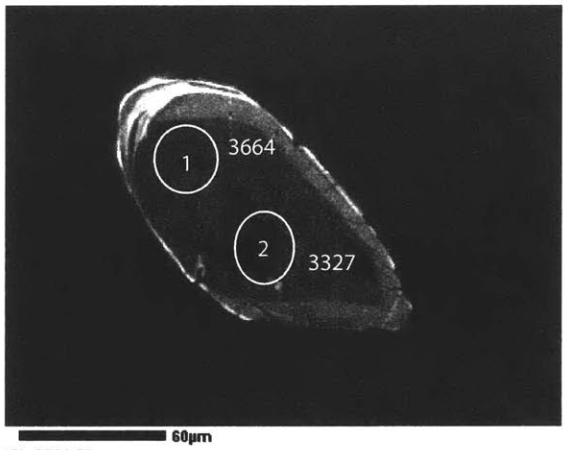

grain 4

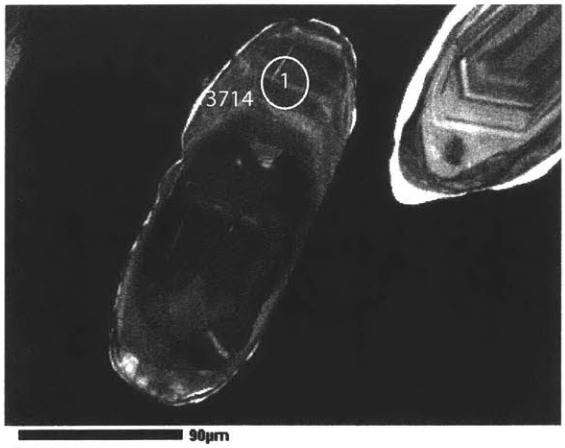

grain 9

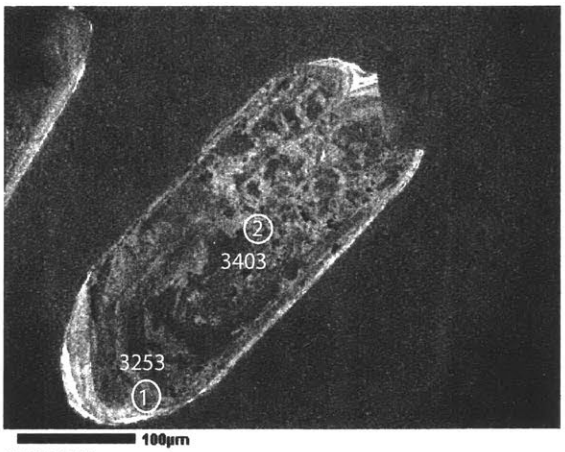

grain 6

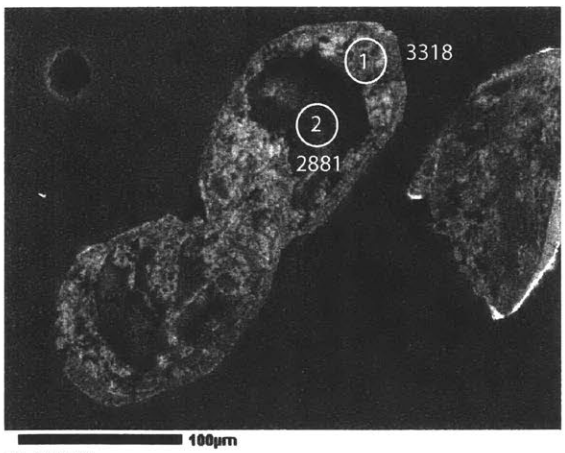

grain 13

SAB91-52 zircons

0	1	2	3	4	5			
STDS		s s	p	p	s s			
STDS			p	p				
14	13	12	11	10	9	8	7	6

R.Safipour

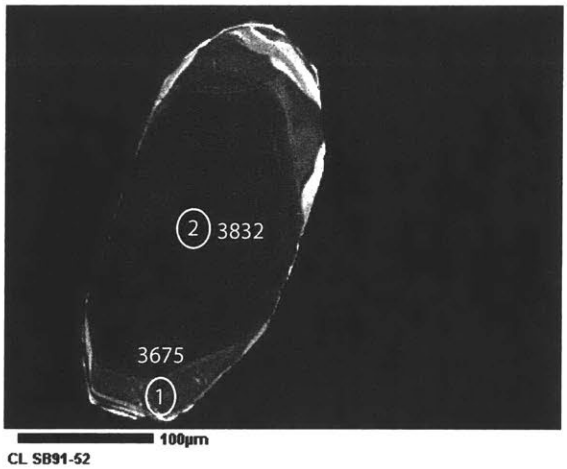

grain 14

SAB91-53 zircons

0	1	2	3	4	5	6		
15	14	13	12	11	10	9	8	7
STDS		s	p	p	s			
STDS		s	p	p	s			
16	17	18	19	20	21	22	23	24
29	28	27	26	25				

R.Safipour

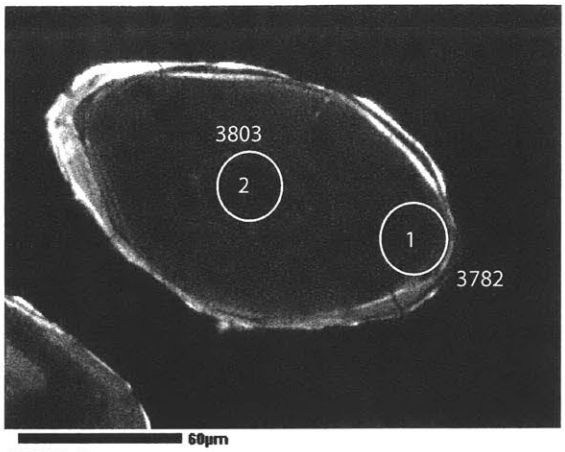

grain 10

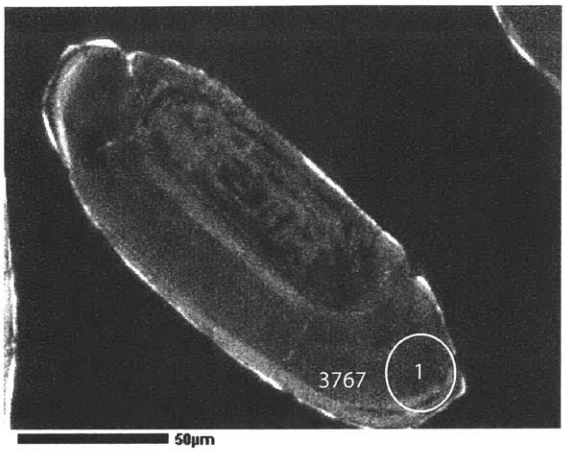

grain 17

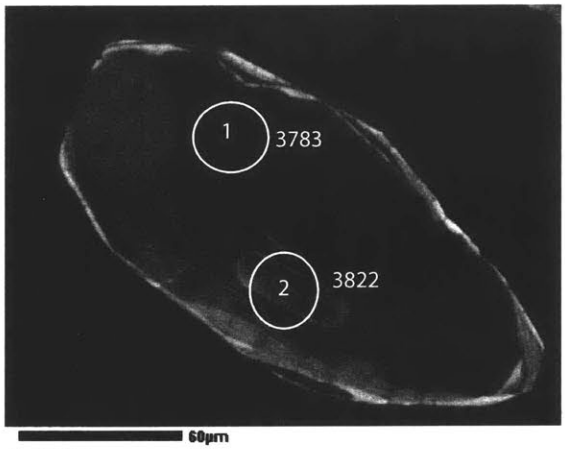

grain 12

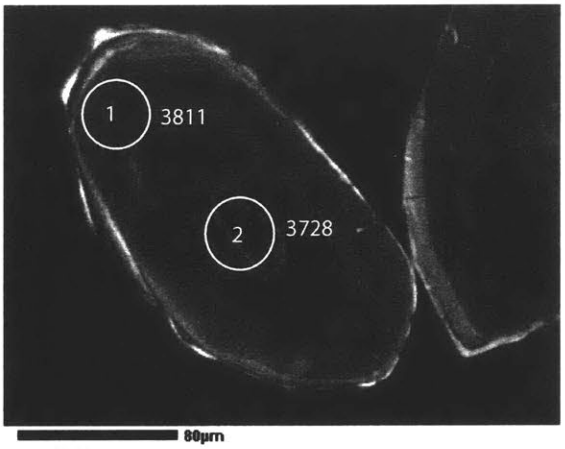

grain 19

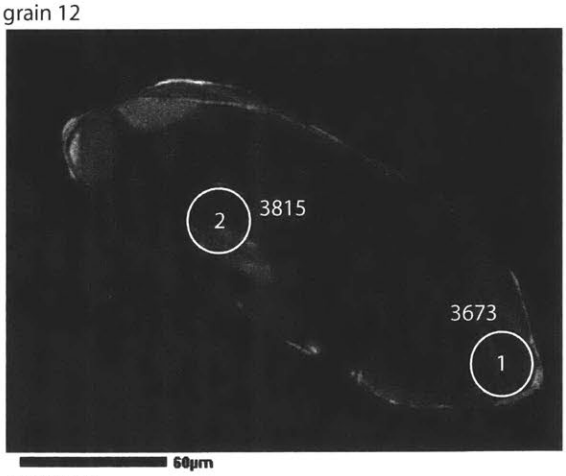

grain 15

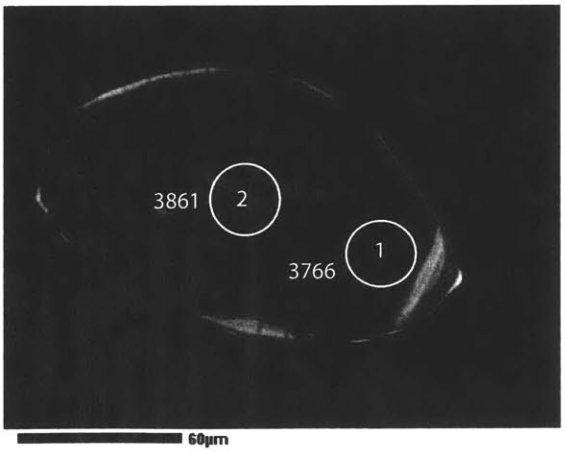

grain 22

SAB91-53 zircons

0	1	2	3	4	5	6		
15	14	13	12	11	10	9	8	7
STDS		s	p	p	s			
STDS		s	p	p	s			
16	17	18	19	20	21	22	23	24
29	28	27	26	25				

R.Safipour

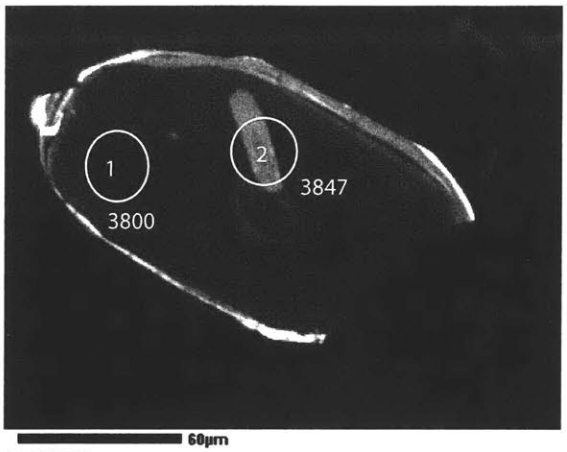

grain 23

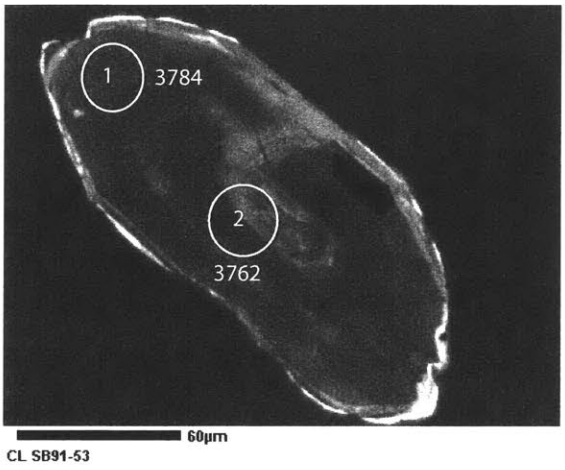

grain 24

SAB91-54 zircons

0 x 1 x 2 3 large grains
8 7 6 5 4 15 16 17 18
STD STD STD
9 10 x 11 x 23 22 21 20 19
14 13 12

R.Safipour

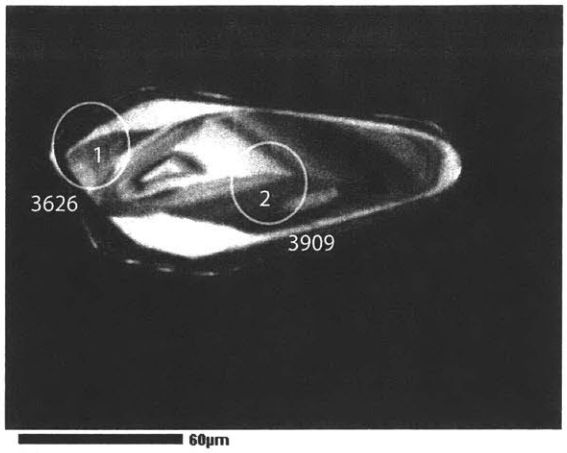

grain 5

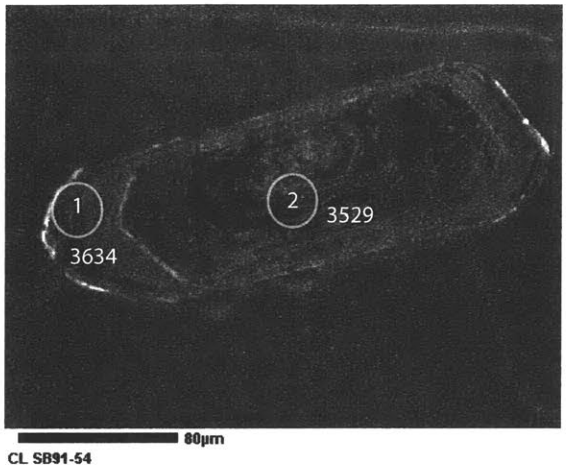

grain 9

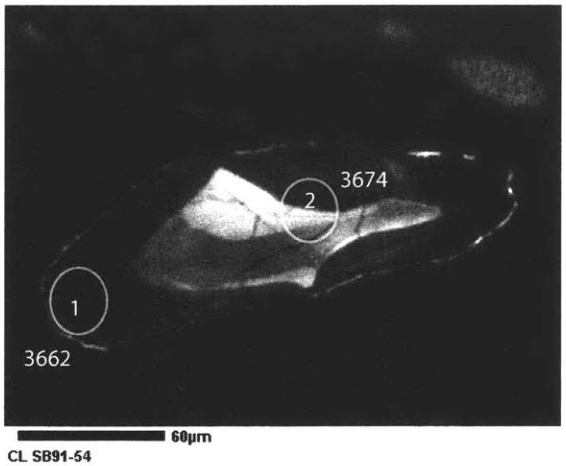

grain 7

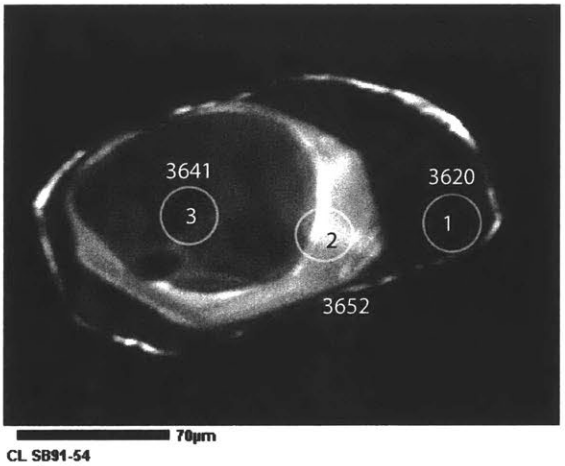

grain 15

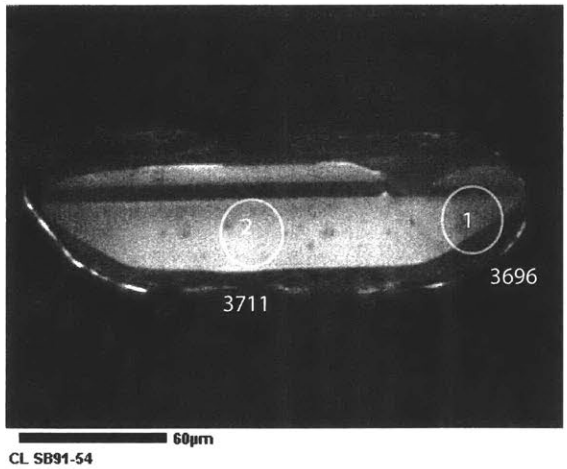

grain 8

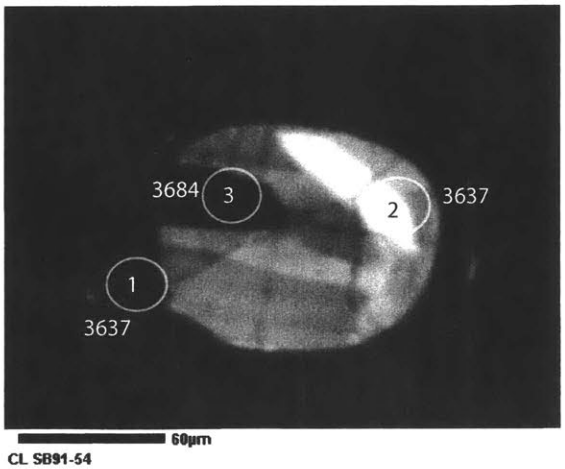

grain 17

SAB91-54 zircons

0 x 1 x 2 3
8 7 6 5 4
STD STD
9 10 x 11 x
14 13 12

large grains
15 16 17 18
STD STD
23 22 21 20 19

R.Safipour

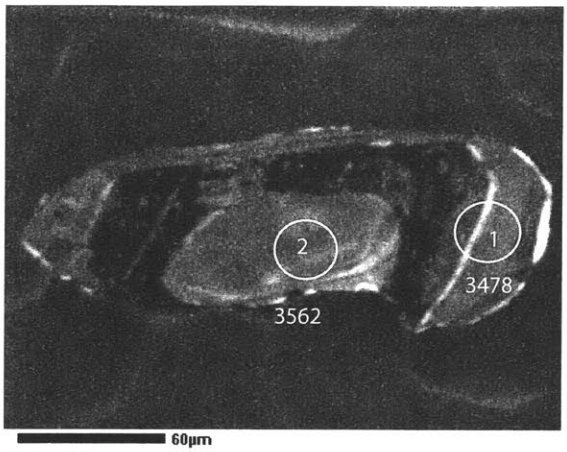

grain 18

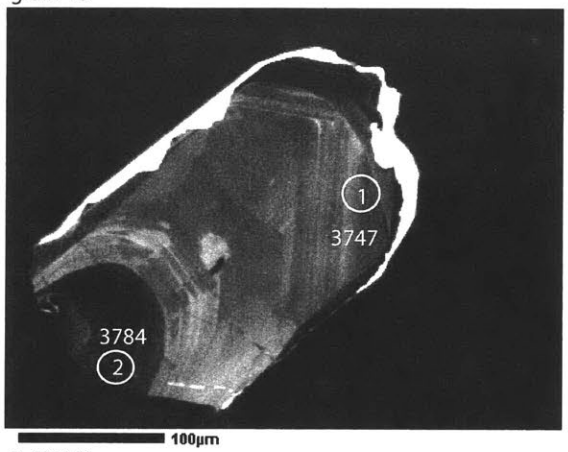

grain 22

SAB91-62 zircons

0	1	2	3	4	5	6				
17	16	15	14	13	12	11	10	9	8	7
18	19	20	21	22	23	24	25	26	27	28
STDS		s	s	P	P	s	s			
STDS				P	P					
39	38	37	36	35	34	33	32	31	30	29
40	41	42	43	44	45	46	47	48	49	50
59	58	57	56	55	54	53	52	51		

R.Safipour

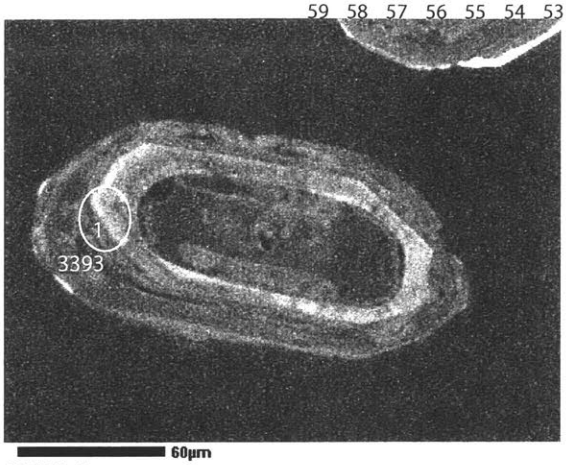

grain 1

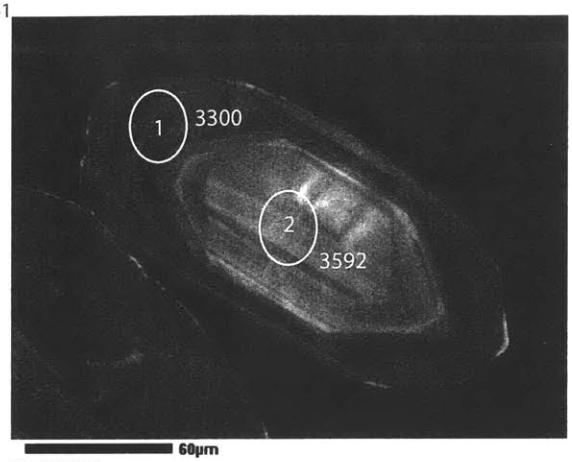

grain 13

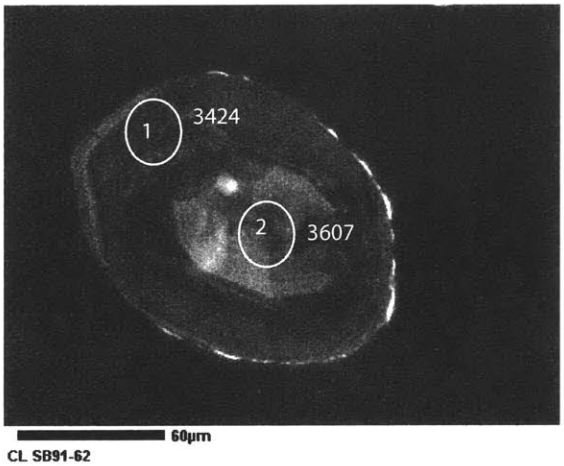

grain 4

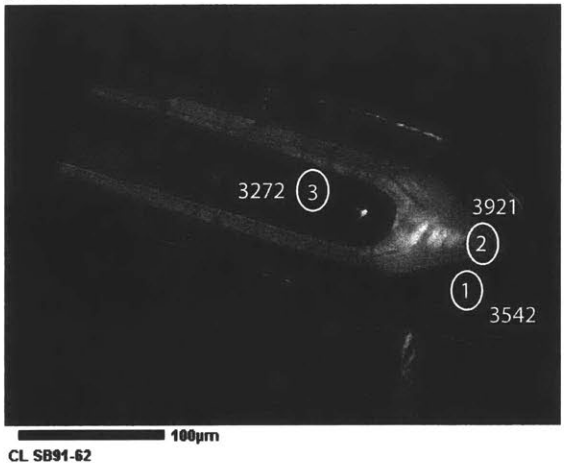

grain 30

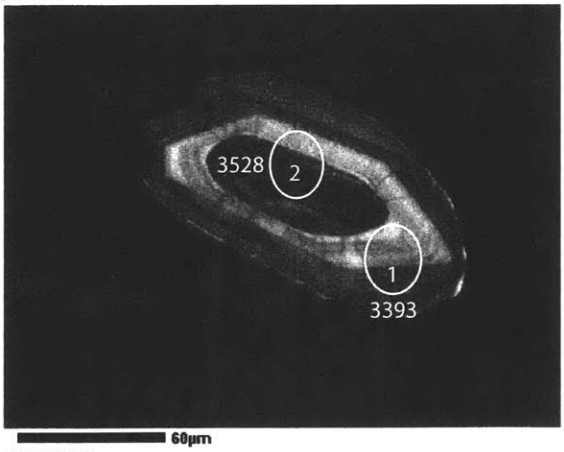

grain 7

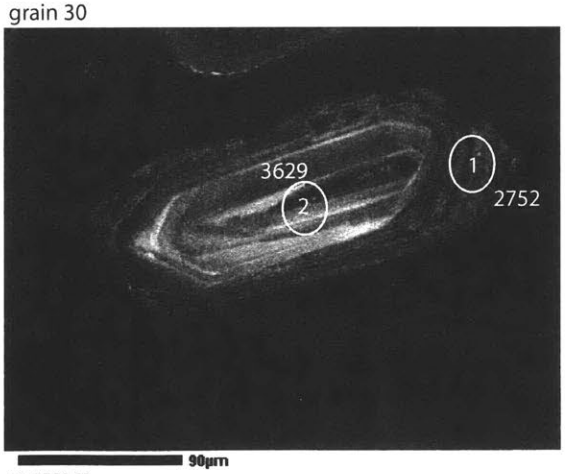

grain 36

SAB91-62 zircons

0	1	2	3	4	5	6				
17	16	15	14	13	12	11	10	9	8	7
18	19	20	21	22	23	24	25	26	27	28
STDS		s	s	P	P		s	s		
STDS				P	P					
39	38	37	36	35	34	33	32	31	30	29
40	41	42	43	44	45	46	47	48	49	50
59	58	57	56	55	54	53	52	51		

R.Safipour

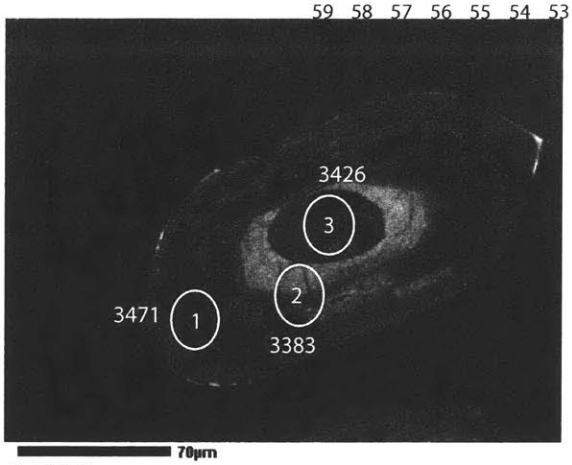

grain 37

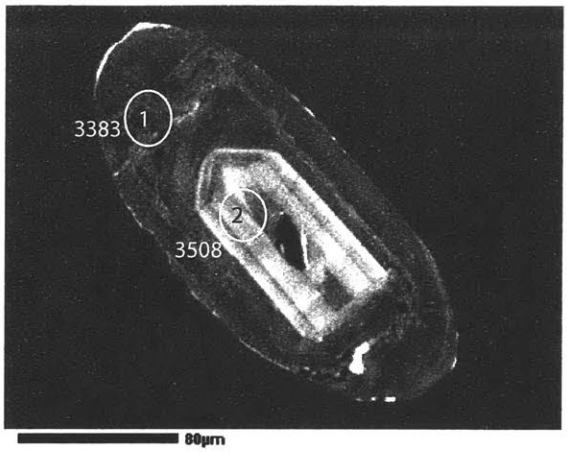

grain 53

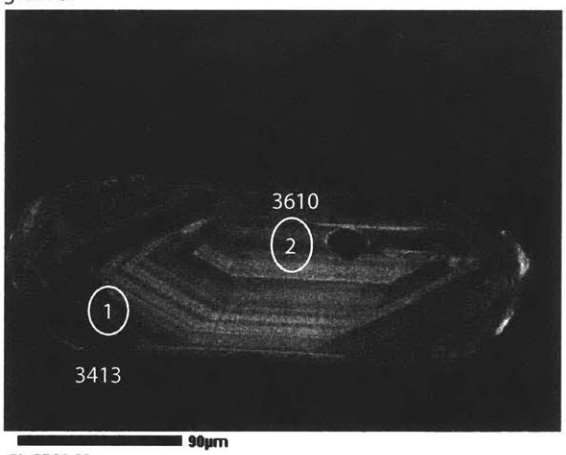

grain 39

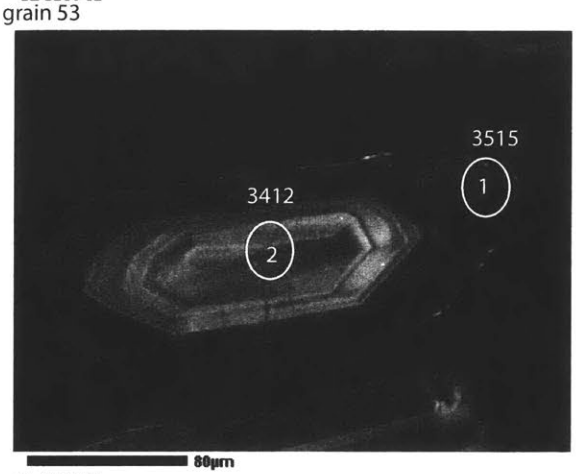

grain 58

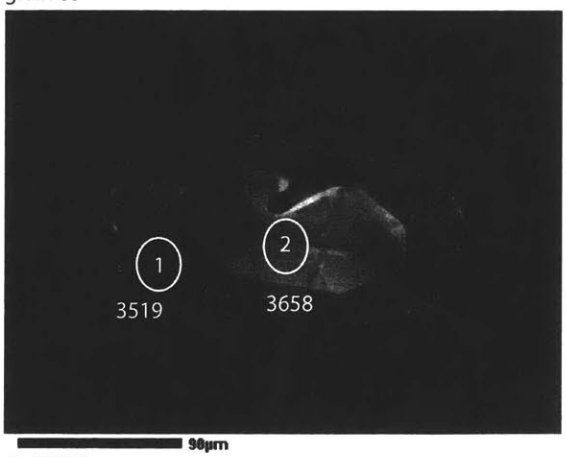

grain 46

SAB91-65 annealed zircons

R.Safipour

0	1	2	3	4	5						
17	16	15	14	13	12	11	10	9	8	7	6
18	19	20	21	22	23	24	25	26	27	28	29
STDS											
STDS											
41	40	39	38	37	36	35	34	33	32	31	30
42	43	44	45	46	47	48	49	50	X	51	52

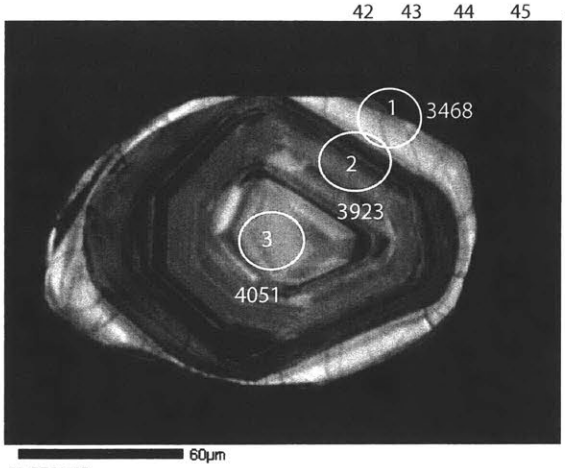

grain 0

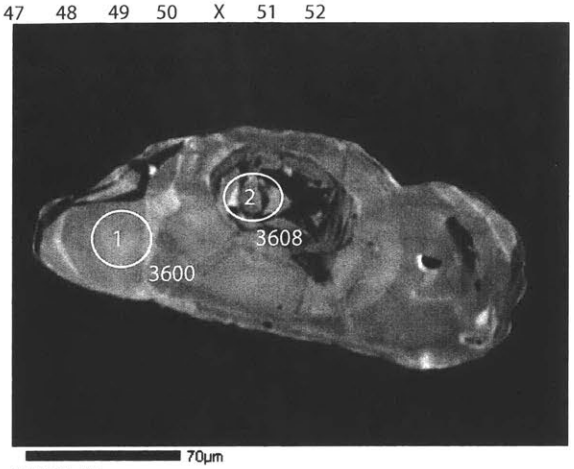

grain 4

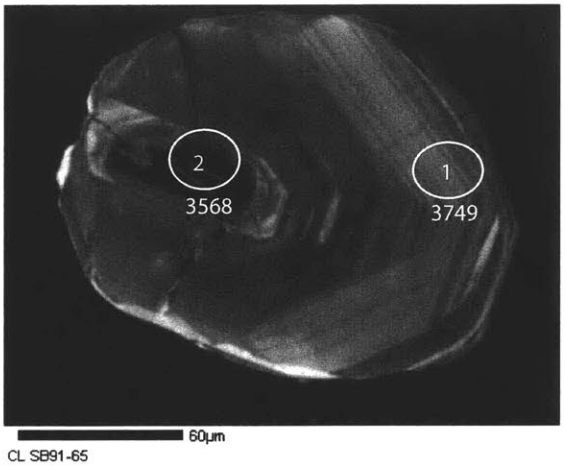

grain 1

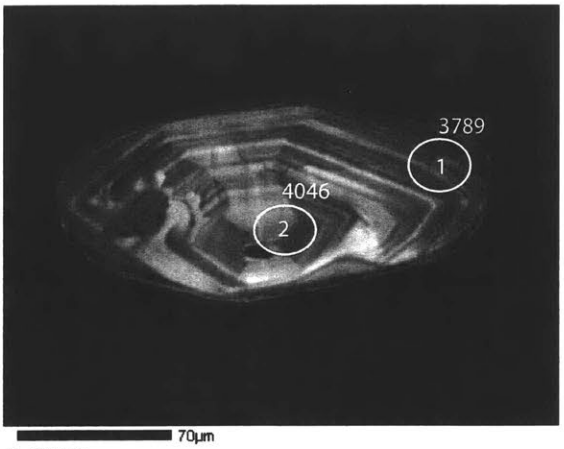

grain 5

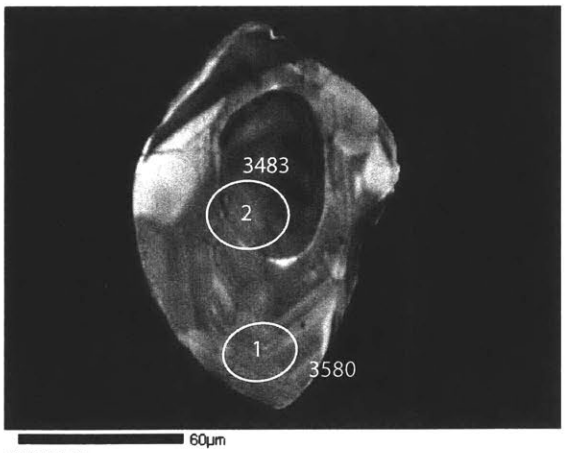

grain 2

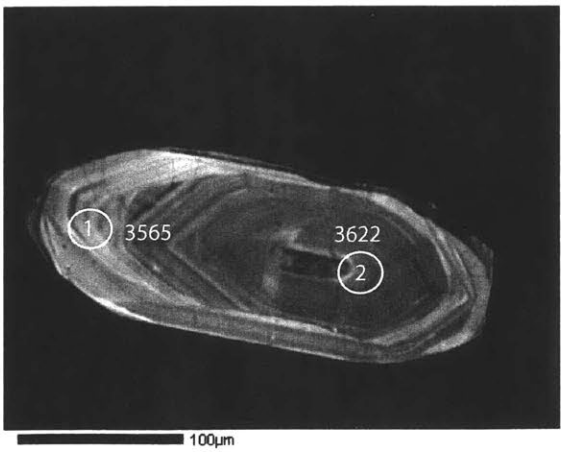

grain 7

SAB91-65 annealed zircons

R.Safipour

0	1	2	3	4	5						
17	16	15	14	13	12	11	10	9	8	7	6
18	19	20	21	22	23	24	25	26	27	28	29
STDS											
STDS											
41	40	39	38	37	36	35	34	33	32	31	30
42	43	44	45	46	47	48	49	50	X	51	52

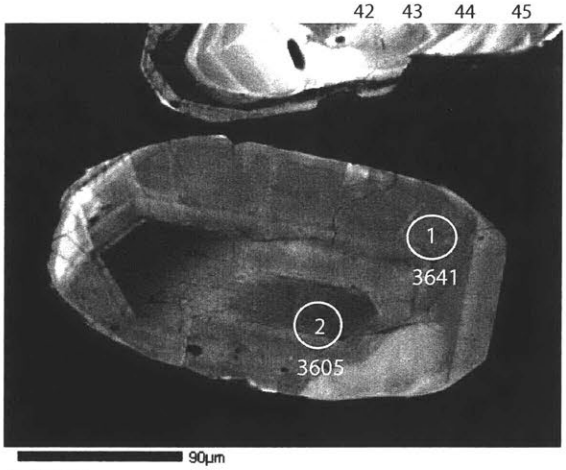

grain 13

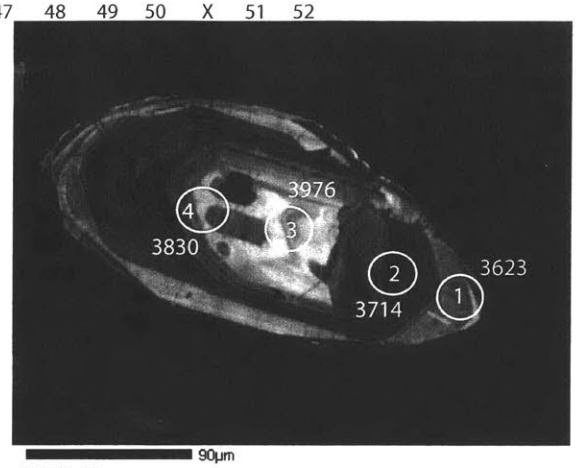

grain 32

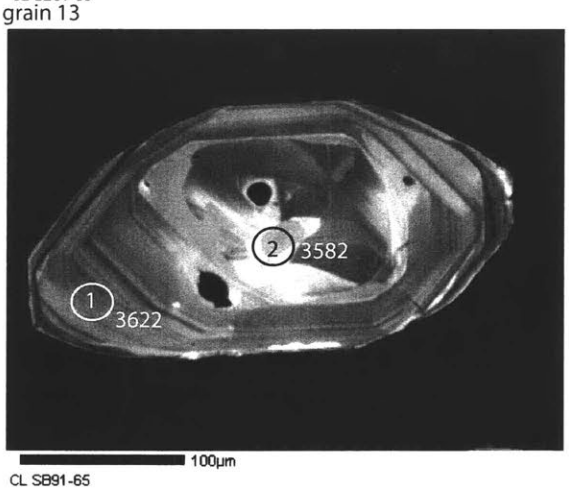

grain 16

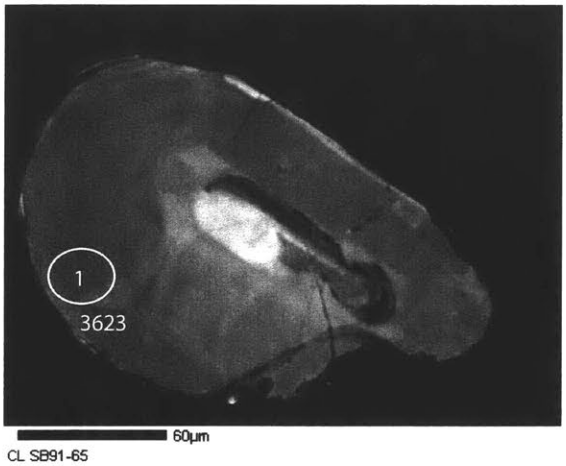

grain 36

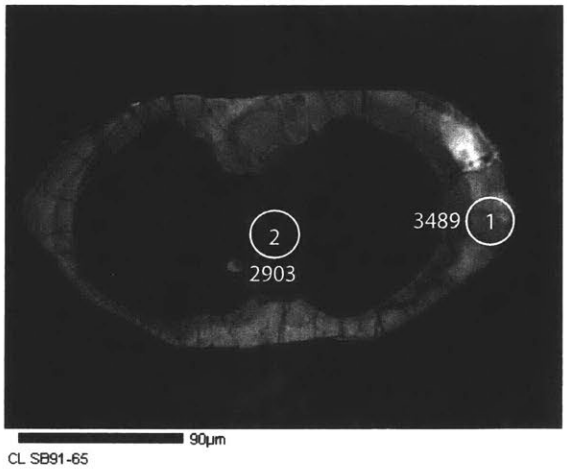

grain 28

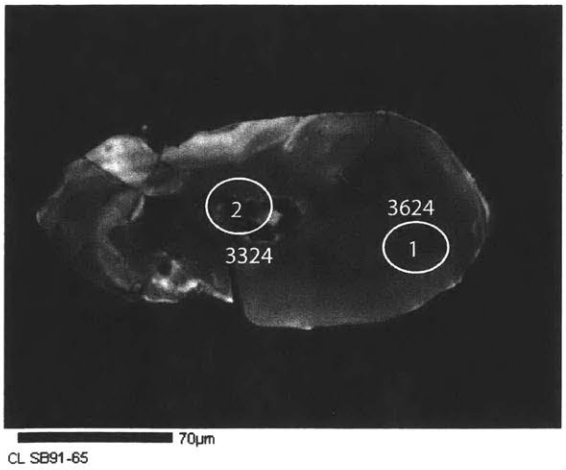

grain 52

SAB91-79 zircons

	0	1	2	3	4	5	
13	12	11	10	9	8	7	6
STDS		s	p	p	s		
STDS		s	p	p	s		
14	15	16	17	18	19	20	21
26	25	24	23	22			

R.Safipour

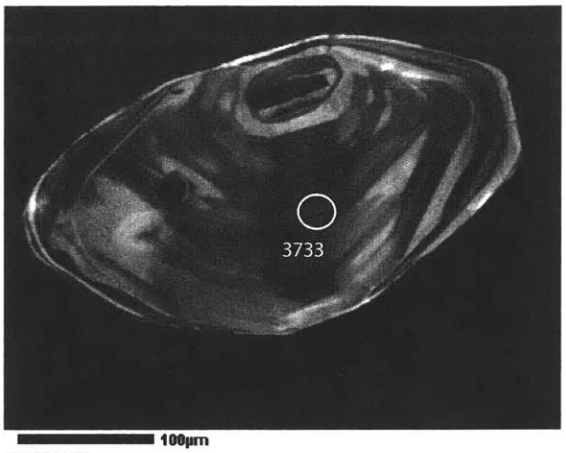

grain 1

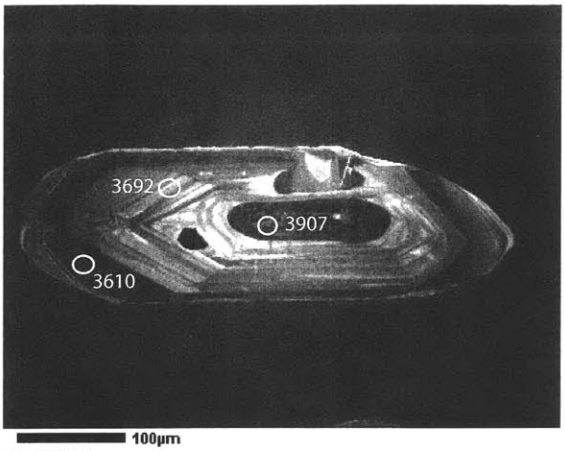

grain 8

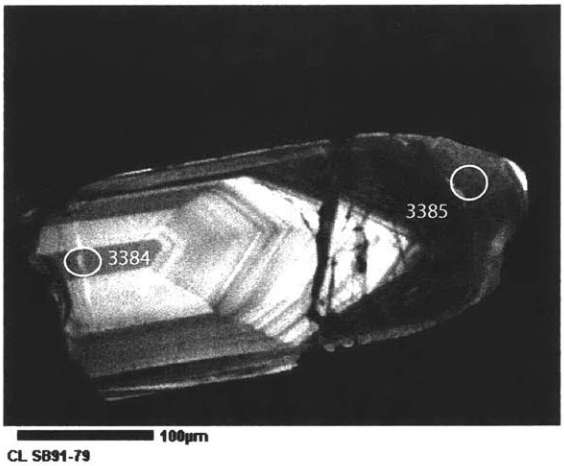

grain 3

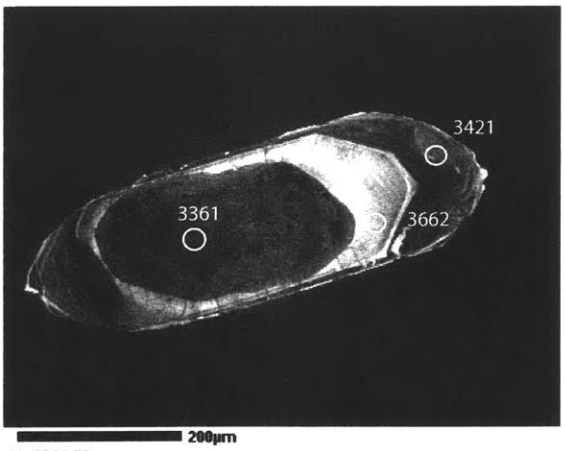

grain 9

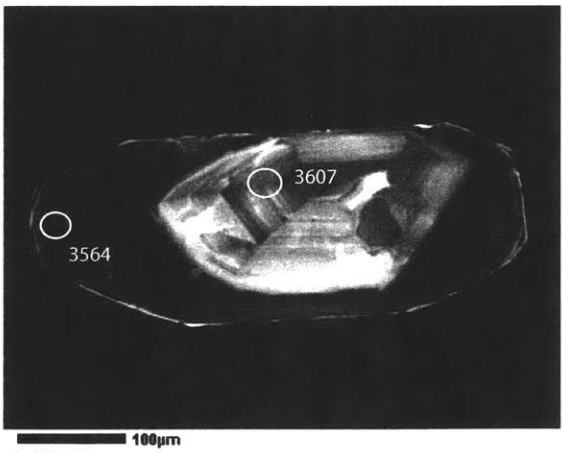

grain 4

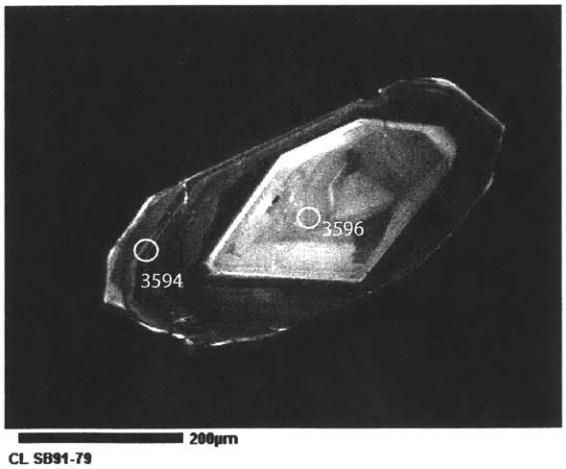

grain 10

SAB91-79 zircons

	0	1	2	3	4	5	
13	12	11	10	9	8	7	6
STDS		s	p	p	s		
STDS		s	p	p	s		
14	15	16	17	18	19	20	21
26	25	24	23	22			

R.Safipour

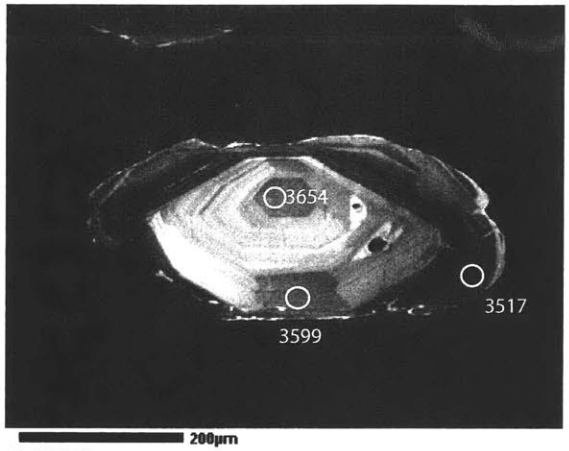

grain 11

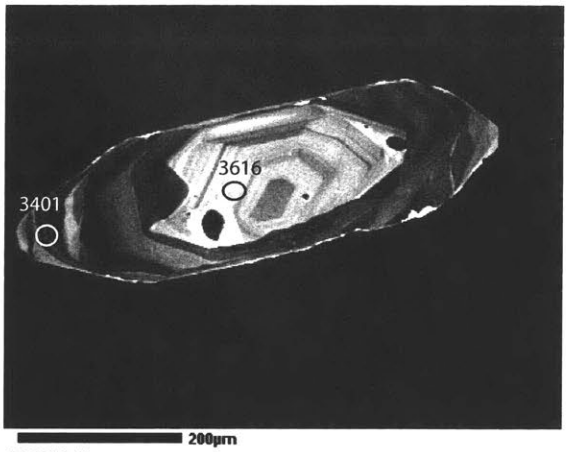

grain 14

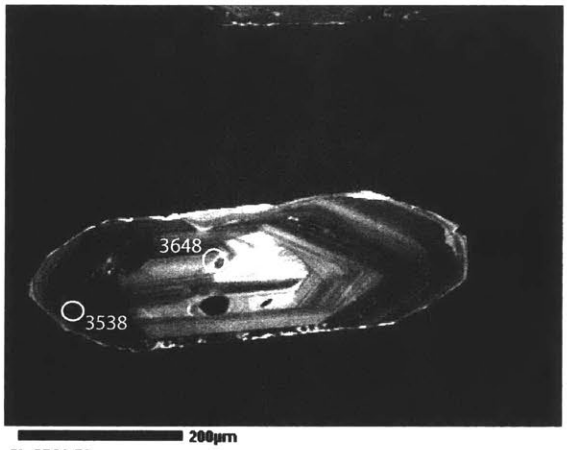

grain 12

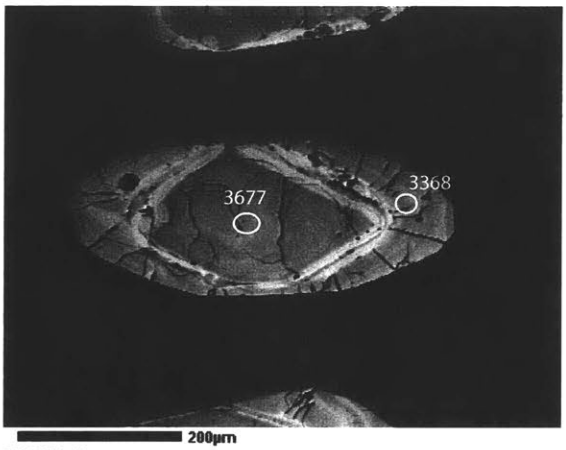

grain 15

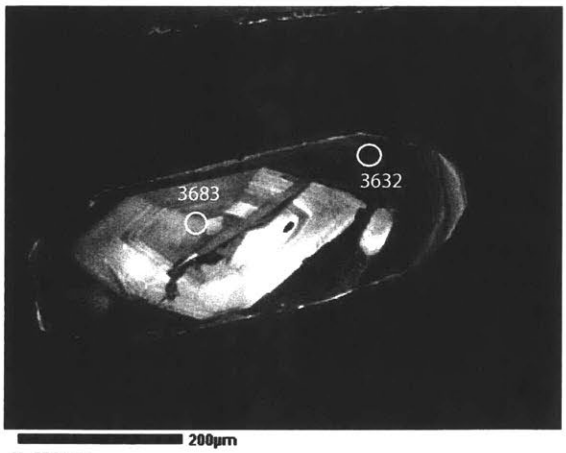

grain 13

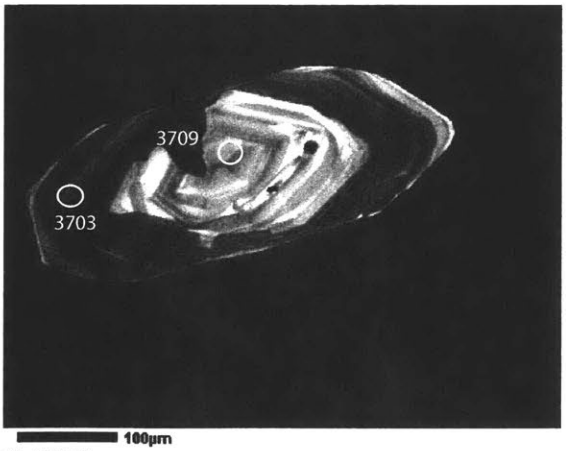

grain 17

SAB91-79 zircons

R.Safipour

	0	1	2	3	4	5	
13	12	11	10	9	8	7	6
STDS		s	p	p	s		
STDS		s	p	p	s		
14	15	16	17	18	19	20	21
26	25	24	23	22			

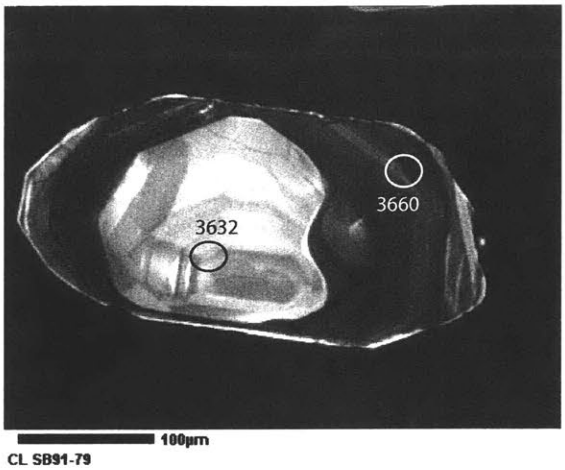

grain 24

SAB94-77 zircons

Grain Map

11	10	9	8	7	6	5	4	3	2	1	0
12	13	14	15	16	17	18	19	20	21	22	23
33	32	31	30	29	28	27	26	25	24		

R.Safipour

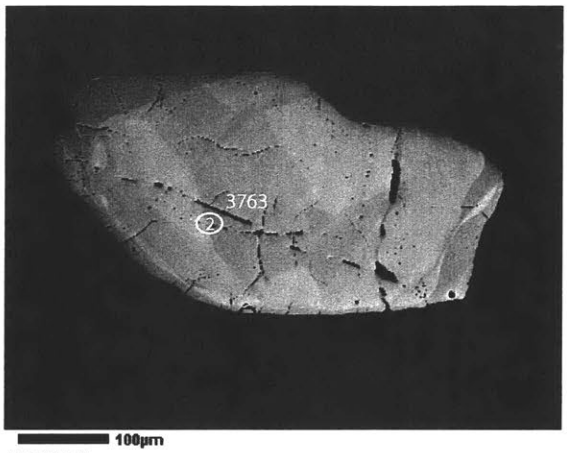

grain 0

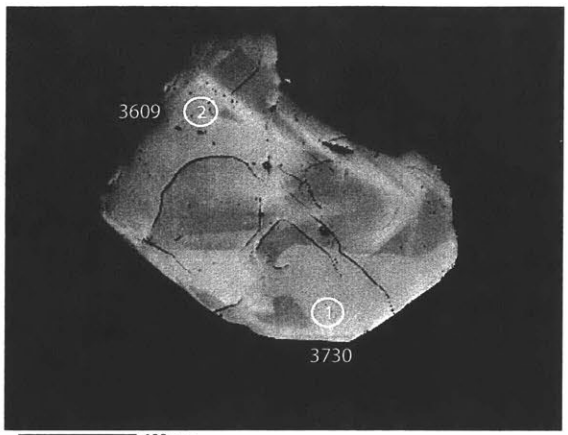

grain 13

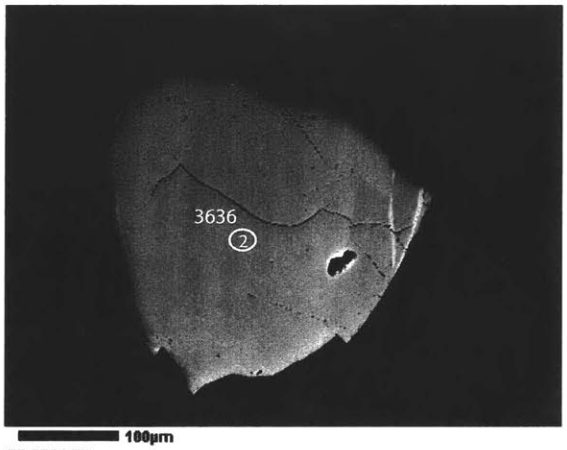

grain 2

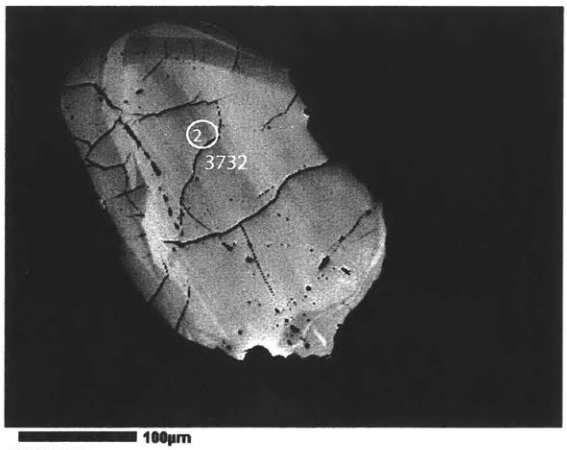

grain 14

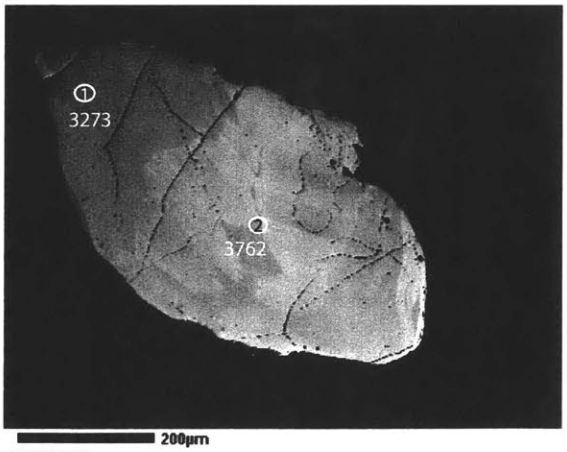

grain 12

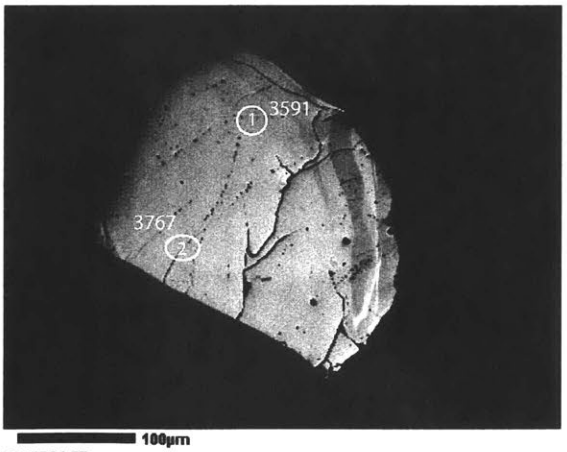

grain 15

SAB94-77 zircons

Grain Map

11	10	9	8	7	6	5	4	3	2	1	0
12	13	14	15	16	17	18	19	20	21	22	23
33	32	31	30	29	28	27	26	25	24		

R.Safipour

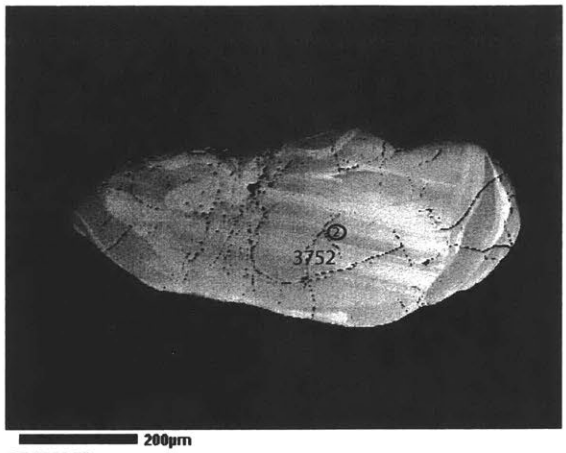

grain 17

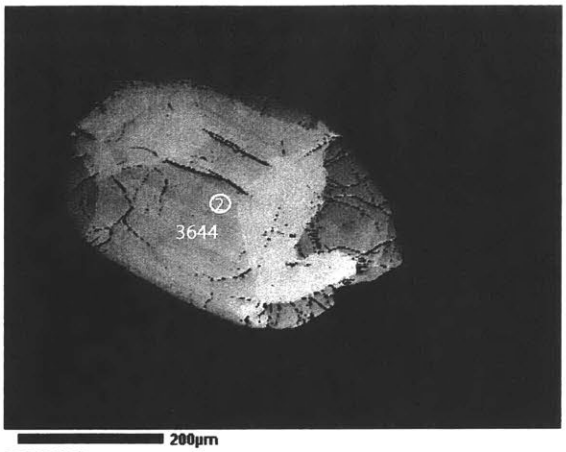

grain 25

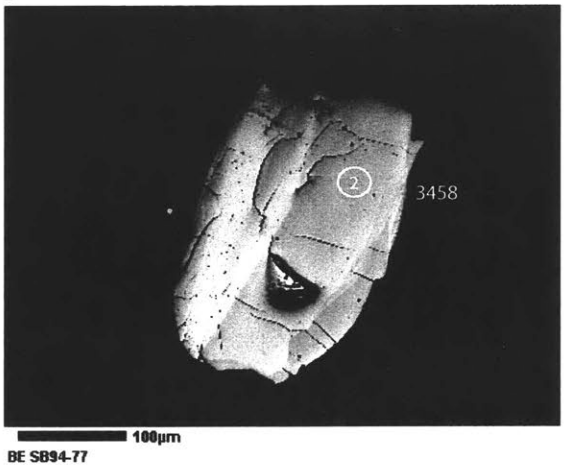

grain 18

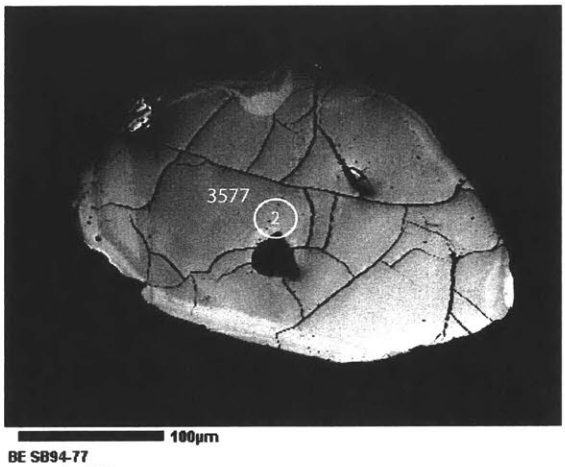

grain 26

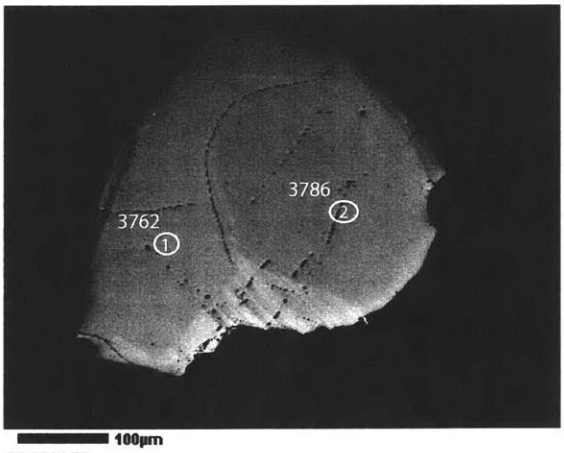

grain 24

SAB94-134 annealed zircons

0	1	2	3	4	5	6		
15	14	13	12	11	10	9	8	7
STDS		x	p	p	s			
STDS		s	p	p	s			
16	17	18	19	20	21	22	23	24
28	27	26	25					

R.Safipour

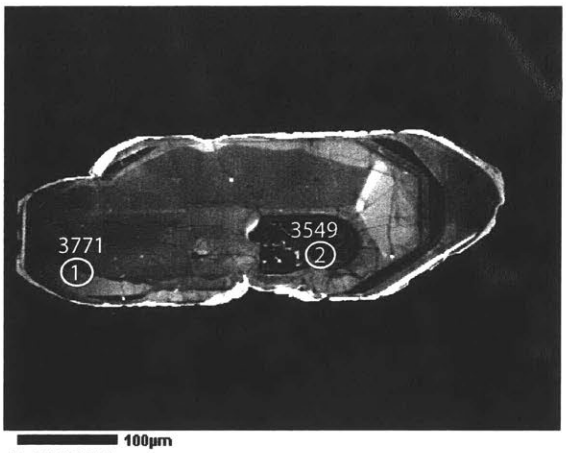

grain 0

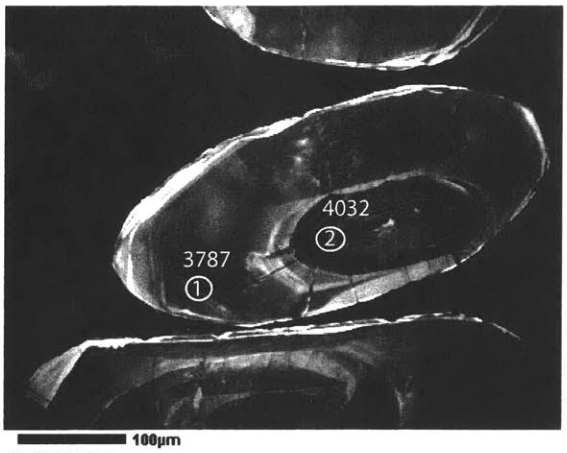

grain 9

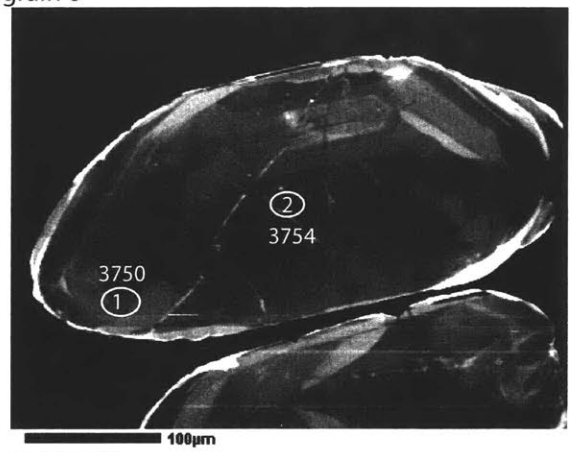

grain 1

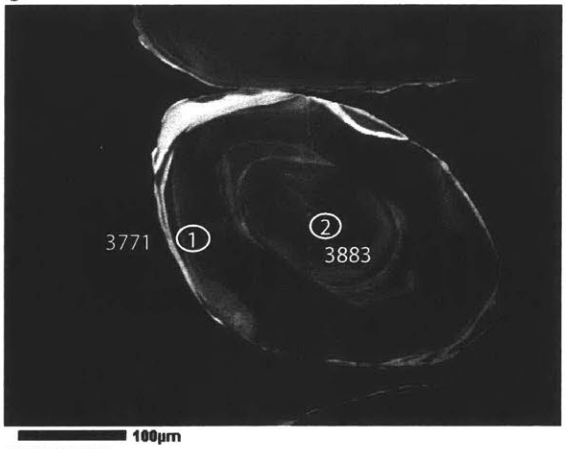

grain 10

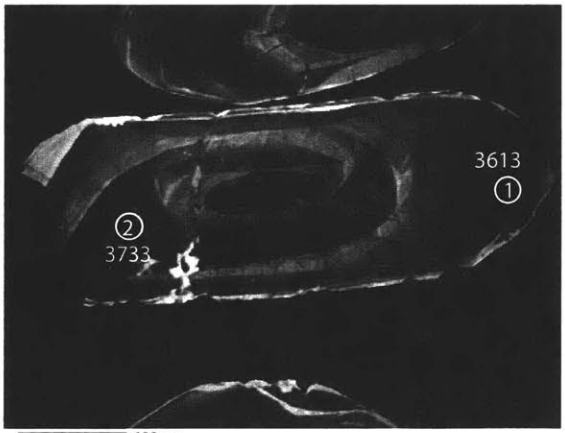

grain 8

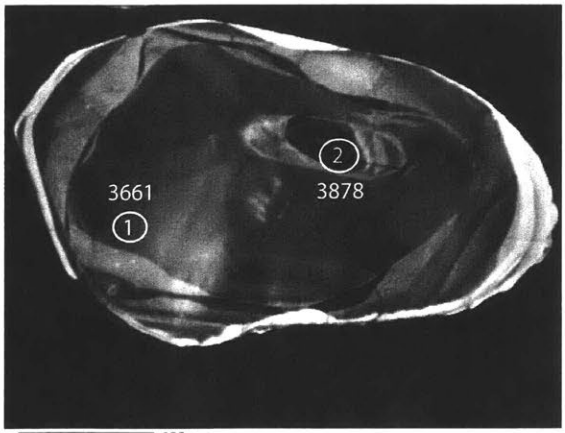

grain 14

SAB94-134 annealed zircons

0	1	2	3	4	5	6		
15	14	13	12	11	10	9	8	7
STDS		x	p	p	s			
STDS		s	p	p	s			
16	17	18	19	20	21	22	23	24
28	27	26	25					

R.Safipour

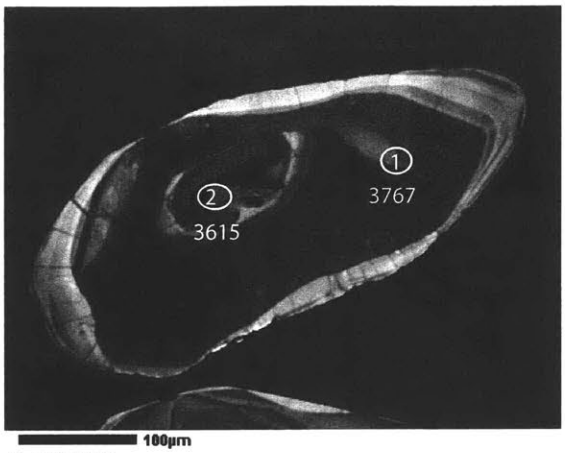

grain 15

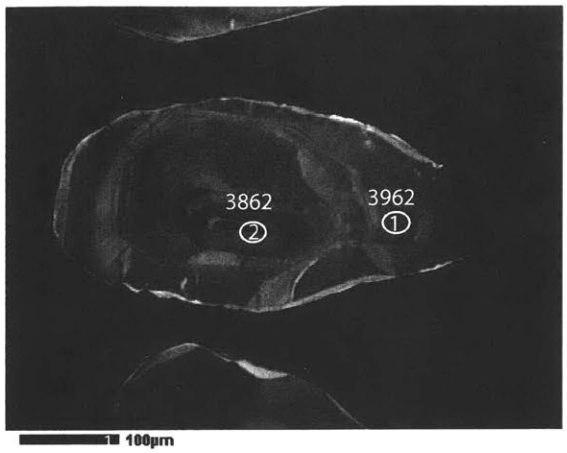

grain 23

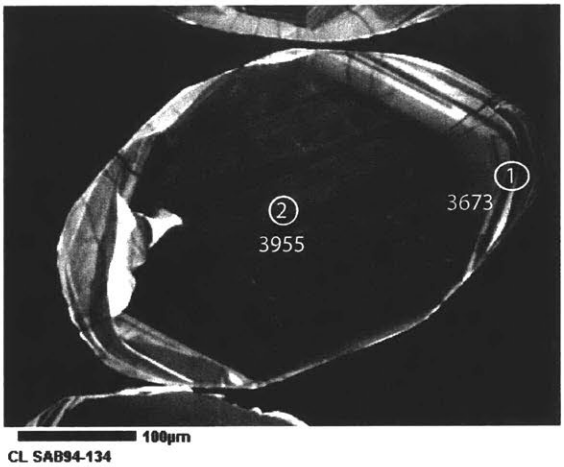

grain 19

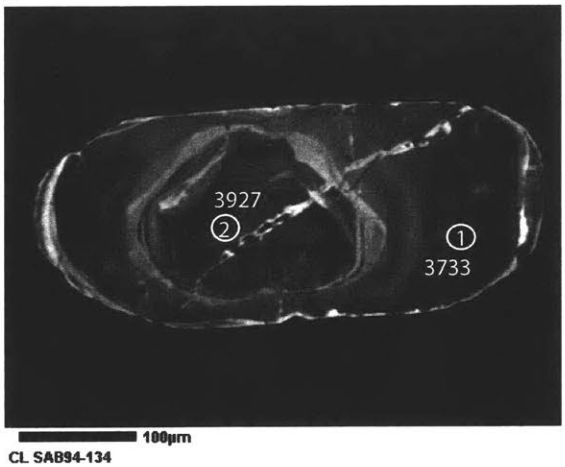

grain 25

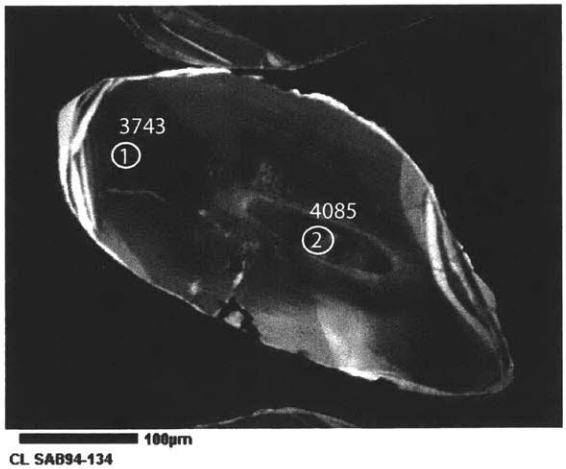

grain 20

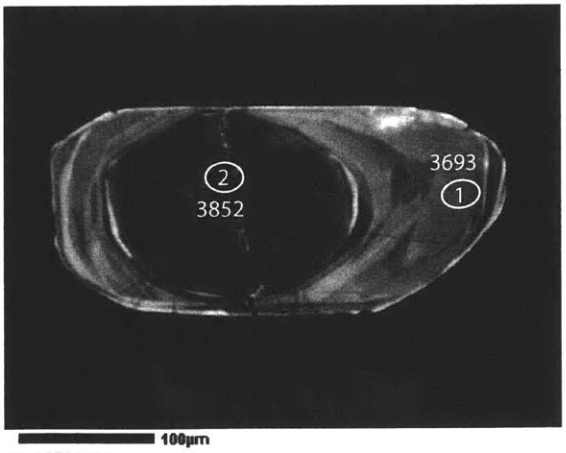

grain 27

SAB96-60 zircons

Grain Map

R.Safipour

0 1 2 3 4 5
10 9 8 7 6

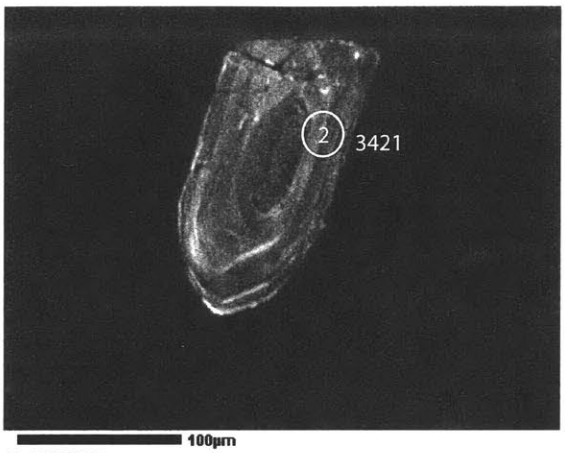

grain 1

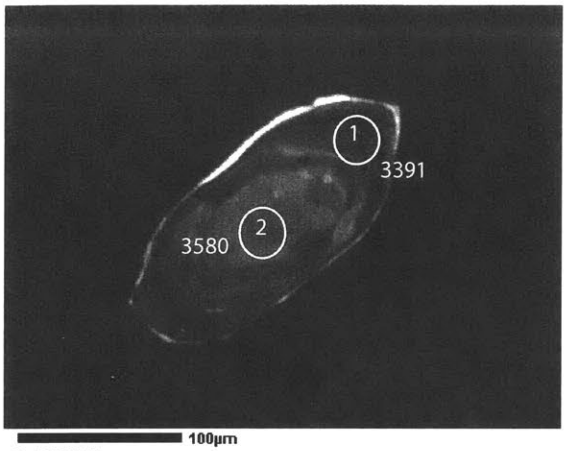

grain 4

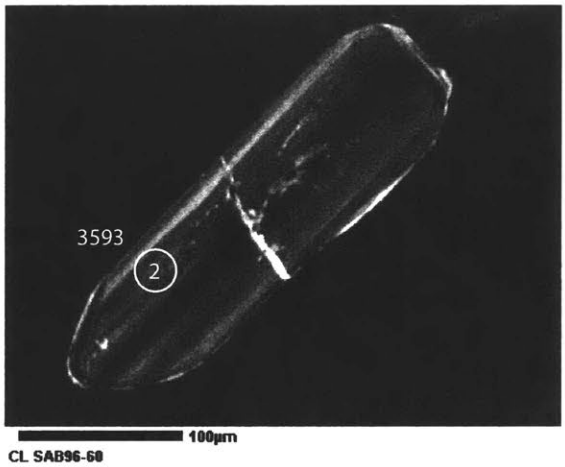

grain 2

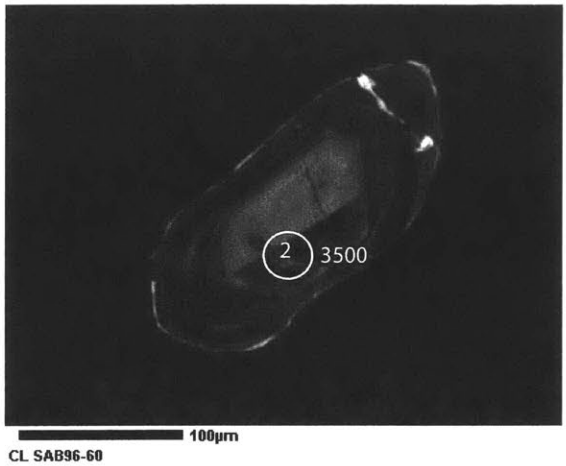

grain 6

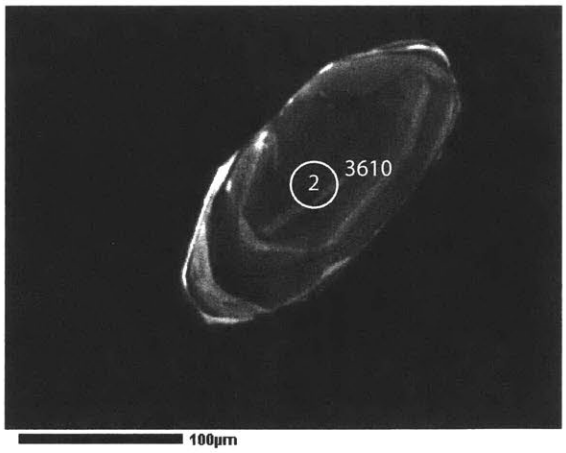

grain 3

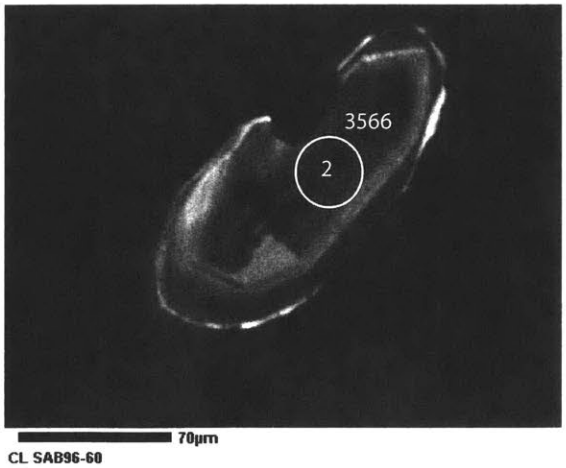

grain 8

SAB96-60 zircons

Grain Map

R.Safipour

0 1 2 3 4 5
10 9 8 7 6

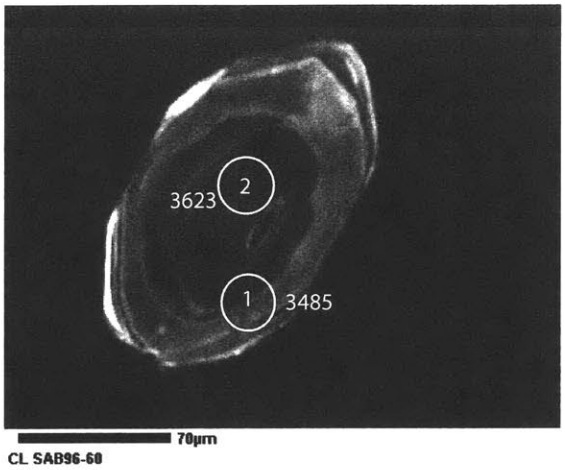

grain 9

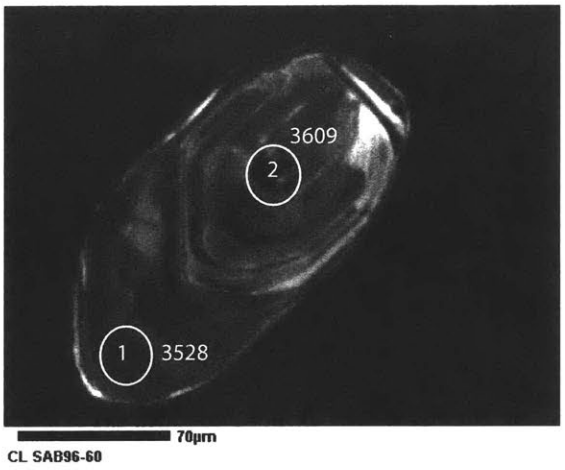

grain 10

SAB96-76 zircons

Grain Map

R.Safipour

0 1 2 3 4
8 7 6 5

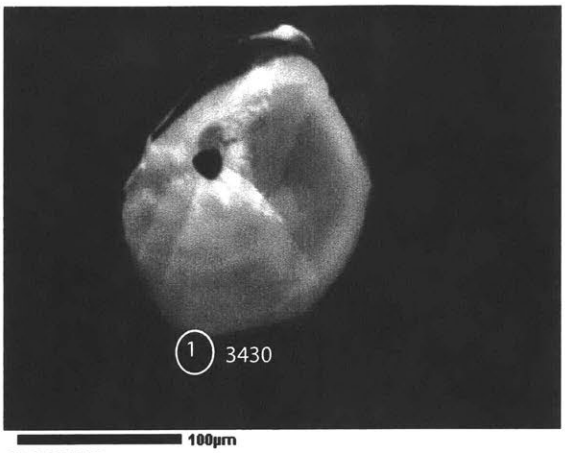

grain 0

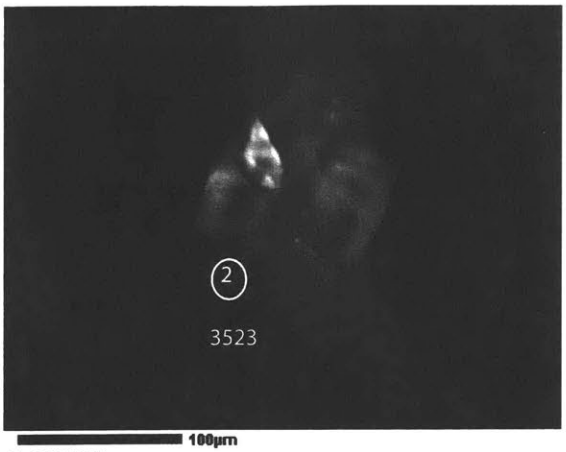

grain 5

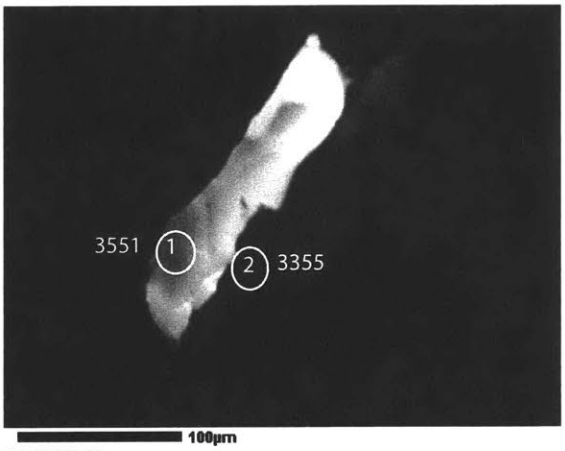

grain 1

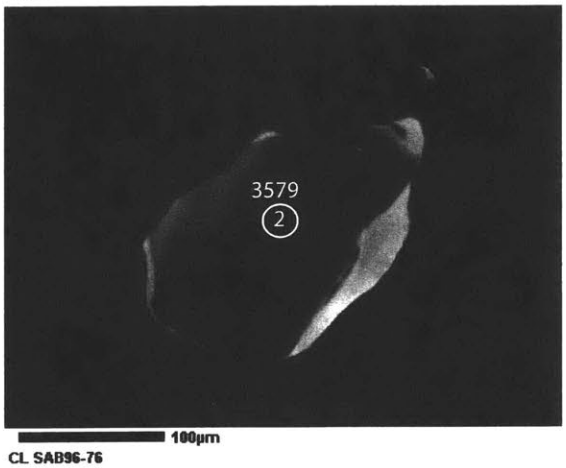

grain 6

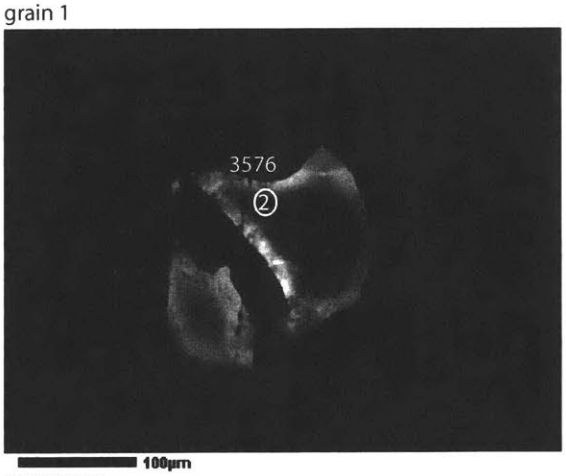

grain 3

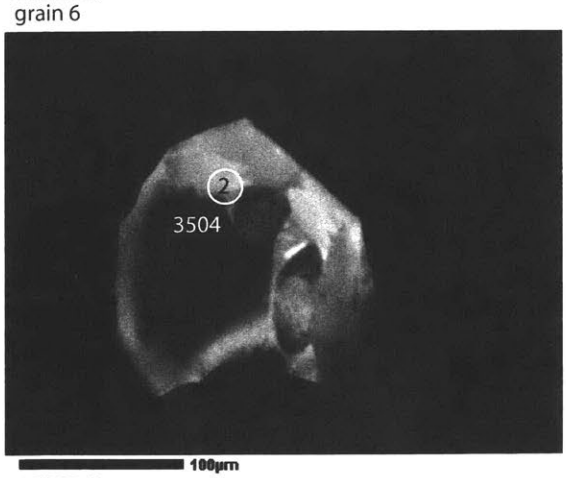

grain 7

SAB96-76 zircons

Grain Map

R.Safipour

0 1 2 3 4
8 7 6 5

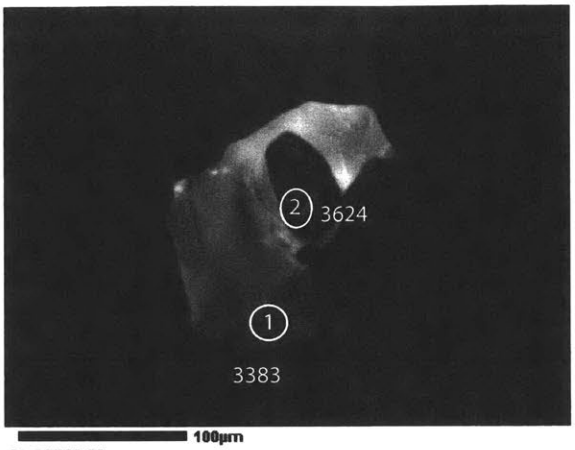

CL SAB96-76
grain 8

Appendix B

Tables of U/Pb isotopic data.

SAB89-28																	
U-Pb geochronologic analyses.																	
							Isotope ratios						Apparent ages (Ma)				
grain-spot	U	206Pb	U/Th	206Pb*	±	207Pb*	±	206Pb*	±	error	206Pb*	±	207Pb*	±	206Pb*	±	Conc
	(ppm)	204Pb		207Pb*	(%)	235U*	(%)	238U	(%)	corr.	238U*	(Ma)	235U	(Ma)	207Pb*	(Ma)	(%)
05-1	176	20271	5.7	3.9005	1.8	21.0838	5.6	0.5964	5.3	0.95	3015.5	128.4	3142.5	54.6	3224.6	28.3	93.5
05-2	6	4236	6.8	4.0353	15.9	22.6609	17.9	0.6632	8.2	0.46	3279.6	211.4	3212.5	175.7	3170.8	253.7	103.4
09-1	57	20043	4.4	3.5840	4.7	26.8471	5.7	0.6979	3.2	0.56	3412.5	84.8	3377.9	55.6	3357.4	73.3	101.6
09-2	48	28232	4.0	3.5836	1.7	25.5478	3.1	0.6640	2.7	0.85	3282.7	68.2	3329.4	30.6	3357.6	25.9	97.8
10-1	102	34210	4.2	3.6688	2.1	24.5574	4.0	0.6534	3.4	0.85	3241.6	85.4	3290.8	38.6	3320.9	33.1	97.6
10-2	11	2665	5.4	3.6159	3.0	26.1657	5.2	0.6862	4.2	0.81	3368.1	109.7	3352.7	50.6	3343.6	47.6	100.7
12-1	60	33681	6.4	3.5210	2.7	26.6730	4.9	0.6811	4.1	0.83	3348.7	106.6	3371.5	47.9	3385.1	42.0	98.9
12-2	9	2974	6.5	3.5539	3.9	26.3598	5.9	0.6794	4.4	0.75	3342.2	115.0	3360.0	57.7	3370.6	61.0	99.2
14-1	472	16484	11.1	4.9588	3.2	11.4046	11.5	0.4102	11.0	0.96	2215.7	207.1	2556.8	107.8	2839.7	52.5	78.0
14-2	51	17484	114.8	3.7563	3.7	23.6244	4.0	0.6436	1.5	0.38	3203.2	38.4	3253.0	39.4	3283.9	58.8	97.5
14-3	50	72986	38.5	3.4613	5.7	26.4344	6.5	0.6636	3.1	0.47	3281.1	78.4	3362.7	63.7	3411.7	89.4	96.2
18-1	420	61894	8.3	3.9586	2.9	21.6519	3.2	0.6216	1.4	0.43	3116.4	34.6	3168.2	31.4	3201.2	46.2	97.4
18-2	104	15891	42.0	3.5000	1.9	24.9531	3.1	0.6334	2.5	0.80	3163.1	61.5	3306.4	30.2	3394.4	29.1	93.2
21-1	252	8290	7.3	3.9316	1.5	21.7768	2.1	0.6210	1.5	0.70	3113.7	37.1	3173.8	20.7	3212.0	23.9	96.9
21-2	11	5707	5.3	3.6506	5.0	25.6291	6.0	0.6786	3.3	0.55	3338.9	85.7	3332.5	58.3	3328.6	77.8	100.3
22-1	520	67585	14.9	3.8362	1.9	22.4036	3.3	0.6233	2.8	0.83	3123.1	68.3	3201.4	32.5	3250.8	29.6	96.1
22-2	102	21010	56.7	3.4363	4.8	28.8197	5.6	0.7182	2.9	0.52	3489.5	78.4	3447.4	55.3	3423.0	75.0	101.9
EKCO2-51	38	20218	2.1	3.6240	2.4	25.9916	4.5	0.6832	3.8	0.84	3356.5	99.2	3346.2	44.1	3340.1	38.2	100.5
EKCO2-51	40	12850	2.7	3.8390	1.8	23.7002	2.1	0.6599	1.0	0.49	3266.7	25.9	3256.1	20.2	3249.6	28.5	100.5

SAB91-35																	
U-Pb geochronologic analyses.																	
							Isotope ratios						Apparent ages (Ma)				
grain-spot	U	206Pb	U/Th	206Pb*	±	207Pb*	±	206Pb*	±	error	206Pb*	±	207Pb*	±	206Pb*	±	Conc
	(ppm)	204Pb		207Pb*	(%)	235U*	(%)	238U	(%)	corr.	238U*	(Ma)	235U	(Ma)	207Pb*	(Ma)	(%)
04-1	550	11439	7.4	3.1828	2.4	30.2102	4.9	0.6974	4.2	0.87	3410.6	112.3	3493.7	47.9	3541.6	37.0	96.3
04-2	651	15230	14.0	3.1290	2.0	30.7054	4.8	0.6968	4.4	0.91	3408.6	116.5	3509.7	47.6	3567.8	31.1	95.5
05-1	693	83471	9.3	3.0530	2.0	32.9273	7.9	0.7291	7.6	0.97	3530.0	207.2	3578.4	77.8	3605.6	30.5	97.9
05-2	2604	11240	3.6	4.0337	3.0	14.9272	4.1	0.4367	2.8	0.69	2335.8	55.5	2810.6	39.2	3171.5	47.4	73.7
06-2	465	85745	6.5	3.0501	2.0	32.6702	4.5	0.7227	4.1	0.90	3506.2	109.8	3570.7	44.5	3607.1	30.2	97.2
10-2	952	115606	10.6	3.2866	2.8	27.6012	8.1	0.6579	7.7	0.94	3259.1	195.8	3405.0	80.0	3492.1	43.3	93.3
12-1	449	38288	20.2	3.2288	2.6	29.3494	7.1	0.6873	6.7	0.93	3372.3	174.9	3465.3	70.3	3519.5	40.1	95.8
12-2	241	27507	3.5	3.1448	2.4	33.3757	6.3	0.7613	5.8	0.93	3648.8	161.6	3591.8	61.8	3560.1	36.5	102.5
15-1	363	1676	8.5	3.2667	3.6	28.1751	6.2	0.6675	5.0	0.81	3296.4	128.6	3425.2	60.6	3501.4	56.3	94.1
15-2	1021	20933	3.5	3.3820	5.1	28.0155	5.8	0.6872	2.7	0.48	3371.8	71.9	3419.6	56.5	3447.8	78.6	97.8
17-1	751	122342	7.2	3.0302	1.7	34.3938	3.1	0.7559	2.6	0.84	3629.1	71.0	3621.4	30.2	3617.1	25.6	100.3
17-2	425	14123	7.1	3.1846	2.3	30.1206	5.8	0.6957	5.3	0.92	3404.3	141.0	3490.8	57.1	3540.7	35.6	96.1
19-1	521	22090	20.3	4.0086	2.5	20.2640	5.6	0.5891	5.1	0.90	2985.9	120.9	3104.0	54.6	3181.4	39.4	93.9
19-2	782	147838	3.4	3.0703	3.5	33.4997	5.8	0.7460	4.6	0.79	3592.7	126.2	3595.4	57.1	3596.9	54.2	99.9
25-1	730	124640	11.0	3.7328	1.6	23.9097	3.6	0.6473	3.2	0.90	3217.7	82.1	3264.7	35.3	3293.7	25.3	97.7
25-2	1707	40880	10.9	4.1714	1.6	17.0438	5.2	0.5156	4.9	0.95	2680.7	108.1	2937.3	49.8	3118.1	25.6	86.0
29-1	658	96099	6.9	3.0296	3.0	33.7998	4.2	0.7427	3.0	0.70	3580.5	81.6	3604.2	41.8	3617.4	46.3	99.0
EKCO2-51	39	12920	1.2	3.8096	1.8	23.4447	3.8	0.6478	3.4	0.88	3219.5	84.9	3245.6	37.1	3261.7	28.5	98.7
EKCO2-51	27	12218	2.1	3.8001	2.3	23.9898	5.1	0.6612	4.6	0.89	3271.7	116.8	3268.0	49.9	3265.7	36.7	100.2

SAB91-37-3 non-annealed grains																	
U-Pb geochronologic analyses.																	
							Isotope ratios						Apparent ages (Ma)				
grain-spot	U	206Pb	U/Th	206Pb*	±	207Pb*	±	206Pb*	±	error	206Pb*	±	207Pb*	±	206Pb*	±	Conc
	(ppm)	204Pb		207Pb*	(%)	235U*	(%)	238U	(%)	corr.	238U*	(Ma)	235U	(Ma)	207Pb*	(Ma)	(%)
00-2	953	38945	1.9	2.5527	5.3	41.4542	6.1	0.7675	3.0	0.49	3671.6	84.3	3806.1	60.8	3877.7	80.5	94.7
01-1	1263	28398	11.0	4.9079	5.9	11.3819	6.4	0.4051	2.7	0.42	2192.7	49.8	2554.9	60.2	2856.5	95.5	76.8
01-2	130	25298	1.6	3.0769	2.2	31.0412	6.0	0.6927	5.5	0.93	3393.0	145.9	3520.4	58.6	3593.6	33.8	94.4
02-1	192	31432	6.1	3.1497	1.6	31.1069	3.7	0.7106	3.3	0.90	3460.7	87.8	3522.4	36.0	3557.7	24.9	97.3
02-2	2613	11102	7.4	4.5602	6.4	11.7921	6.8	0.3900	2.1	0.32	2122.9	38.7	2588.0	63.4	2975.5	103.5	71.3
04-2	342	9706	6.3	3.7300	3.0	20.6968	6.7	0.5599	6.0	0.90	2866.2	138.9	3124.5	65.0	3294.9	46.8	87.0
05-1	274	8697	3.4	3.0571	1.2	32.8172	2.0	0.7276	1.7	0.82	3524.6	44.8	3575.1	19.9	3603.6	18.0	97.8
05-2	675	3769	4.2	2.9987	2.7	30.0707	4.1	0.6540	3.1	0.76	3243.8	80.1	3489.1	40.4	3633.1	40.7	89.3
06-2	759	25248	3.4	2.8260	5.5	32.2444	7.2	0.6609	4.7	0.65	3270.5	119.8	3557.8	70.8	3723.7	83.0	87.8
07-2	43	16695	1.0	3.1307	2.6	31.3149	4.3	0.7110	3.4	0.79	3462.3	91.1	3529.0	42.4	3567.0	40.6	97.1
08-1	442	10518	12.1	2.4574	3.9	47.1820	4.4	0.8409	2.1	0.47	3934.0	60.4	3934.6	43.6	3934.9	58.1	100.0
08-2	494	13156	6.7	2.3801	2.1	41.9580	4.2	0.7243	3.7	0.87	3512.0	99.9	3818.1	41.9	3982.8	30.7	88.2
09-1	222	6904	5.0	3.2774	1.8	30.7808	4.8	0.7317	4.4	0.92	3539.6	120.7	3512.1	47.2	3496.4	28.5	101.2
09-2	512	27614	6.4	2.9788	1.9	36.4425	5.8	0.7873	5.5	0.94	3743.5	155.9	3678.5	57.6	3643.3	29.5	102.8
10-1	230	6924	6.0	3.0680	2.7	32.3482	6.6	0.7198	6.0	0.91	3495.3	162.2	3561.0	64.9	3598.1	41.2	97.1
10-2	710	19293	11.7	3.1943	3.1	31.0372	5.5	0.7191	4.6	0.83	3492.5	123.8	3520.2	54.5	3536.0	47.7	98.8
11-1	411	63597	6.2	3.1415	3.0	33.0241	4.4	0.7524	3.2	0.73	3616.4	88.0	3581.3	42.9	3561.7	45.7	101.5
11-2	349	30940	2.1	2.3655	1.8	46.3143	3.9	0.7946	3.5	0.89	3769.7	99.3	3916.1	38.8	3992.0	26.5	94.4
EKCO2-51	33	7867	2.6	3.9252	1.7	22.6431	2.8	0.6446	2.2	0.79	3207.1	55.8	3211.7	27.3	3214.6	27.4	99.8
EKCO2-51	36	7929	2.5	3.8653	1.5	23.4527	2.4	0.6575	1.9	0.78	3257.3	48.6	3245.9	23.6	3238.9	23.8	100.6
EKCO2-51	48	25391	2.3	3.8505	2.2	23.7149	4.8	0.6623	4.2	0.89	3276.0	108.7	3256.7	46.4	3244.9	34.4	101.0
EKCO2-51	31	10239	2.1	3.8630	3.4	24.1254	4.9	0.6759	3.5	0.71	3328.7	90.0	3273.5	47.6	3239.8	54.3	102.7

SAB91-37-3 annealed grains																
U-Pb geochronologic analyses.																
							Isotope ratios						Apparent ages (Ma)			
grain-spot	U	206Pb	U/Th	206Pb*	±	207Pb*	±	206Pb*	±	error	206Pb*	±	207Pb*	±	206Pb*	±
	(ppm)	204Pb		207Pb*	(%)	235U*	(%)	238U	(%)	corr.	238U*	(Ma)	235U	(Ma)	207Pb*	(Ma)
00-1	218	72559	2.0	3.0941	1.0	32.6085	2.0	0.7317	1.7	0.86	3539.9	45.8	3568.8	19.3	3585.1	15.5
00-2	1041	13184	7.7	3.8097	7.1	14.7252	11.7	0.4069	9.3	0.80	2200.6	172.9	2797.7	111.2	3261.7	111.3
01-1	318	21173	3.9	2.8365	2.7	38.0296	4.2	0.7824	3.3	0.78	3725.6	92.3	3720.7	41.6	3718.0	40.4
01-2	325	201265	7.6	3.0681	1.1	32.9001	5.3	0.7321	5.2	0.98	3541.2	140.9	3577.6	52.1	3598.1	16.9
02-1	375	2698	6.3	3.1510	18.1	21.9741	18.1	0.5022	1.6	0.09	2623.2	35.1	3182.6	177.8	3557.1	280.6
02-2	565	3139	2.0	2.9255	2.9	25.0256	8.9	0.5310	8.4	0.95	2745.6	188.8	3309.2	87.4	3670.9	44.5
03-2	473	17357	3.8	3.0271	9.2	22.4081	13.5	0.4920	9.9	0.73	2579.1	210.9	3201.6	132.0	3618.7	140.7
05-1	527	14570	13.5	2.6626	3.1	38.7264	3.2	0.7479	1.0	0.32	3599.6	28.7	3738.7	31.9	3814.0	46.1
07-1	424	20114	5.9	3.2551	4.2	27.8981	4.6	0.6586	1.9	0.40	3261.8	47.4	3415.5	45.3	3507.0	65.4
08-1	375	9320	5.9	2.9745	6.2	27.8754	6.8	0.6014	2.9	0.43	3035.3	70.9	3414.7	67.1	3645.6	94.7
08-2	364	6358	4.1	2.9700	6.5	27.2190	10.6	0.5863	8.3	0.79	2974.4	198.3	3391.4	104.0	3647.9	100.0
10-1	213	89348	3.4	3.1226	1.8	32.8877	3.0	0.7448	2.5	0.81	3588.4	67.7	3577.2	29.9	3571.0	27.4
10-2	543	30173	3.3	2.5654	1.6	41.9264	2.5	0.7801	1.9	0.76	3717.4	52.5	3817.3	24.3	3870.2	24.1
11-1	251	17453	3.0	3.0283	1.5	34.4522	4.9	0.7567	4.7	0.95	3632.1	130.0	3623.1	48.6	3618.1	23.2
11-2	571	45426	1.8	2.4514	5.1	48.3214	5.4	0.8591	1.9	0.36	3997.5	57.8	3958.3	54.0	3938.5	76.0
12-1	236	12597	4.1	3.2598	2.0	29.9819	4.4	0.7088	3.9	0.89	3454.1	105.1	3486.2	43.3	3504.7	30.8
12-2	842	7885	7.7	3.7961	6.5	15.6941	10.3	0.4321	8.0	0.77	2315.1	154.9	2858.4	98.5	3267.3	102.7
13-1	258	81146	2.3	2.4938	2.1	45.9256	3.9	0.8306	3.3	0.84	3897.9	95.9	3907.8	38.9	3912.8	32.2
13-2	389	96316	1.9	2.3664	3.3	50.0945	5.1	0.8598	3.8	0.75	3999.6	113.0	3994.2	50.3	3991.4	50.0
14-1	231	9313	3.5	3.0118	1.6	28.6170	6.0	0.6251	5.8	0.97	3130.1	144.3	3440.5	59.2	3626.5	23.9
14-2	56	144960	1.4	3.1041	3.7	33.0898	7.3	0.7450	6.3	0.87	3588.9	173.7	3583.3	72.0	3580.1	56.1
15-1	588	14140	9.6	3.3428	1.9	24.3098	2.3	0.5894	1.3	0.57	2986.9	31.6	3280.9	22.4	3465.8	29.1
15-2	728	5150	3.8	4.0502	10.5	13.7264	14.6	0.4032	10.1	0.69	2183.8	187.1	2731.0	138.7	3165.0	167.0
16-1	166	1963	2.1	3.0507	3.1	30.5126	3.6	0.6751	1.9	0.53	3325.6	50.2	3503.5	35.7	3606.8	47.2
16-2	264	18316	1.5	3.0699	1.9	33.5837	6.2	0.7477	5.9	0.95	3599.2	161.4	3597.9	60.7	3597.2	29.2
17-1	320	24787	3.1	3.0629	1.4	33.0313	2.2	0.7338	1.7	0.77	3547.5	46.1	3581.5	21.7	3600.6	21.6

17-2	136	38433	2.7	2.9670	3.4	35.6918	3.5	0.7680	0.7	0.19	3673.6	18.8	3658.0	34.4	3649.4	52.3
18-1	280	44982	2.9	3.0426	1.9	32.1201	2.9	0.7088	2.2	0.75	3453.9	58.0	3554.0	28.6	3610.8	29.6
18-2	432	13508	6.6	2.8800	2.1	32.2912	6.2	0.6745	5.8	0.94	3323.2	150.9	3559.2	61.1	3694.8	32.6
19-1	187	21330	3.6	3.0720	7.2	33.5277	7.6	0.7470	2.5	0.33	3596.5	69.5	3596.2	75.4	3596.1	110.9
20-1	117	26033	1.2	3.0886	2.1	32.4516	2.4	0.7269	1.2	0.50	3522.0	32.0	3564.1	23.4	3587.8	31.6
21-1	116	100330	2.7	2.8479	2.4	37.7684	3.5	0.7801	2.6	0.73	3717.4	72.9	3713.9	34.9	3711.9	36.7
21-2	352	8943	5.5	2.8596	5.4	32.6469	6.5	0.6771	3.7	0.57	3333.2	95.5	3570.0	64.0	3705.7	81.6
22-1	261	69600	3.2	3.1383	1.9	31.8537	3.0	0.7250	2.3	0.78	3514.9	62.3	3545.8	29.2	3563.3	28.8
22-2	538	28369	1.6	2.7072	2.5	37.5374	5.4	0.7370	4.8	0.89	3559.5	130.5	3707.8	53.3	3788.9	37.9
23-1	943	15400	13.6	3.3946	4.7	23.6718	7.8	0.5828	6.2	0.80	2960.2	147.2	3255.0	75.9	3442.0	73.0
23-2	274	6867	1.6	3.1272	2.9	31.5072	5.1	0.7146	4.2	0.83	3475.8	112.3	3535.0	49.9	3568.7	44.0
24-1	111	137024	2.7	3.1698	3.4	32.4299	3.6	0.7455	1.3	0.35	3591.1	34.7	3563.4	35.8	3547.9	52.5
24-2	636	13682	5.0	3.8094	5.3	14.7465	11.5	0.4074	10.3	0.89	2203.1	191.7	2799.0	110.2	3261.8	83.0
25-2	422	5440	3.1	2.8450	4.6	29.4773	9.2	0.6082	7.9	0.87	3063.0	193.6	3469.5	90.3	3713.5	69.8
26-1	294	186420	3.5	3.1064	2.9	32.3911	4.2	0.7298	3.1	0.73	3532.5	83.0	3562.3	41.1	3579.0	43.8
26-2	298	9869	4.8	2.9868	1.5	33.2781	4.1	0.7209	3.8	0.93	3499.4	103.2	3588.9	40.6	3639.2	23.4
27-1	191	33928	4.8	3.4628	2.8	27.7684	3.4	0.6974	1.9	0.56	3410.7	50.1	3411.0	33.4	3411.1	44.0
27-2	1009	8376	3.1	3.1695	6.3	22.8884	9.4	0.5261	7.1	0.75	2725.2	156.7	3222.2	92.1	3548.1	96.9
28-2	791	8104	5.6	3.2808	3.4	19.7815	7.4	0.4707	6.6	0.89	2486.6	135.4	3080.7	71.5	3494.8	52.6
29-2	836	7318	3.1	3.1112	2.1	23.9956	4.2	0.5414	3.7	0.87	2789.5	83.1	3268.2	41.1	3576.7	31.8
30-2	1139	2420	4.6	3.9982	3.8	11.6198	5.3	0.3369	3.6	0.68	1872.0	58.3	2574.3	49.2	3185.5	60.7
32-2	527	7189	3.0	3.4226	2.1	23.6551	3.0	0.5872	2.2	0.73	2978.0	52.7	3254.3	29.6	3429.2	32.4
EKCO2-51	22	18651	1.5	3.8146	2.0	22.7966	4.6	0.6307	4.2	0.90	3152.3	104.0	3218.3	44.9	3259.7	31.2
EKCO2-51	32	30472	1.6	3.8215	2.9	23.6325	3.9	0.6550	2.6	0.66	3247.7	65.6	3253.4	37.7	3256.8	45.5

SAB91-52																	
U-Pb geochronologic analyses.																	
							Isotope ratios						Apparent ages (Ma)				
grain-spot	U	206Pb	U/Th	206Pb*	±	207Pb*	±	206Pb*	±	error	206Pb*	±	207Pb*	±	206Pb*	±	Conc
	(ppm)	204Pb		207Pb*	(%)	235U*	(%)	238U	(%)	corr.	238U*	(Ma)	235U	(Ma)	207Pb*	(Ma)	(%)
01-1	279	10091	1.7	2.7840	2.5	36.3177	2.7	0.7333	1.2	0.43	3545.7	31.9	3675.1	26.9	3746.4	37.4	94.6
01-2	553	7101	2.6	3.2801	3.0	24.5693	5.6	0.5845	4.8	0.85	2967.1	113.4	3291.3	54.8	3495.1	45.8	84.9
04-1	615	11820	2.6	2.9387	2.4	33.3161	3.8	0.7101	2.9	0.77	3458.8	78.7	3590.0	37.5	3664.1	36.8	94.4
04-2	1294	587	3.5	3.6544	7.4	12.0529	8.2	0.3194	3.7	0.45	1787.0	57.8	2608.5	77.4	3327.0	115.5	53.7
06-1	834	3729	5.1	3.7341	5.4	15.7404	6.7	0.4263	4.0	0.59	2289.0	76.1	2861.2	64.1	3293.2	85.2	69.5
06-2	1134	44754	13.4	3.4809	4.8	24.4038	5.4	0.6161	2.6	0.47	3094.4	62.7	3284.7	53.0	3402.9	74.6	90.9
08-1	135	43427	9.9	3.6665	2.4	24.6933	2.6	0.6566	0.9	0.36	3254.1	23.8	3296.2	25.1	3321.8	37.6	98.0
08-2	106	25514	1.1	3.0400	2.1	34.3706	3.2	0.7578	2.5	0.76	3636.2	68.9	3620.7	32.1	3612.2	32.2	100.7
09-1	179	32578	1.5	2.8448	2.2	36.6584	4.4	0.7563	3.9	0.87	3630.8	107.4	3684.4	43.9	3713.6	33.1	97.8
13-1	1449	2183	5.6	3.6744	3.7	17.8943	4.2	0.4769	2.0	0.46	2513.6	40.8	2984.1	40.7	3318.5	58.7	75.7
13-2	2939	1483	6.7	4.8343	6.8	6.9754	7.7	0.2446	3.6	0.47	1410.4	45.6	2108.3	68.6	2881.0	110.8	49.0
14-1	112	26534	1.8	2.9176	1.9	35.3874	2.7	0.7488	2.0	0.71	3603.1	53.8	3649.5	27.1	3675.1	29.5	98.0
14-2	510	25644	3.9	2.6309	2.8	39.7450	4.5	0.7584	3.5	0.77	3638.3	96.5	3764.4	44.4	3832.1	42.8	94.9
EKCO2-51	22	5509	2.1	3.8781	2.9	23.2079	3.8	0.6528	2.4	0.63	3239.0	60.9	3235.7	36.9	3233.7	46.4	100.2

SAB91-53																	
U-Pb geochronologic analyses.																	
							Isotope ratios						Apparent ages (Ma)				
grain-spot	U	206Pb	U/Th	206Pb*	±	207Pb*	±	206Pb*	±	error	206Pb*	±	207Pb*	±	206Pb*	±	Conc
	(ppm)	204Pb		207Pb*	(%)	235U*	(%)	238U	(%)	corr.	238U*	(Ma)	235U	(Ma)	207Pb*	(Ma)	(%)
10-1	375	25054	1.5	2.7192	1.4	39.1391	3.9	0.7719	3.6	0.93	3687.7	102.2	3749.2	38.7	3782.2	21.5	97.5
10-2	415	33465	1.2	2.6827	1.8	41.2746	7.3	0.8031	7.1	0.97	3800.1	203.9	3801.8	72.8	3802.7	27.7	99.9
12-1	316	43098	1.3	2.7177	1.6	38.3942	4.9	0.7568	4.6	0.95	3632.4	127.5	3730.1	48.1	3783.1	24.0	96.0
12-2	560	13470	3.1	2.6482	3.4	38.3086	12.7	0.7358	12.2	0.96	3554.9	334.2	3727.9	126.1	3822.2	51.3	93.0
15-1	200	13987	4.2	2.9219	1.5	35.0137	4.2	0.7420	3.9	0.93	3578.0	107.9	3639.0	41.6	3672.8	23.1	97.4
15-2	507	20356	7.2	2.6609	2.3	41.7107	4.9	0.8050	4.4	0.88	3806.9	125.1	3812.2	48.9	3815.0	34.9	99.8
17-1	390	4016	1.2	2.7470	2.4	33.1879	3.3	0.6612	2.3	0.70	3271.9	59.3	3586.2	32.5	3766.8	35.8	86.9
19-1	448	6845	1.0	2.6681	1.8	38.6565	3.7	0.7480	3.2	0.87	3600.2	88.3	3736.9	36.4	3810.9	27.2	94.5
19-2	677	31821	1.6	2.8188	7.9	28.7078	9.3	0.5869	4.9	0.53	2976.8	116.4	3443.6	91.4	3727.6	120.6	79.9
22-1	497	16633	1.8	2.7476	1.6	39.1059	3.2	0.7793	2.8	0.87	3714.5	78.2	3748.3	31.6	3766.4	24.1	98.6
22-2	223	7222	2.1	2.5812	3.1	43.1954	3.3	0.8086	1.2	0.37	3820.0	35.5	3846.9	33.1	3861.0	46.7	98.9
23-1	333	23960	1.3	2.6871	2.5	41.3198	5.4	0.8053	4.8	0.89	3807.9	138.9	3802.9	54.0	3800.2	38.0	100.2
23-2	272	21435	1.4	2.6047	2.0	43.5126	3.2	0.8220	2.5	0.77	3867.4	71.8	3854.2	31.8	3847.3	30.8	100.5
24-1	342	61334	1.3	2.7166	1.6	40.5404	4.5	0.7988	4.2	0.94	3784.7	120.0	3784.0	44.3	3783.6	23.5	100.0
24-2	505	26916	1.0	2.7560	2.8	32.6520	7.4	0.6527	6.9	0.93	3238.6	175.7	3570.2	73.3	3761.8	41.9	86.1
EKCO2-51	38	48270	2.0	3.8231	1.3	23.9915	3.4	0.6652	3.2	0.92	3287.4	81.9	3268.0	33.6	3256.2	20.8	101.0
EKCO2-51	33	10490	2.2	3.8366	2.0	23.6727	3.3	0.6587	2.6	0.78	3262.2	65.3	3255.0	31.8	3250.6	32.1	100.4

SAB91-54																	
U-Pb geochronologic analyses.																	
							Isotope ratios						Apparent ages (Ma)				
grain-spot	U	206Pb	U/Th	206Pb*	±	207Pb*	±	206Pb*	±	error	206Pb*	±	207Pb*	±	206Pb*	±	Conc
	(ppm)	204Pb		207Pb*	(%)	235U*	(%)	238U	(%)	corr.	238U*	(Ma)	235U	(Ma)	207Pb*	(Ma)	(%)
05-1	410	15468	18.4	3.0133	3.2	28.4351	3.4	0.6214	1.0	0.29	3115.6	24.5	3434.2	33.2	3625.7	49.6	85.9
05-2	324	18674	5.9	2.4998	4.6	40.6200	9.9	0.7364	8.7	0.88	3557.4	238.8	3785.9	98.2	3909.2	69.5	91.0
07-1	618	29653	49.1	2.9423	4.4	33.9926	4.8	0.7254	1.9	0.40	3516.3	51.8	3609.8	47.3	3662.2	67.3	96.0
07-2	285	48884	10.3	2.9187	2.0	36.2400	3.9	0.7671	3.3	0.86	3670.3	92.9	3673.0	38.3	3674.5	30.5	99.9
08-1	145	69100	2.5	2.8780	2.0	36.6422	3.6	0.7648	3.0	0.84	3661.9	84.9	3683.9	35.7	3695.9	29.7	99.1
08-2	77	26674	1.6	2.8504	1.8	36.8229	5.8	0.7612	5.5	0.95	3648.8	152.7	3688.8	57.1	3710.6	27.4	98.3
09-1	548	4623	19.2	2.9964	1.7	32.1680	6.0	0.6991	5.8	0.96	3417.1	154.1	3555.5	59.6	3634.3	25.8	94.0
09-2	1218	4051	8.5	3.2098	3.3	19.8746	11.2	0.4627	10.7	0.96	2451.4	217.9	3085.3	108.4	3528.6	50.7	69.5
15-1	845	6116	31.7	3.0254	5.2	22.2673	7.5	0.4886	5.4	0.72	2564.6	113.6	3195.5	72.6	3619.5	79.5	70.9
15-2	134	8083	2.0	2.9627	7.8	36.1250	8.3	0.7762	2.8	0.34	3703.5	79.7	3669.9	82.1	3651.6	119.3	101.4
15-3	258	35173	2.9	2.6149	2.7	42.3369	4.2	0.8029	3.3	0.78	3799.6	93.9	3827.0	41.8	3841.3	40.2	98.9
17-1	507	10248	22.0	2.9917	2.2	34.1327	2.4	0.7406	1.0	0.41	3572.8	27.2	3613.9	23.7	3636.7	33.5	98.2
17-2	80	712	3.6	2.9921	3.1	35.0815	3.3	0.7613	1.0	0.30	3649.0	27.4	3640.9	32.5	3636.5	48.0	100.3
17-3	116	228	2.6	2.9006	3.7	24.2870	9.7	0.5109	9.0	0.92	2660.6	196.3	3280.0	95.4	3684.0	57.1	72.2
18-1	581	11773	21.0	3.3172	7.4	16.8692	10.9	0.4058	7.9	0.73	2195.9	147.8	2927.4	104.7	3477.7	115.4	63.1
18-2	482	10879	11.5	3.1402	13.4	23.3325	15.4	0.5314	7.5	0.49	2747.3	168.5	3240.9	150.6	3562.4	207.0	77.1
21-1	86	22264	0.8	2.7833	1.1	39.6113	3.7	0.7996	3.5	0.95	3787.7	100.0	3761.0	36.4	3746.8	17.3	101.1
21-2	350	32910	8.8	2.7168	2.0	39.1118	3.1	0.7707	2.4	0.77	3683.2	66.5	3748.5	30.4	3783.5	29.6	97.3

SAB91-62																	
U-Pb geochronologic analyses.																	
							Isotope ratios						Apparent ages (Ma)				
grain-spot	U	206Pb	U/Th	206Pb*	±	207Pb*	±	206Pb*	±	error	206Pb*	±	207Pb*	±	206Pb*	±	Conc
	(ppm)	204Pb		207Pb*	(%)	235U*	(%)	238U	(%)	corr.	238U*	(Ma)	235U	(Ma)	207Pb*	(Ma)	(%)
01-1	1149	6170	4.0	3.5033	3.8	23.6880	5.7	0.6019	4.2	0.74	3037.4	101.5	3255.6	55.2	3393.0	59.4	89.5
04-1	826	27140	9.2	3.4340	5.5	23.3248	11.3	0.5809	9.9	0.87	2952.5	233.9	3240.6	110.5	3424.1	85.7	86.2
04-2	227	97265	3.4	3.0511	4.6	32.0497	6.0	0.7092	3.9	0.65	3455.6	103.5	3551.8	59.1	3606.6	70.3	95.8
07-1	819	4117	11.2	3.5038	4.7	22.0030	5.9	0.5591	3.5	0.59	2863.1	80.2	3183.9	57.1	3392.7	73.9	84.4
07-2	309	1782	9.6	3.2109	6.1	22.2610	9.0	0.5184	6.6	0.74	2692.4	145.5	3195.2	87.5	3528.1	94.0	76.3
13-1	1585	30670	3.8	3.7173	5.4	18.3567	6.3	0.4949	3.2	0.51	2591.8	68.5	3008.6	60.5	3300.3	84.6	78.5
13-2	87	25035	2.2	3.0796	2.1	33.0677	4.0	0.7386	3.4	0.85	3565.3	92.3	3582.6	39.1	3592.3	31.9	99.2
30-1	1041	69507	15.7	3.1811	1.5	30.4553	3.8	0.7026	3.5	0.92	3430.7	93.4	3501.6	37.6	3542.4	23.3	96.8
30-2	217	113621	2.7	2.4797	3.0	46.7953	4.6	0.8416	3.5	0.77	3936.4	104.3	3926.4	46.0	3921.3	44.8	100.4
30-3	2069	9789	2.7	3.7858	15.9	16.6316	17.7	0.4567	7.7	0.44	2424.8	156.5	2913.8	171.2	3271.6	252.2	74.1
36-1	1876	5543	4.3	5.2327	4.8	11.7559	5.0	0.4461	1.7	0.33	2378.1	33.2	2585.2	47.2	2751.7	78.3	86.4
36-2	190	84339	1.2	3.0062	1.9	34.0166	3.4	0.7417	2.9	0.83	3576.8	78.5	3610.5	33.9	3629.3	29.3	98.6
37-1	816	32464	11.6	3.3306	5.8	24.2476	6.5	0.5857	2.9	0.45	2972.0	70.0	3278.4	63.8	3471.5	90.5	85.6
37-2	335	12501	4.2	3.5250	6.5	23.3478	8.3	0.5969	5.3	0.63	3017.4	127.2	3241.6	81.4	3383.3	100.8	89.2
37-3	929	19493	5.1	3.4289	2.0	25.3078	2.3	0.6294	1.3	0.56	3147.1	32.6	3320.2	23.0	3426.3	30.3	91.9
39-1	848	7456	3.1	3.4594	4.9	23.1838	8.1	0.5817	6.4	0.79	2955.6	152.7	3234.7	79.0	3412.6	76.6	86.6
39-2	268	7995	1.7	3.0450	3.8	32.9295	6.7	0.7272	5.5	0.83	3523.1	150.4	3578.5	66.1	3609.6	57.7	97.6
46-1	957	6642	3.6	3.2305	3.2	26.7444	6.4	0.6266	5.5	0.86	3136.2	137.1	3374.2	62.7	3518.7	49.9	89.1
46-2	150	7047	1.5	2.9500	5.6	35.9060	5.9	0.7682	1.9	0.32	3674.3	52.9	3663.9	58.8	3658.2	86.3	100.4
53-1	1192	30694	15.1	3.5267	5.1	21.2586	7.0	0.5437	4.9	0.69	2799.1	110.8	3150.5	68.4	3382.6	79.3	82.7
53-2	332	47394	2.5	3.2634	4.7	30.3408	5.9	0.7181	3.6	0.61	3489.0	96.2	3497.9	57.9	3503.0	72.4	99.6
58-1	521	3974	10.2	3.2390	7.2	21.1069	9.5	0.4958	6.3	0.65	2595.9	133.6	3143.5	92.8	3514.6	111.6	73.9
58-2	130	6541	2.0	3.4599	7.4	24.5238	12.5	0.6154	10.2	0.81	3091.6	249.6	3289.4	123.0	3412.3	114.7	90.6
EKCO2-51	71	8134	1.9	3.8465	2.8	23.2812	5.2	0.6495	4.4	0.84	3226.2	111.4	3238.8	50.7	3246.6	44.1	99.4
EKCO2-51	36	38229	2.2	3.5946	1.6	25.7797	2.3	0.6721	1.6	0.71	3313.9	42.5	3338.2	22.7	3352.8	25.6	98.8

SAB91-65																	
U-Pb geochronologic analyses.																	
							Isotope ratios						Apparent ages (Ma)				
grain-spot	U	206Pb	U/Th	206Pb*	±	207Pb*	±	206Pb*	±	error	206Pb*	±	207Pb*	±	206Pb*	±	Conc
	(ppm)	204Pb		207Pb*	(%)	235U*	(%)	238U	(%)	corr.	238U*	(Ma)	235U	(Ma)	207Pb*	(Ma)	(%)
00-1	127	13237	3.8	3.3384	4.4	25.2684	4.4	0.6118	0.7	0.17	3077.2	18.1	3318.6	43.4	3467.9	67.9	88.7
00-2	575	77335	8.1	2.4773	1.4	43.0311	1.9	0.7732	1.3	0.69	3692.3	37.7	3843.1	19.2	3922.8	21.0	94.1
00-3	205	12271	1.8	2.2744	5.3	52.9127	8.4	0.8728	6.5	0.78	4044.8	195.9	4048.7	84.0	4050.6	79.2	99.9
01-1	180	55285	2.9	2.7797	1.1	39.4250	6.1	0.7948	6.0	0.98	3770.5	171.6	3756.4	60.5	3748.8	16.1	100.6
01-2	614	22927	6.0	3.1297	3.1	30.2180	3.2	0.6859	1.1	0.34	3367.0	29.4	3493.9	31.9	3567.5	46.9	94.4
02-1	186	11694	1.7	3.1049	8.9	31.3879	14.1	0.7068	11.0	0.78	3446.4	293.3	3531.3	139.9	3579.8	136.9	96.3
02-2	179	13433	3.2	3.3053	9.6	28.4208	10.4	0.6813	3.8	0.37	3349.4	99.8	3433.7	102.1	3483.3	149.6	96.2
04-1	237	77563	1.8	3.0638	3.0	33.3466	3.4	0.7410	1.6	0.48	3574.2	44.4	3590.9	33.6	3600.2	46.1	99.3
04-2	738	56628	6.4	3.0482	7.0	29.6791	7.4	0.6561	2.4	0.33	3252.2	61.8	3476.2	73.2	3608.0	108.0	90.1
05-1	579	7879	10.6	2.7064	4.1	38.0773	4.3	0.7474	1.3	0.30	3597.9	35.6	3721.9	42.3	3789.4	61.7	94.9
05-2	188	31489	4.6	2.2822	3.8	53.5061	6.0	0.8856	4.7	0.77	4088.7	141.7	4059.8	60.3	4045.6	57.0	101.1
07-1	105	17079	1.6	3.1342	1.4	31.1012	2.5	0.7070	2.1	0.83	3447.0	56.1	3522.3	24.8	3565.3	21.4	96.7
07-2	405	29266	1.1	3.0198	1.4	34.5810	2.8	0.7574	2.4	0.86	3634.6	66.1	3626.8	27.4	3622.4	21.9	100.3
13-1	293	102099	1.9	2.9836	1.7	35.1214	2.7	0.7600	2.1	0.78	3644.2	57.9	3642.1	26.2	3640.9	25.3	100.1
13-2	799	72592	1.4	3.0549	2.3	34.7618	2.6	0.7702	1.1	0.44	3681.4	32.0	3631.9	25.7	3604.7	35.9	102.1
16-1	95	23753	1.3	3.0209	2.0	34.3767	3.9	0.7532	3.4	0.87	3619.3	93.9	3620.9	38.7	3621.8	30.0	99.9
16-2	122	44667	1.1	3.1001	3.5	32.6319	4.4	0.7337	2.8	0.63	3547.2	76.1	3569.6	43.7	3582.1	53.0	99.0
28-1	90	7732	2.3	3.2924	3.9	26.5853	4.1	0.6348	1.2	0.30	3168.6	31.0	3368.3	40.0	3489.3	60.2	90.8
28-2	1947	32546	9.1	4.7706	3.9	10.3816	4.7	0.3592	2.6	0.56	1978.4	44.5	2469.4	43.3	2902.6	62.9	68.2
32-1	184	9198	2.1	3.2011	3.2	30.5478	3.4	0.7092	1.1	0.33	3455.5	30.2	3504.6	33.6	3532.8	49.7	97.8
32-2	915	31898	24.9	2.8445	1.7	34.5437	3.3	0.7126	2.8	0.85	3468.4	75.9	3625.7	32.7	3713.8	26.3	93.4
32-3	353	35627	3.7	2.3903	4.4	49.5494	5.5	0.8590	3.3	0.60	3997.0	97.7	3983.3	54.8	3976.4	66.2	100.5
32-4	853	214199	8.1	2.6349	2.6	37.8392	6.0	0.7231	5.4	0.90	3507.7	145.6	3715.7	59.3	3829.9	39.8	91.6
36-1	227	62316	1.2	3.0189	1.6	34.0827	3.8	0.7463	3.5	0.91	3593.7	96.7	3612.4	38.0	3622.8	24.2	99.2
52-1	237	58374	1.1	3.0170	1.9	33.9448	5.4	0.7428	5.1	0.94	3580.8	139.9	3608.4	53.7	3623.8	29.6	98.8
52-2	258	22263	21.8	3.6607	3.6	21.1428	5.9	0.5613	4.7	0.79	2872.2	107.8	3145.2	57.0	3324.3	56.2	86.4
EKCO2-51	39	13221	1.6	3.8887	2.4	23.0427	4.4	0.6499	3.7	0.84	3227.8	93.7	3228.7	42.7	3229.3	37.4	100.0
EKCO2-51	41	13206	2.1	3.8816	2.7	23.6204	8.5	0.6650	8.0	0.95	3286.4	206.3	3252.9	82.6	3232.2	42.8	101.7

SAB91-79																	
U-Pb geochronologic analyses.																	
							Isotope ratios						Apparent ages (Ma)				
grain-spot	U	206Pb	U/Th	206Pb*	±	207Pb*	±	206Pb*	±	error	206Pb*	±	207Pb*	±	206Pb*	±	Conc
	(ppm)	204Pb		207Pb*	(%)	235U*	(%)	238U	(%)	corr.	238U*	(Ma)	235U	(Ma)	207Pb*	(Ma)	(%)
01-1	98	51313	0.7	2.8092	1.4	38.4061	4.0	0.7825	3.8	0.94	3726.1	106.7	3730.4	39.8	3732.7	21.3	99.8
03-1	116	6781	4.2	3.5208	2.0	24.9944	5.2	0.6382	4.8	0.92	3182.1	121.1	3308.0	51.0	3385.2	31.0	94.0
03-2	77	8066	1.3	3.5225	3.9	27.2186	5.5	0.6954	3.8	0.70	3403.1	101.5	3391.4	53.9	3384.4	61.3	100.6
04-1	94	185390	2.8	3.1376	3.2	32.6066	4.6	0.7420	3.4	0.73	3577.9	93.1	3568.8	45.7	3563.6	48.6	100.4
04-2	95	73037	1.3	3.0498	4.0	32.7076	4.7	0.7235	2.4	0.52	3509.1	64.9	3571.8	45.9	3607.2	61.2	97.3
08-1	197	107880	2.5	3.0434	1.6	33.6516	3.8	0.7428	3.5	0.90	3580.9	95.3	3599.9	37.9	3610.5	25.2	99.2
08-2	57	50466	1.1	2.8848	2.0	36.9585	6.0	0.7733	5.7	0.94	3692.7	159.1	3692.4	59.4	3692.3	30.4	100.0
08-3	563	46652	1.8	2.5040	7.1	43.1844	8.0	0.7843	3.8	0.48	3732.5	108.8	3846.6	80.0	3906.7	106.5	95.5
09-1	76	12235	4.1	3.4406	2.2	28.1787	6.2	0.7032	5.8	0.93	3432.6	155.2	3425.3	61.3	3421.1	34.8	100.3
09-2	54	7326	1.2	2.9421	2.2	35.7778	3.9	0.7634	3.3	0.83	3656.8	91.5	3660.3	38.9	3662.3	33.2	99.9
09-3	2207	12519	7.0	3.5768	3.5	21.6752	7.5	0.5623	6.7	0.88	2876.1	154.6	3169.3	73.2	3360.6	54.8	85.6
10-1	123	40545	1.9	3.0762	3.2	32.6611	6.4	0.7287	5.5	0.86	3528.5	149.2	3570.4	62.8	3594.0	49.5	98.2
10-2	89	26259	1.3	3.0717	2.0	33.2861	5.7	0.7415	5.4	0.94	3576.3	147.4	3589.1	56.4	3596.3	30.1	99.4
11-1	166	68504	2.8	3.2345	3.7	30.7825	4.5	0.7221	2.5	0.55	3504.0	66.5	3512.1	44.1	3516.8	57.8	99.6
11-2	93	21413	0.8	3.0654	2.1	33.4562	5.6	0.7438	5.2	0.93	3584.6	143.6	3594.1	55.6	3599.4	32.7	99.6
11-3	102	18740	0.8	2.9585	2.0	35.5311	4.6	0.7624	4.1	0.90	3653.0	114.9	3653.5	45.3	3653.8	30.9	100.0
12-1	236	13809	2.8	3.1909	2.0	28.7220	9.6	0.6647	9.4	0.98	3285.4	241.0	3444.1	94.1	3537.7	30.5	92.9
12-2	84	13914	1.6	2.9695	2.5	35.3969	4.1	0.7623	3.2	0.79	3652.8	89.5	3649.8	40.1	3648.1	37.9	100.1
13-1	194	46650	2.6	3.0015	1.4	34.6836	2.1	0.7550	1.6	0.77	3626.0	45.2	3629.7	21.0	3631.7	20.8	99.8
13-2	58	35364	1.7	2.9017	1.3	36.4907	4.0	0.7680	3.8	0.95	3673.3	106.4	3679.8	39.7	3683.4	19.5	99.7
14-1	106	32447	12.7	3.4847	1.5	26.7358	3.6	0.6757	3.2	0.90	3327.9	83.4	3373.8	34.9	3401.2	24.0	97.8
14-2	53	18088	1.1	3.0319	2.0	34.0859	2.7	0.7495	1.9	0.69	3605.7	51.6	3612.5	26.7	3616.3	30.1	99.7
15-1	71	19877	1.8	3.5595	2.3	25.7512	3.8	0.6648	3.0	0.80	3285.7	77.7	3337.1	37.0	3368.1	35.6	97.6
15-2	67	25030	1.3	2.9132	1.9	36.2903	2.4	0.7668	1.5	0.63	3669.0	42.5	3674.4	23.7	3677.3	28.2	99.8
17-1	133	25956	1.8	2.8637	1.9	37.3888	4.7	0.7766	4.3	0.91	3704.6	119.8	3703.9	46.0	3703.5	28.8	100.0
17-2	94	104034	1.3	2.8542	1.3	37.5457	4.1	0.7772	3.9	0.95	3707.1	109.4	3708.0	40.5	3708.5	19.7	100.0
24-1	179	32927	2.3	2.9465	1.8	35.5904	2.7	0.7606	2.0	0.74	3646.3	55.4	3655.2	26.7	3660.0	28.0	99.6
24-2	61	19931	0.6	3.0014	1.5	34.8070	2.5	0.7577	2.0	0.80	3635.8	54.7	3633.2	24.4	3631.8	23.0	100.1
EKCO2-51	41	10126	1.4	3.8085	2.7	22.9704	7.5	0.6345	7.0	0.93	3167.3	174.5	3225.7	73.0	3262.2	42.9	97.1
EKCO2-51	21	5359	2.1	3.7765	2.1	24.1120	6.5	0.6604	6.2	0.95	3268.8	158.2	3272.9	63.7	3275.5	33.5	99.8

SAB94-77																	
U-Pb geochronologic analyses.																	
							Isotope ratios						Apparent ages (Ma)				
grain-spot	U	206Pb	U/Th	206Pb*	±	207Pb*	±	206Pb*	±	error	206Pb*	±	207Pb*	±	206Pb*	±	Conc
	(ppm)	204Pb		207Pb*	(%)	235U*	(%)	238U	(%)	corr.	238U*	(Ma)	235U	(Ma)	207Pb*	(Ma)	(%)
00-2	197	44734	2.4	2.7531	1.3	37.6544	4.4	0.7519	4.2	0.95	3614.4	117.3	3710.9	44.0	3763.4	20.0	96.0
02-2	48	11405	1.7	2.9929	1.7	34.9450	2.1	0.7585	1.3	0.61	3638.9	35.3	3637.1	20.7	3636.1	25.6	100.1
12-1	77	14649	0.9	3.7825	2.3	24.3485	3.6	0.6680	2.8	0.77	3298.0	72.0	3282.4	35.2	3273.0	36.0	100.8
12-2	152	39860	1.0	2.7561	1.4	39.0031	3.4	0.7796	3.1	0.92	3715.8	86.7	3745.7	33.2	3761.7	20.5	98.8
13-1	124	33544	1.8	2.8151	1.8	38.1659	3.3	0.7792	2.8	0.84	3714.3	77.6	3724.2	32.3	3729.6	26.8	99.6
13-2	361	59491	0.8	3.0470	2.0	34.3324	3.2	0.7587	2.5	0.77	3639.5	69.0	3619.6	31.6	3608.7	31.1	100.9
14-2	58	40699	1.4	2.8097	1.7	38.5746	4.9	0.7861	4.6	0.94	3739.1	129.7	3734.8	48.2	3732.5	25.6	100.2
15-1	69	4398	1.4	3.0821	2.6	34.0227	3.9	0.7605	3.0	0.75	3646.2	82.2	3610.7	38.6	3591.1	39.4	101.5
15-2	47	5037	1.7	2.7459	1.9	39.6478	3.5	0.7896	3.0	0.85	3751.7	85.3	3761.9	35.0	3767.4	28.4	99.6
17-2	60	16828	1.3	2.7730	2.3	39.5970	3.4	0.7964	2.5	0.74	3776.1	71.2	3760.7	33.4	3752.5	34.6	100.6
18-2	129	52451	1.4	3.3600	2.0	28.9851	4.6	0.7063	4.2	0.91	3444.6	112.4	3453.0	45.6	3457.9	30.2	99.6
24-1	105	21390	2.1	2.7563	2.1	40.1354	5.5	0.8023	5.0	0.92	3797.5	144.4	3774.0	54.2	3761.6	32.3	101.0
24-2	67	41306	1.6	2.7117	1.9	41.4593	4.1	0.8154	3.6	0.89	3844.0	105.1	3806.2	40.6	3786.4	28.5	101.5
25-2	321	85538	4.0	2.9771	1.3	35.6782	5.6	0.7704	5.5	0.97	3682.1	154.0	3657.6	55.7	3644.2	19.4	101.0
26-2	61	5443	1.7	3.1107	2.0	33.5520	3.4	0.7570	2.8	0.81	3633.1	76.4	3597.0	33.7	3576.9	31.1	101.6
EKCO2-51	37	9622	2.7	3.9888	4.3	22.6457	7.0	0.6551	5.6	0.79	3248.2	141.9	3211.8	68.3	3189.2	67.8	101.9

SAB94-134																	
U-Pb geochronologic analyses.																	
							Isotope ratios						Apparent ages (Ma)				
grain-spot	U	206Pb	U/Th	206Pb*	±	207Pb*	±	206Pb*	±	error	206Pb*	±	207Pb*	±	206Pb*	±	Conc
	(ppm)	204Pb		207Pb*	(%)	235U*	(%)	238U	(%)	corr.	238U*	(Ma)	235U	(Ma)	207Pb*	(Ma)	(%)
00-1	150	2124	1.0	2.7389	1.5	39.7333	4.2	0.7893	3.9	0.93	3750.6	110.6	3764.1	41.3	3771.2	22.8	99.5
00-2	203	917	1.3	3.1677	5.2	25.4562	11.8	0.5848	10.6	0.90	2968.5	252.5	3325.9	115.7	3548.9	79.4	83.6
01-1	145	43529	0.9	2.7769	1.4	38.9579	4.5	0.7846	4.3	0.95	3733.8	121.3	3744.6	44.5	3750.3	21.0	99.6
01-2	178	34866	0.9	2.7703	1.7	39.3304	2.4	0.7902	1.8	0.73	3754.0	50.1	3754.0	23.9	3754.0	25.1	100.0
08-1	373	10009	5.4	3.0384	1.9	33.5478	4.6	0.7393	4.2	0.91	3567.9	114.5	3596.8	45.2	3613.0	28.8	98.8
08-2	602	3597	3.7	2.8090	1.4	38.8385	4.1	0.7913	3.8	0.94	3757.7	109.4	3741.5	40.5	3732.9	21.1	100.7
09-1	213	55014	0.9	2.7107	1.3	39.7476	2.7	0.7814	2.3	0.87	3722.3	65.0	3764.4	26.3	3786.9	20.0	98.3
09-2	621	37657	1.7	2.3029	1.5	52.8099	4.6	0.8821	4.4	0.95	4076.5	132.0	4046.8	46.0	4032.1	21.9	101.1
10-1	157	21843	0.9	2.7395	1.6	38.6604	3.7	0.7681	3.4	0.90	3674.0	93.8	3737.0	36.9	3770.9	24.9	97.4
10-2	364	18562	1.8	2.5445	1.7	44.2394	2.5	0.8164	1.8	0.72	3847.6	51.6	3870.6	24.6	3882.5	25.9	99.1
14-1	144	189396	1.0	2.7269	1.9	39.9906	3.7	0.7909	3.2	0.86	3756.5	91.1	3770.5	37.0	3777.9	29.1	99.4
14-2	793	5031	9.4	2.7266	1.5	39.8197	4.7	0.7874	4.4	0.94	3744.0	125.5	3766.2	46.4	3778.1	23.4	99.1
15-1	221	4810	2.5	2.7475	3.3	35.9254	6.6	0.7159	5.7	0.87	3480.5	154.4	3664.4	65.4	3766.5	49.8	92.4
15-2	1438	37948	2.3	3.0354	4.4	24.2229	10.0	0.5333	9.0	0.90	2755.2	201.6	3277.4	98.1	3614.5	68.1	76.2
19-1	217	40947	9.0	2.9221	1.5	33.7471	3.1	0.7152	2.8	0.88	3478.0	73.9	3602.7	31.0	3672.7	23.2	94.7
19-2	372	49437	2.1	2.4251	1.5	46.6275	2.7	0.8201	2.3	0.83	3860.7	66.2	3922.8	27.2	3954.7	22.7	97.6
20-1	201	74934	0.8	2.7903	1.4	37.5586	4.2	0.7601	3.9	0.94	3644.6	109.4	3708.4	41.3	3743.0	21.1	97.4
20-2	694	97162	1.6	2.2227	2.2	55.9465	4.2	0.9019	3.6	0.85	4144.0	109.4	4104.3	41.9	4084.9	32.6	101.4
23-1	286	44380	5.0	2.4127	1.8	46.1593	3.1	0.8077	2.5	0.81	3816.7	71.1	3912.8	30.3	3962.4	26.8	96.3
23-2	885	96021	4.2	2.5797	7.0	40.3503	7.2	0.7549	1.7	0.23	3625.7	45.8	3779.3	71.1	3861.8	105.3	93.9
25-1	321	77310	1.8	2.8082	0.7	35.8553	2.6	0.7303	2.5	0.96	3534.4	66.7	3662.5	25.3	3733.3	11.1	94.7
25-2	569	7025	4.2	2.4705	2.4	43.7857	4.6	0.7845	3.9	0.85	3733.5	110.0	3860.4	45.5	3926.9	36.7	95.1
27-1	101	36946	1.7	2.8826	1.6	36.4338	4.7	0.7617	4.4	0.94	3650.5	123.8	3678.3	46.6	3693.5	24.1	98.8
27-2	603	4440	2.7	2.5966	6.0	31.5402	12.2	0.5940	10.7	0.87	3005.5	256.0	3536.0	121.1	3852.0	91.3	78.0
EKCO2-51	118	49986	37.8	3.7902	1.9	23.3781	4.3	0.6426	3.9	0.90	3199.4	98.4	3242.8	42.1	3269.8	29.1	97.8
EKCO2-51	75	28505	8.5	3.8573	2.0	22.7705	3.6	0.6370	3.0	0.83	3177.3	74.5	3217.2	34.9	3242.1	31.7	98.0

SAB96-60																	
U-Pb geochronologic analyses.																	
							Isotope ratios						Apparent ages (Ma)				
grain-spot	U	206Pb	U/Th	206Pb*	±	207Pb*	±	206Pb*	±	error	206Pb*	±	207Pb*	±	206Pb*	±	Conc
	(ppm)	204Pb		207Pb*	(%)	235U*	(%)	238U	(%)	corr.	238U*	(Ma)	235U	(Ma)	207Pb*	(Ma)	(%)
01-2	310	37730	3.3	3.4411	2.0	28.2248	6.1	0.7044	5.8	0.95	3437.4	155.1	3426.9	60.3	3420.8	30.3	100.5
02-2	117	37271	1.8	3.0773	1.4	33.2892	5.2	0.7430	5.1	0.96	3581.6	138.8	3589.2	51.7	3593.5	21.7	99.7
03-2	150	67238	1.8	3.0447	1.7	34.4019	4.6	0.7597	4.3	0.93	3643.1	118.8	3621.6	45.4	3609.8	26.2	100.9
04-1	450	15082	12.3	3.5088	5.9	25.3094	9.8	0.6441	7.9	0.80	3205.0	198.8	3320.2	96.3	3390.5	91.9	94.5
04-2	180	45453	1.1	3.1038	5.0	32.9968	11.6	0.7428	10.5	0.90	3580.9	288.7	3580.5	115.1	3580.3	76.7	100.0
06-2	165	12371	2.4	3.2703	2.3	28.8780	3.5	0.6849	2.6	0.75	3363.3	68.7	3449.4	34.3	3499.8	35.7	96.1
08-2	146	60510	1.6	3.1326	2.8	31.8842	6.6	0.7244	6.0	0.91	3512.5	161.4	3546.7	64.9	3566.1	43.1	98.5
09-1	152	36266	6.4	3.3021	2.7	29.9832	3.4	0.7181	2.1	0.60	3488.8	55.2	3486.3	33.4	3484.8	41.9	100.1
09-2	242	15056	2.0	3.0179	1.6	34.4010	2.1	0.7530	1.4	0.66	3618.4	39.3	3621.6	21.2	3623.4	24.7	99.9
10-1	372	10320	4.8	3.2112	3.7	29.5953	8.5	0.6893	7.7	0.90	3379.9	201.5	3473.5	83.9	3527.9	57.7	95.8
10-2	193	14906	1.8	3.0472	2.8	28.9496	3.6	0.6398	2.3	0.63	3188.2	57.6	3451.8	35.6	3608.6	43.1	88.4

SAB96-76																	
U-Pb geochronologic analyses.																	
							Isotope ratios						Apparent ages (Ma)				
grain-spot	U	206Pb	U/Th	206Pb*	±	207Pb*	±	206Pb*	±	error	206Pb*	±	207Pb*	±	206Pb*	±	Conc
	(ppm)	204Pb		207Pb*	(%)	235U*	(%)	238U	(%)	corr.	238U*	(Ma)	235U	(Ma)	207Pb*	(Ma)	(%)
00-1	33	13627	83.2	3.4215	2.9	29.4933	5.2	0.7319	4.3	0.83	3540.4	116.3	3470.1	50.8	3429.7	45.2	103.2
01-1	13	3556	15.9	3.5889	9.2	23.4723	10.1	0.6110	4.2	0.42	3073.9	102.9	3246.7	98.6	3355.3	143.7	91.6
01-2	111	45683	11.4	3.1626	1.5	31.9223	2.6	0.7322	2.1	0.81	3541.7	57.8	3547.9	25.6	3551.4	23.3	99.7
03-2	3	3296	6.6	3.1118	14.5	31.4940	15.2	0.7108	4.6	0.30	3461.5	123.5	3534.6	151.2	3576.3	224.9	96.8
05-2	7	10800	174.6	3.2206	7.0	28.0532	8.2	0.6553	4.2	0.51	3248.8	105.9	3421.0	80.2	3523.4	108.6	92.2
06-2	26	15470	2.6	3.1074	2.6	32.8860	3.3	0.7412	2.1	0.62	3574.9	57.1	3577.2	33.0	3578.5	40.3	99.9
07-2	9	20931	71.8	3.2613	5.7	30.9281	7.9	0.7315	5.6	0.70	3539.2	151.5	3516.8	78.2	3504.0	87.6	101.0
08-1	6	5379	#DIV/0!	3.5264	13.4	27.3214	14.3	0.6988	4.7	0.33	3416.0	125.4	3395.1	140.5	3382.7	210.7	101.0
08-2	10	6270	3.9	3.0173	5.2	32.7986	5.6	0.7177	2.1	0.38	3487.6	56.8	3574.6	55.3	3623.7	79.6	96.2
EKCO2-51	35	14096	2.2	3.8235	1.5	23.5595	2.3	0.6533	1.7	0.74	3241.2	42.5	3250.3	22.1	3256.0	24.1	99.5
EKCO2-51	23	15483	2.0	3.8255	3.9	23.5722	4.7	0.6540	2.7	0.57	3243.9	69.3	3250.9	46.1	3255.2	61.0	99.7

Appendix C

Concordia plot

SAB89-28 closeup

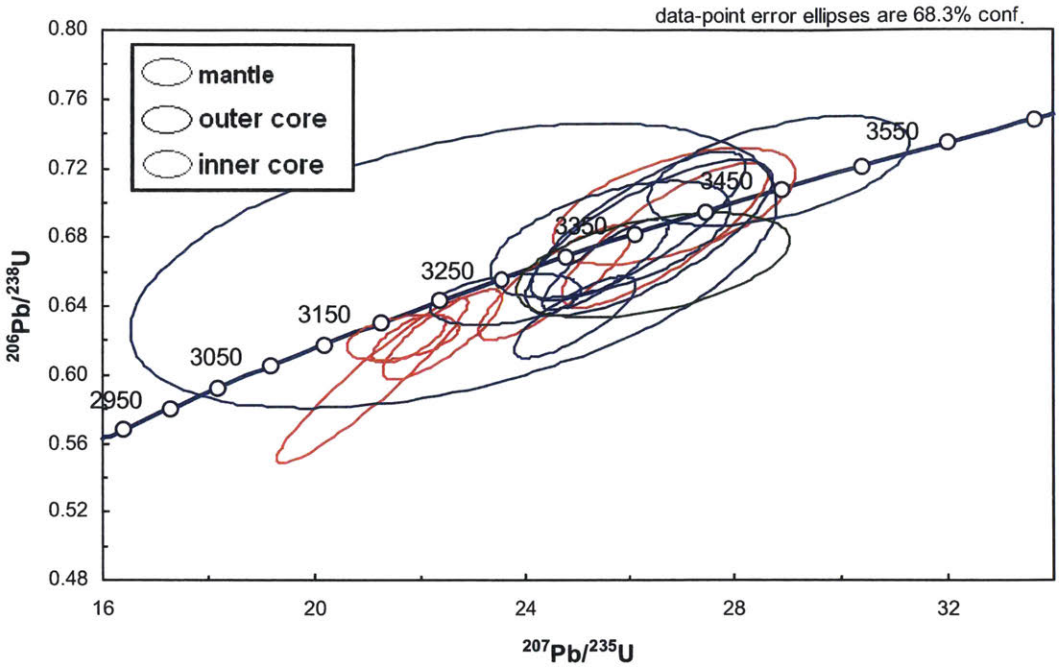

SAB89-28

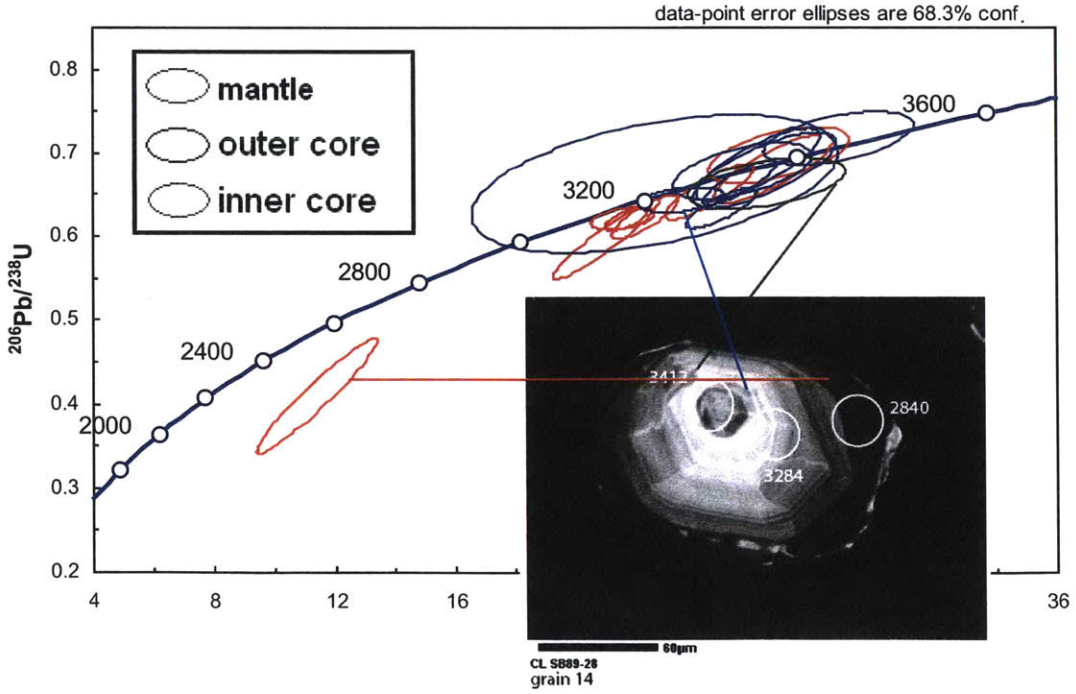

SAB91-35

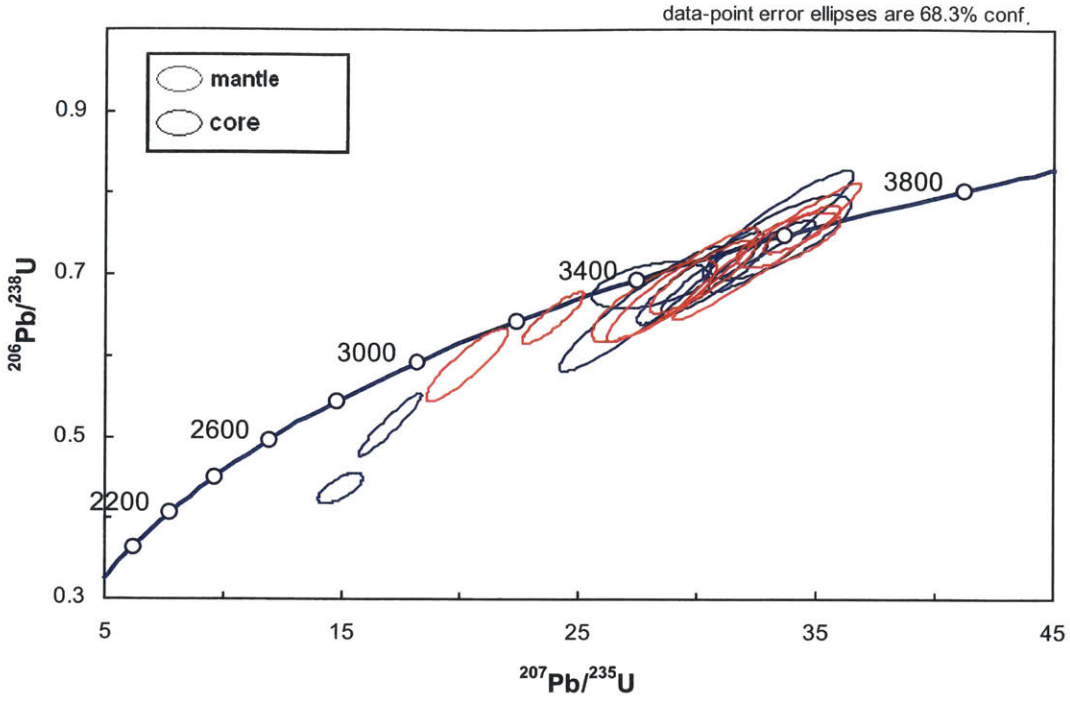

SAB91-35 closeup

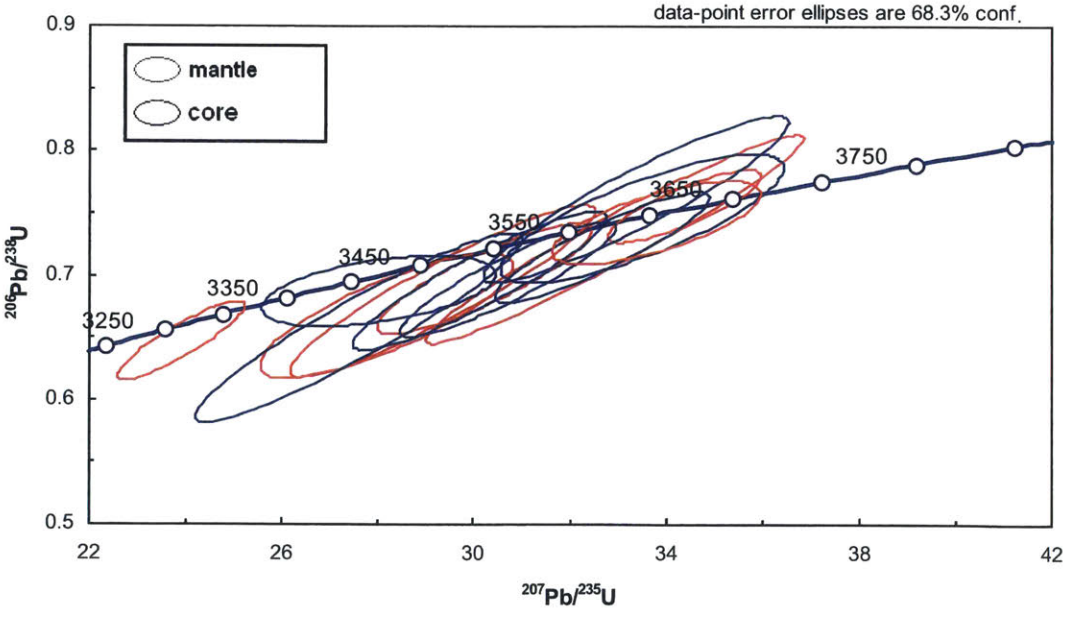

SAB91-37-3 combined data

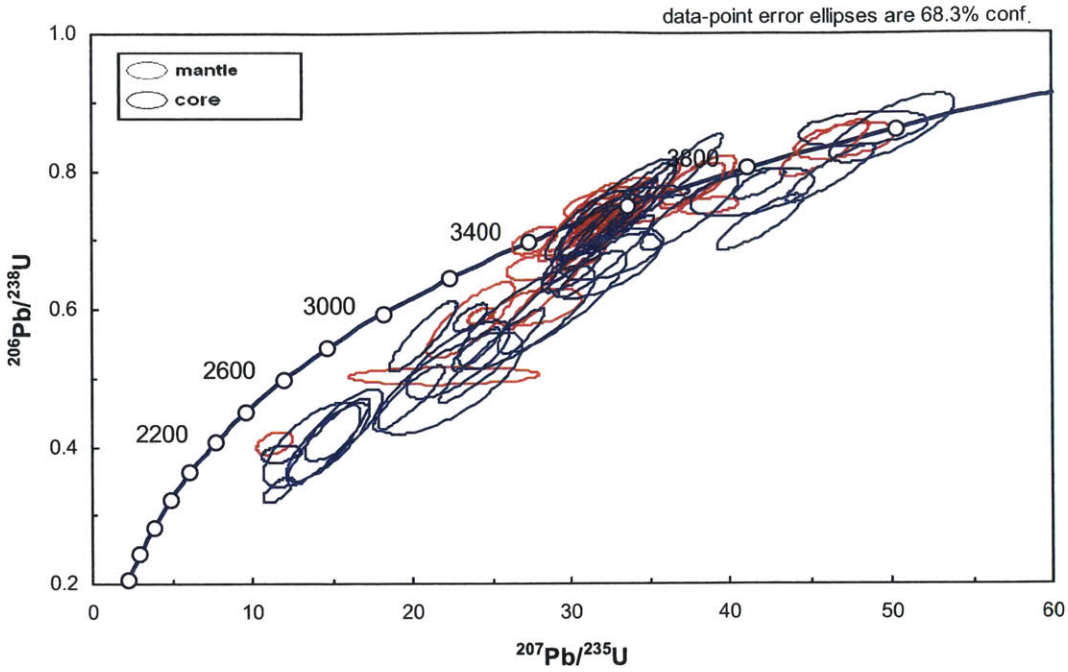

SAB91-37-3 closeup

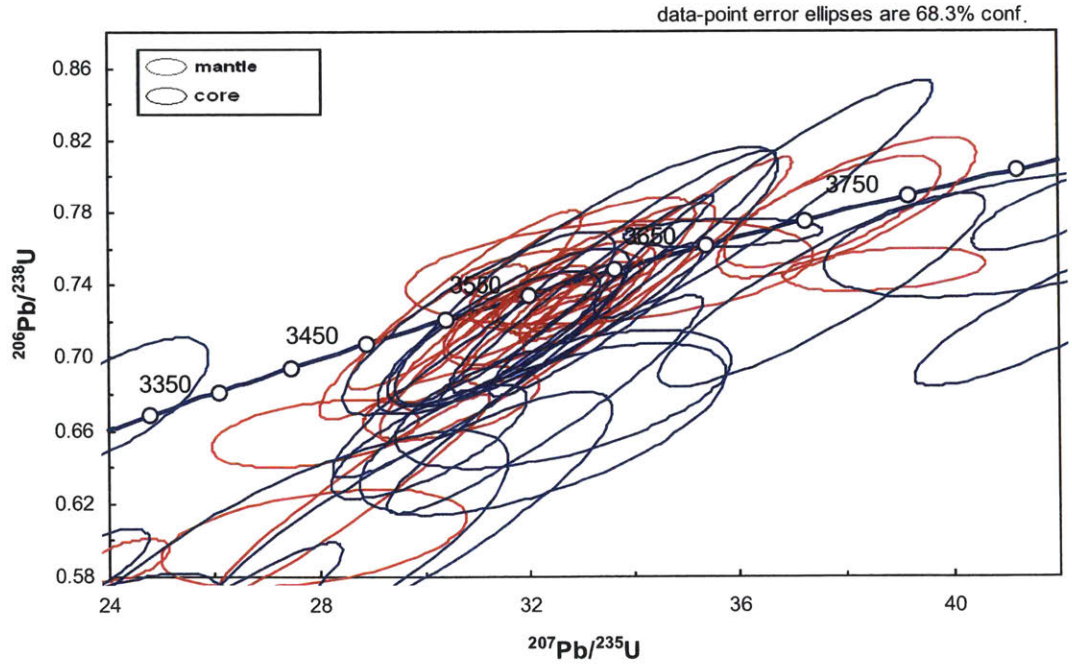

SAB91-52

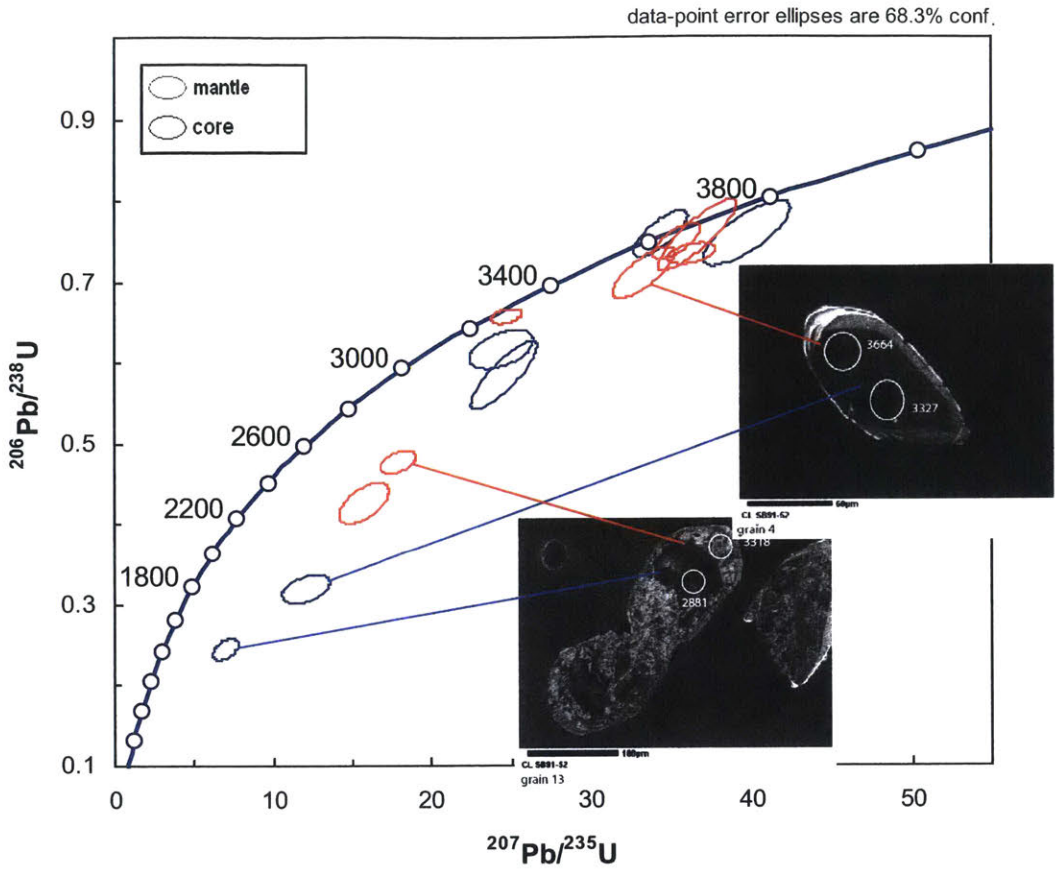
data-point error ellipses are 68.3% conf.
mantle
core
3800
3400
3000
2600
2200
1800
0.9
0.7
0.5
0.3
0.1
0
10
20
30
40
50
$^{206}Pb/^{238}U$
$^{207}Pb/^{235}U$
3664
3327
grain 4
2881
grain 13

SAB91-53

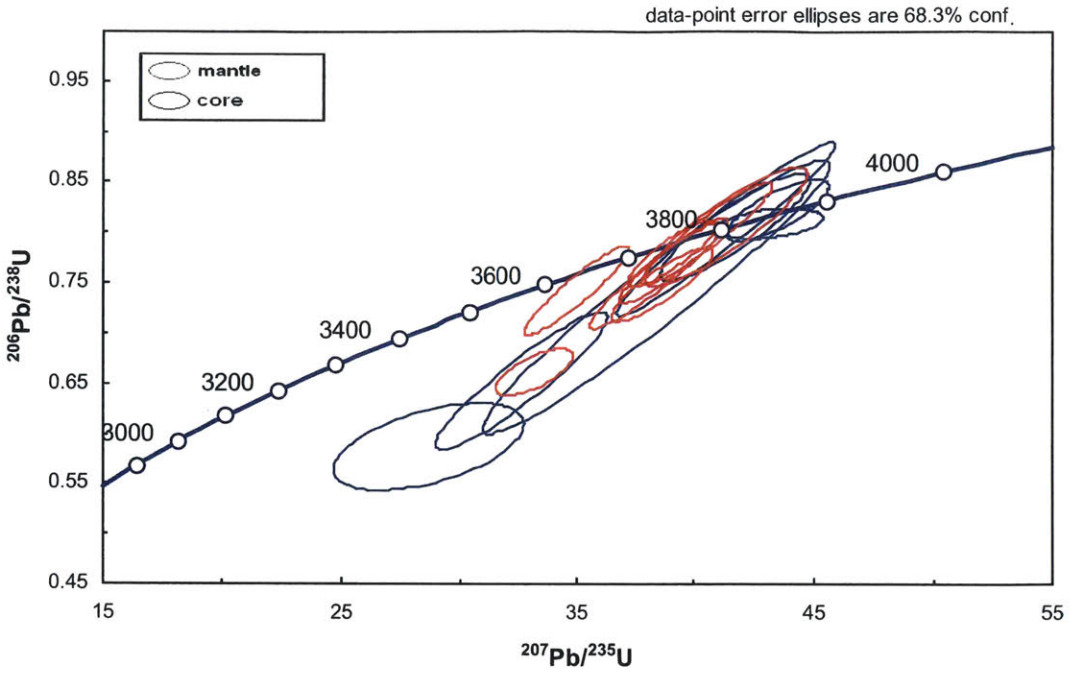

SAB91-53 closeup

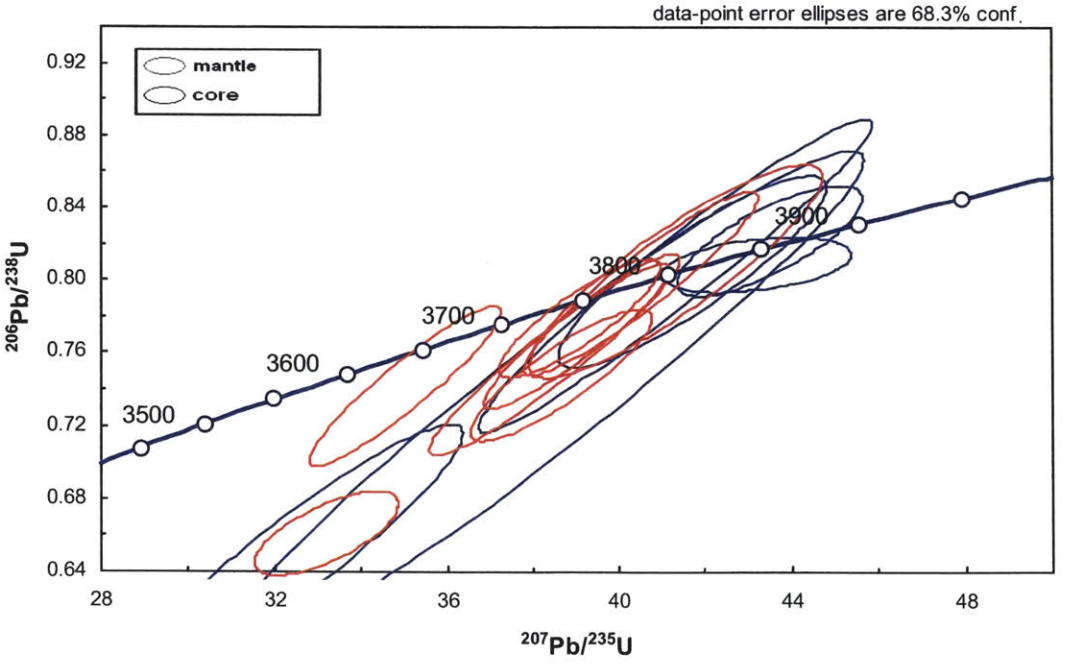

SAB91-54

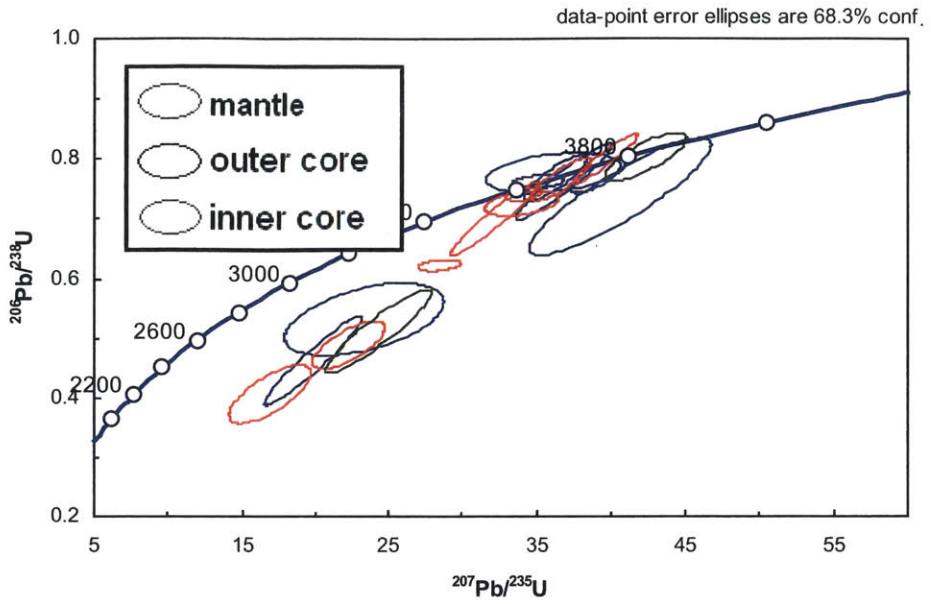

SAB91-54 closeup

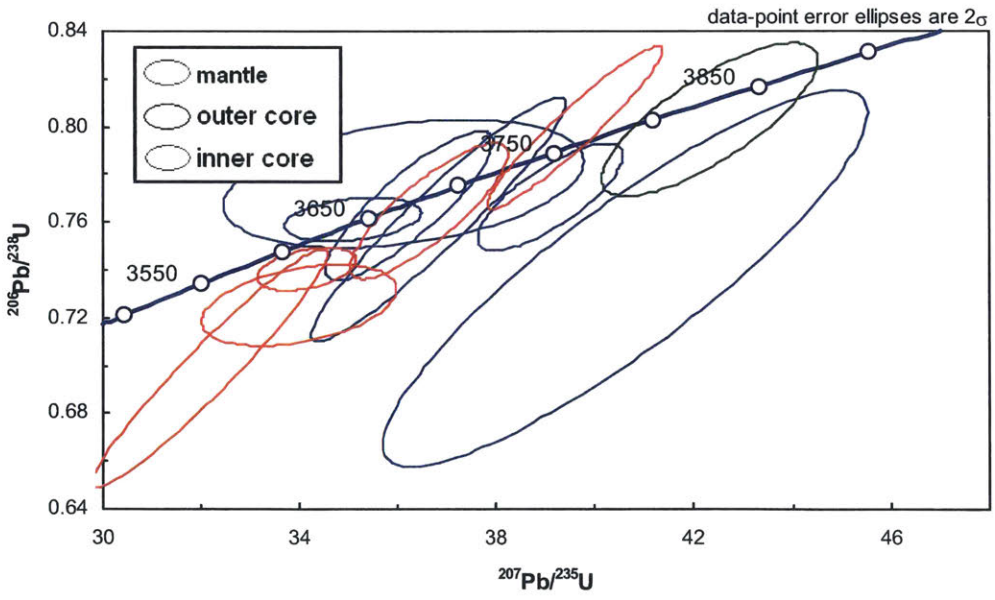

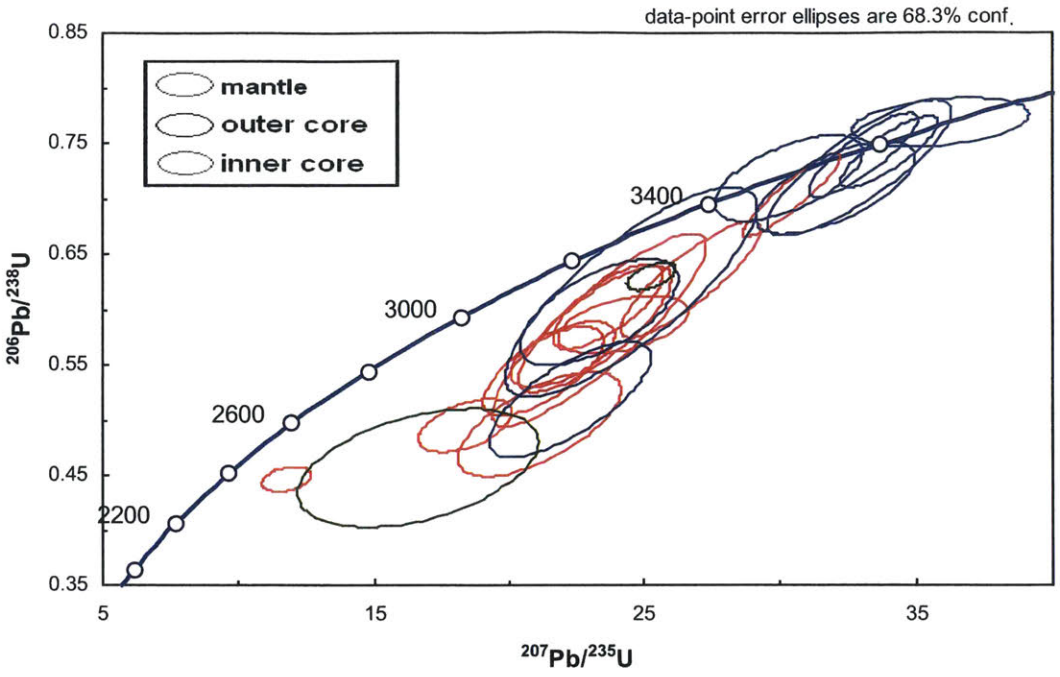
SAB91-62
data-point error ellipses are 68.3% conf.
mantle
outer core
inner core
3400
3000
2600
2200
0.85
0.75
0.65
0.55
0.45
0.35
5
15
25
35
$^{206}Pb/^{238}U$
$^{207}Pb/^{235}U$

SAB91-65

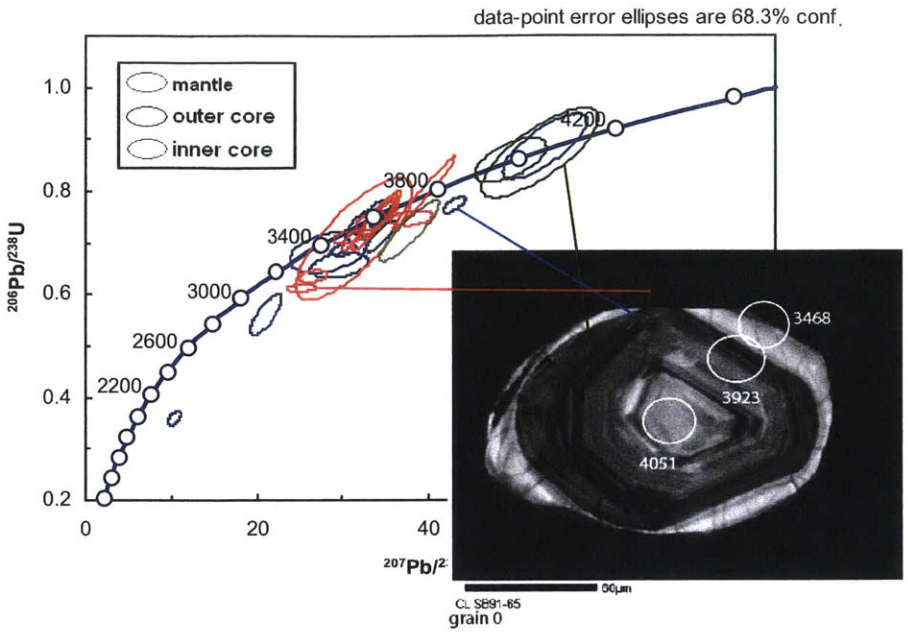

SAB91-65

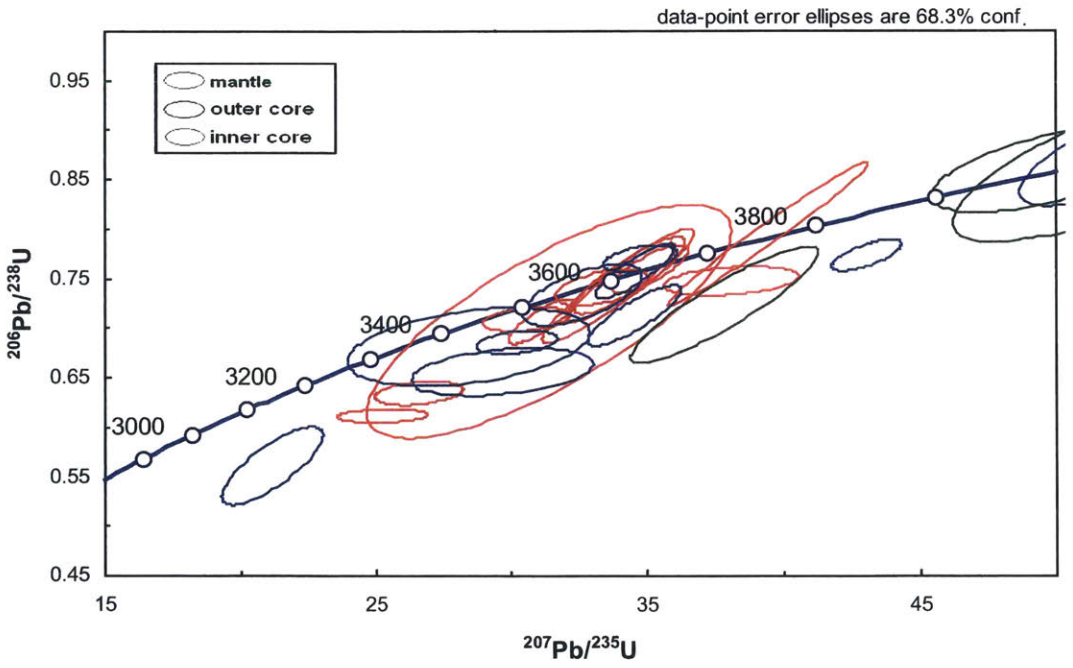

SAB91-79

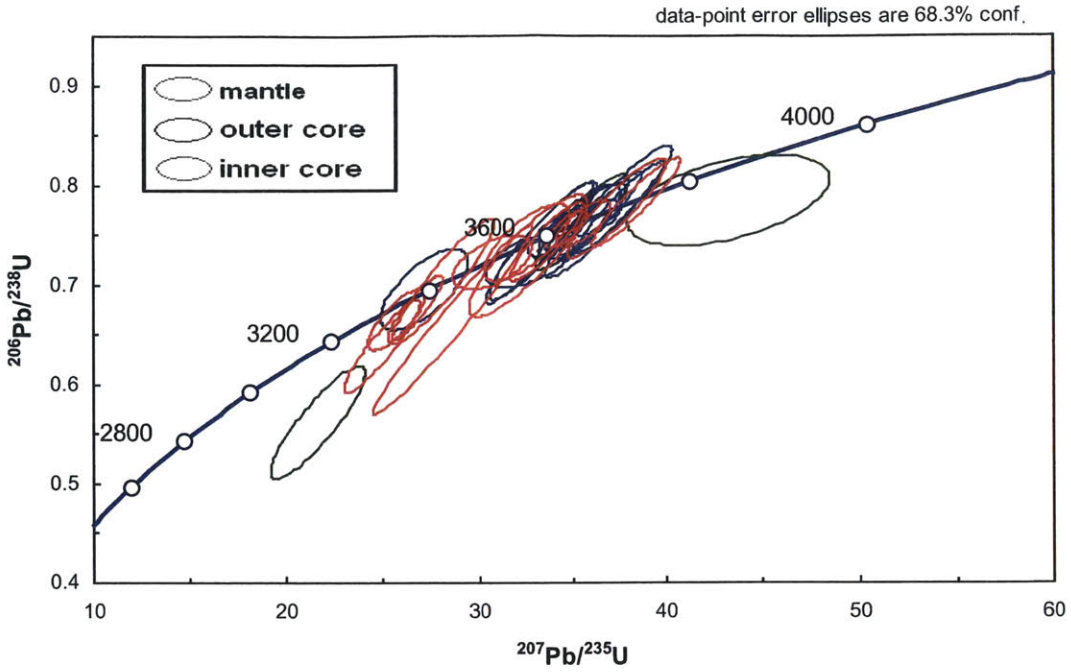

SAB91-79

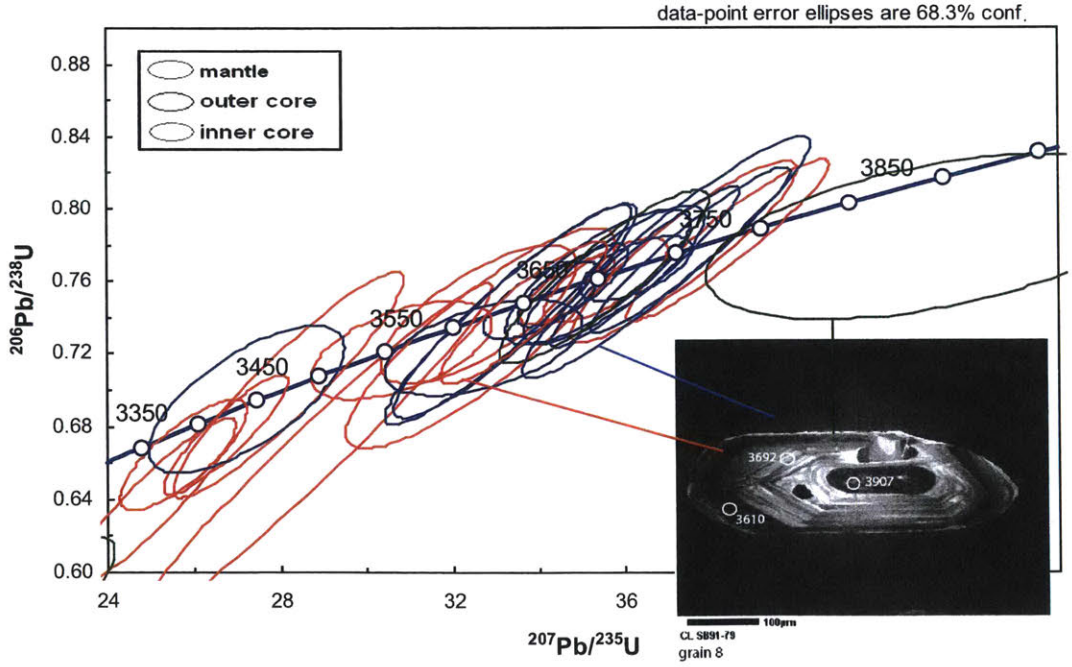

SAB94-77

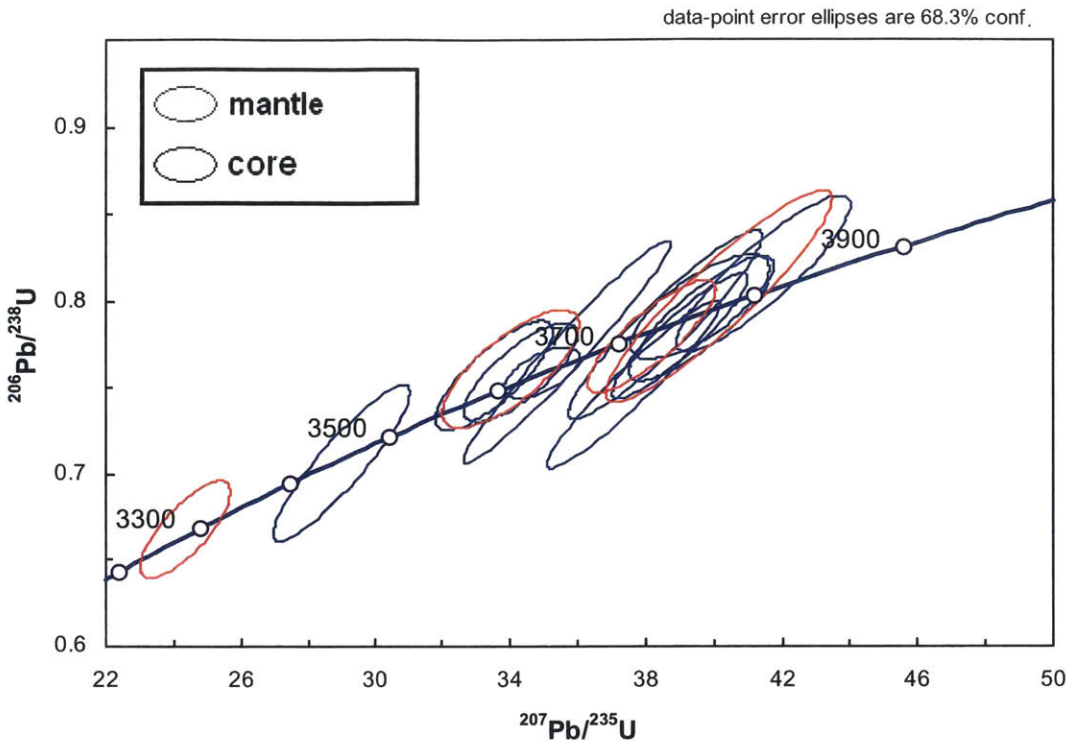
data-point error ellipses are 68.3% conf.
mantle
core
3300
3500
3700
3900
0.6
0.7
0.8
0.9
22
26
30
34
38
42
46
50
$^{206}Pb/^{238}U$
$^{207}Pb/^{235}U$

SAB94-134

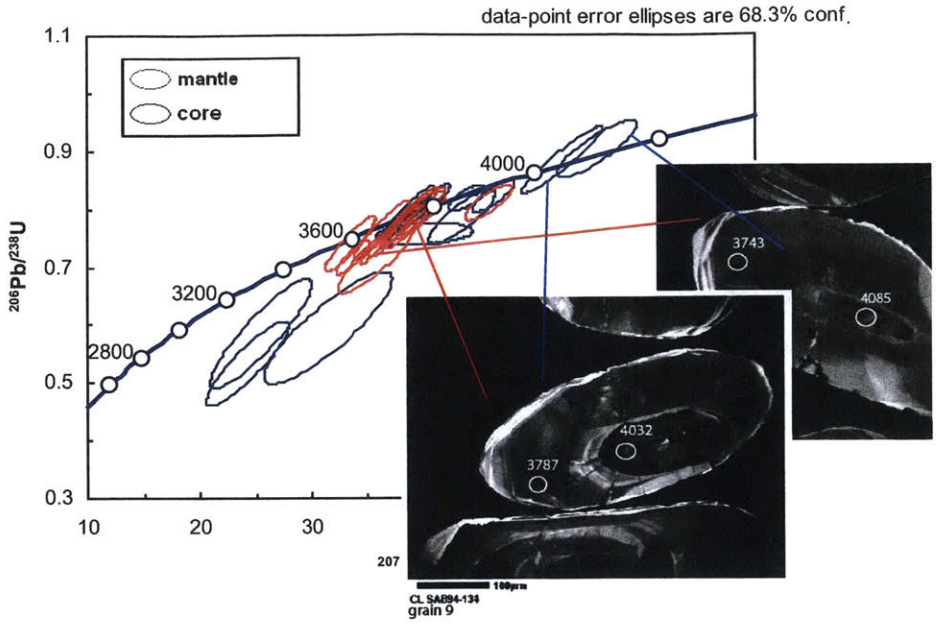

SAB94-134

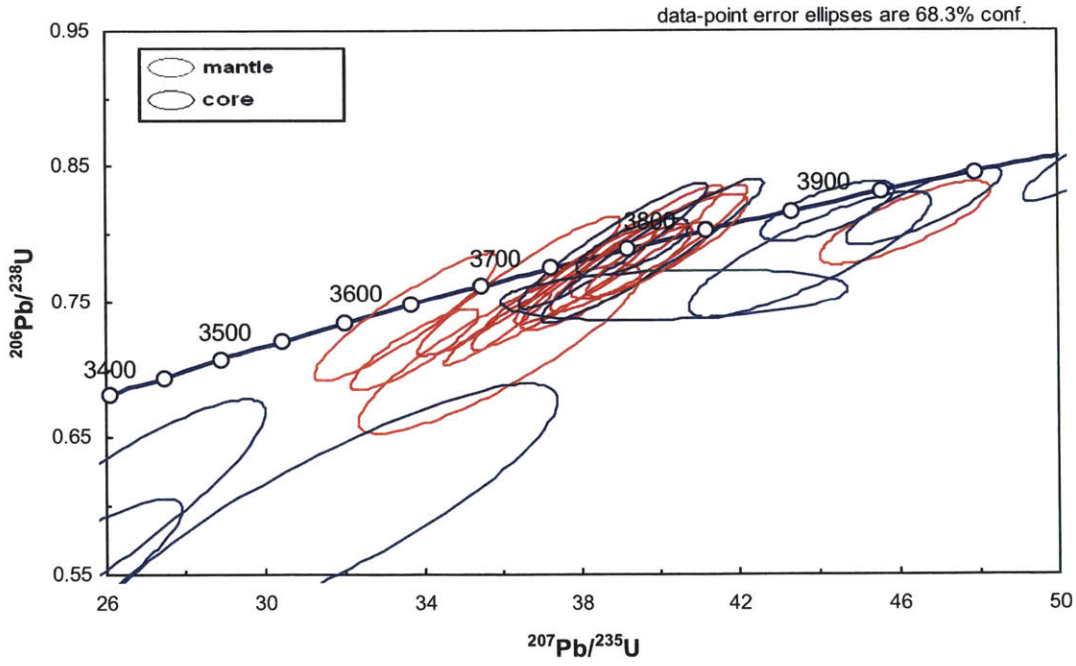

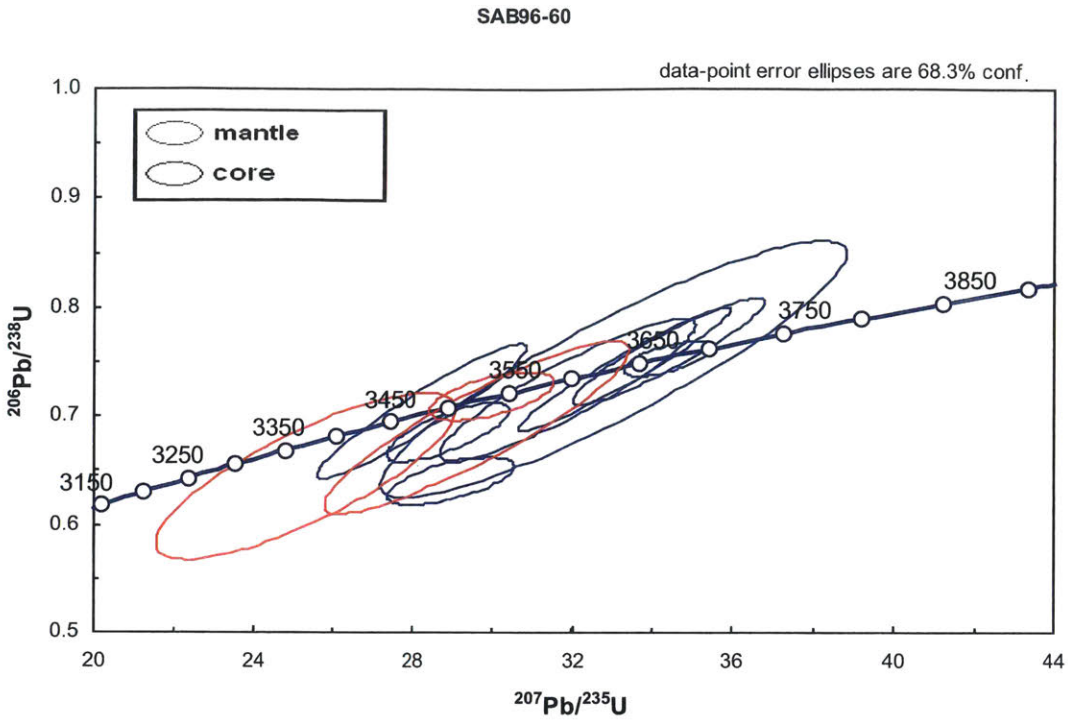
SAB96-60
data-point error ellipses are 68.3% conf.
mantle
core
1.0
0.9
0.8
0.7
0.6
0.5
20
24
28
32
36
40
44
3150
3250
3350
3450
3550
3650
3750
3850
$^{206}Pb/^{238}U$
$^{207}Pb/^{235}U$

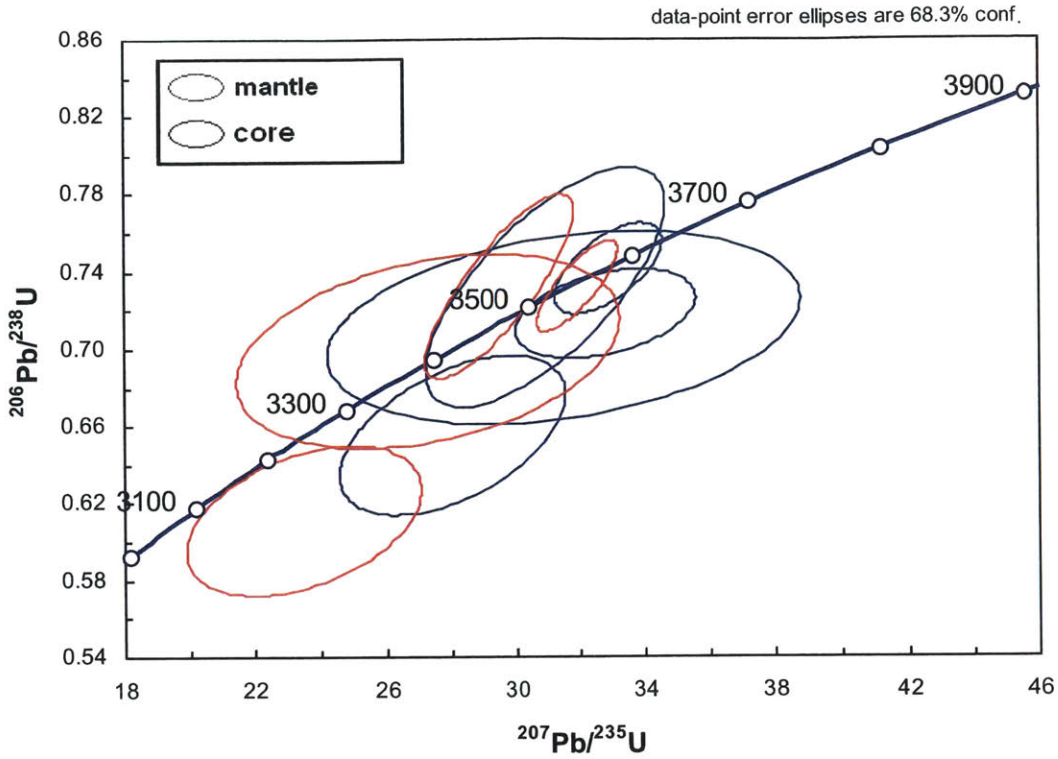
SAB96-76
data-point error ellipses are 68.3% conf.
mantle
core
3900
3700
3500
3300
3100
0.86
0.82
0.78
0.74
0.70
0.66
0.62
0.58
0.54
18
22
26
30
34
38
42
46
$^{206}Pb/^{238}U$
$^{207}Pb/^{235}U$

Appendix D

Plots of U concentration vs. concordance.

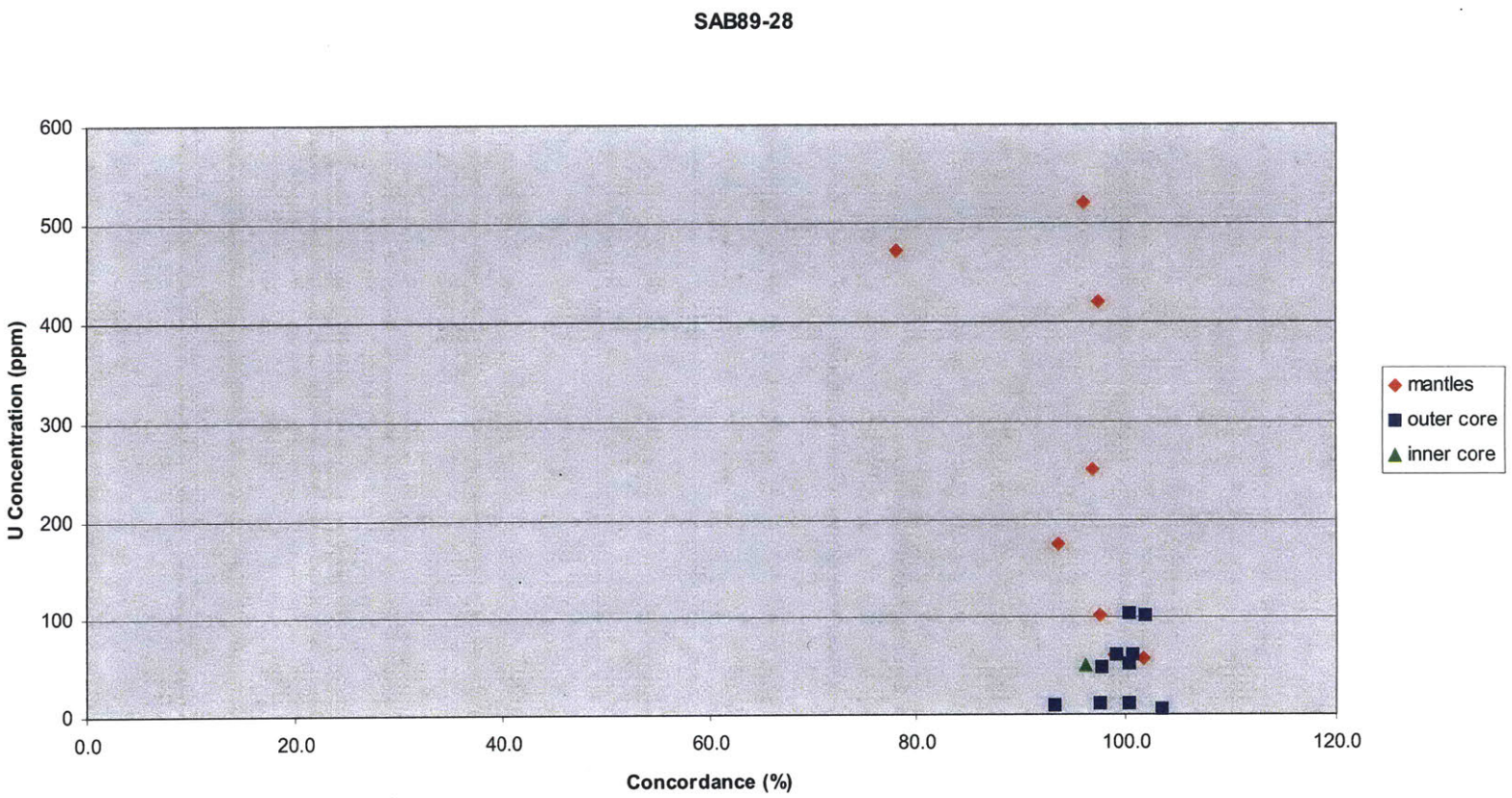
SAB89-28
U Concentration (ppm)
600
500
400
300
200
100
0
0.0
20.0
40.0
60.0
80.0
100.0
120.0
Concordance (%)
mantles
outer core
inner core

SAB91-35

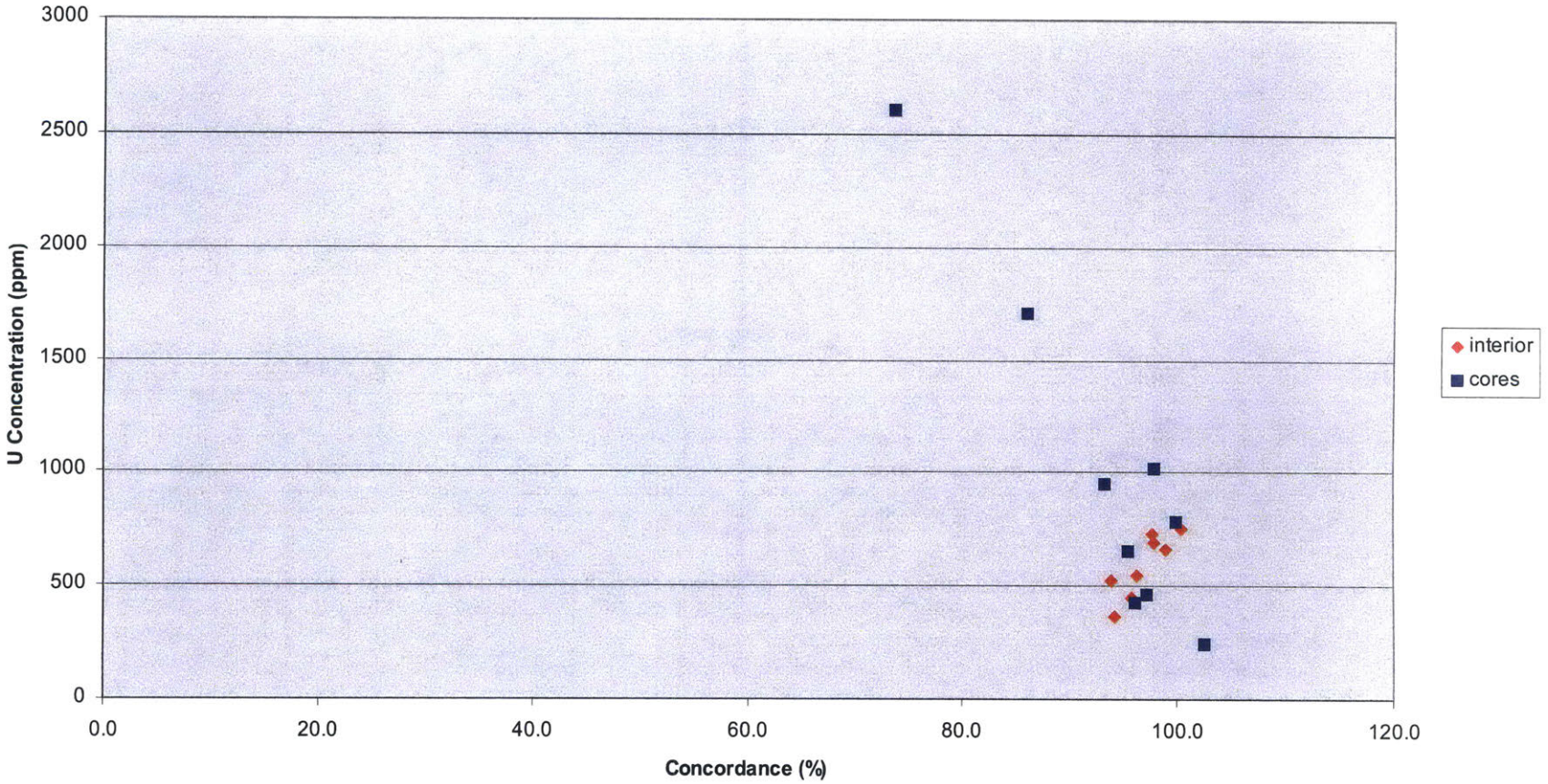
3000
2500
2000
1500
1000
500
0
U Concentration (ppm)
0.0
20.0
40.0
60.0
80.0
100.0
120.0
Concordance (%)
interior
cores

SAB91-37-3

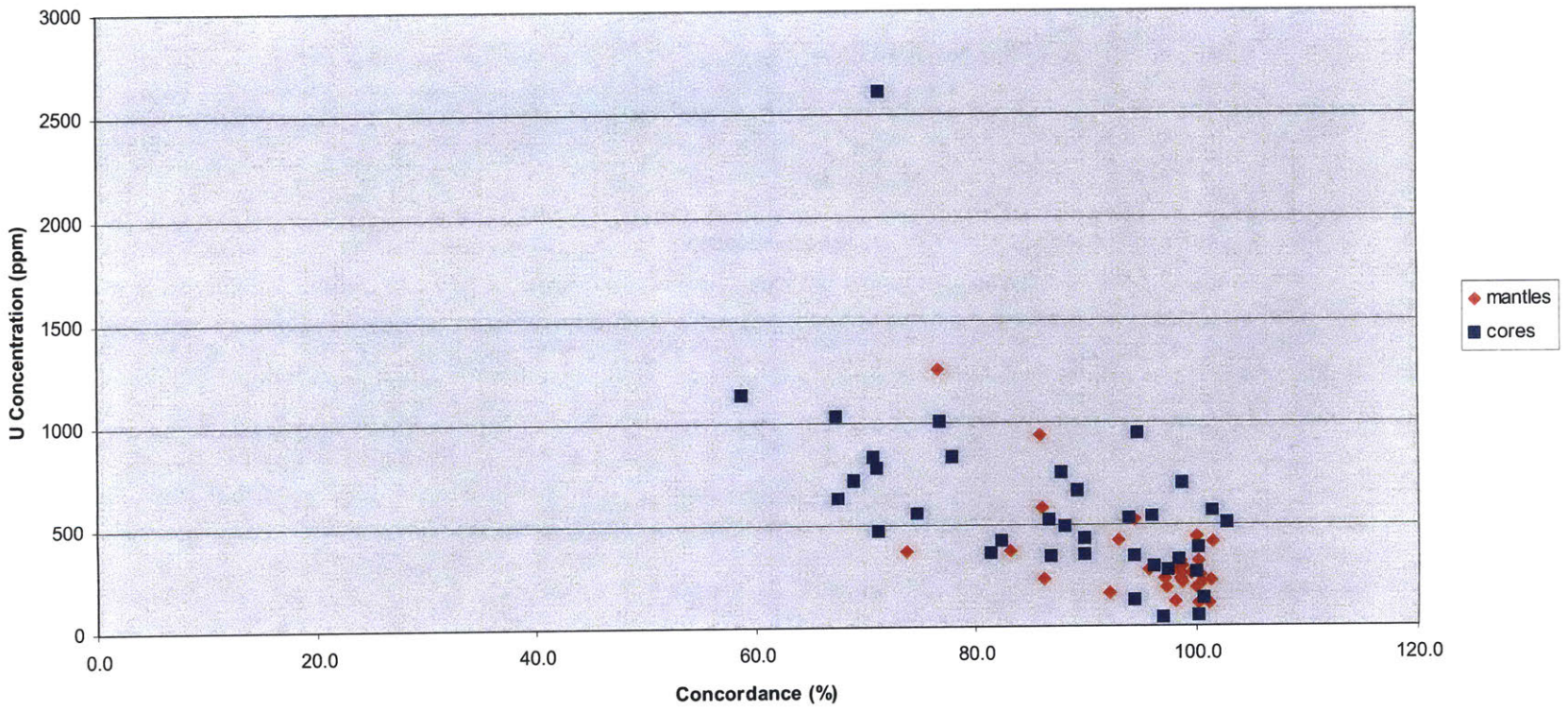
3000
2500
2000
1500
1000
500
0
U Concentration (ppm)
0.0
20.0
40.0
60.0
80.0
100.0
120.0
Concordance (%)
mantles
cores

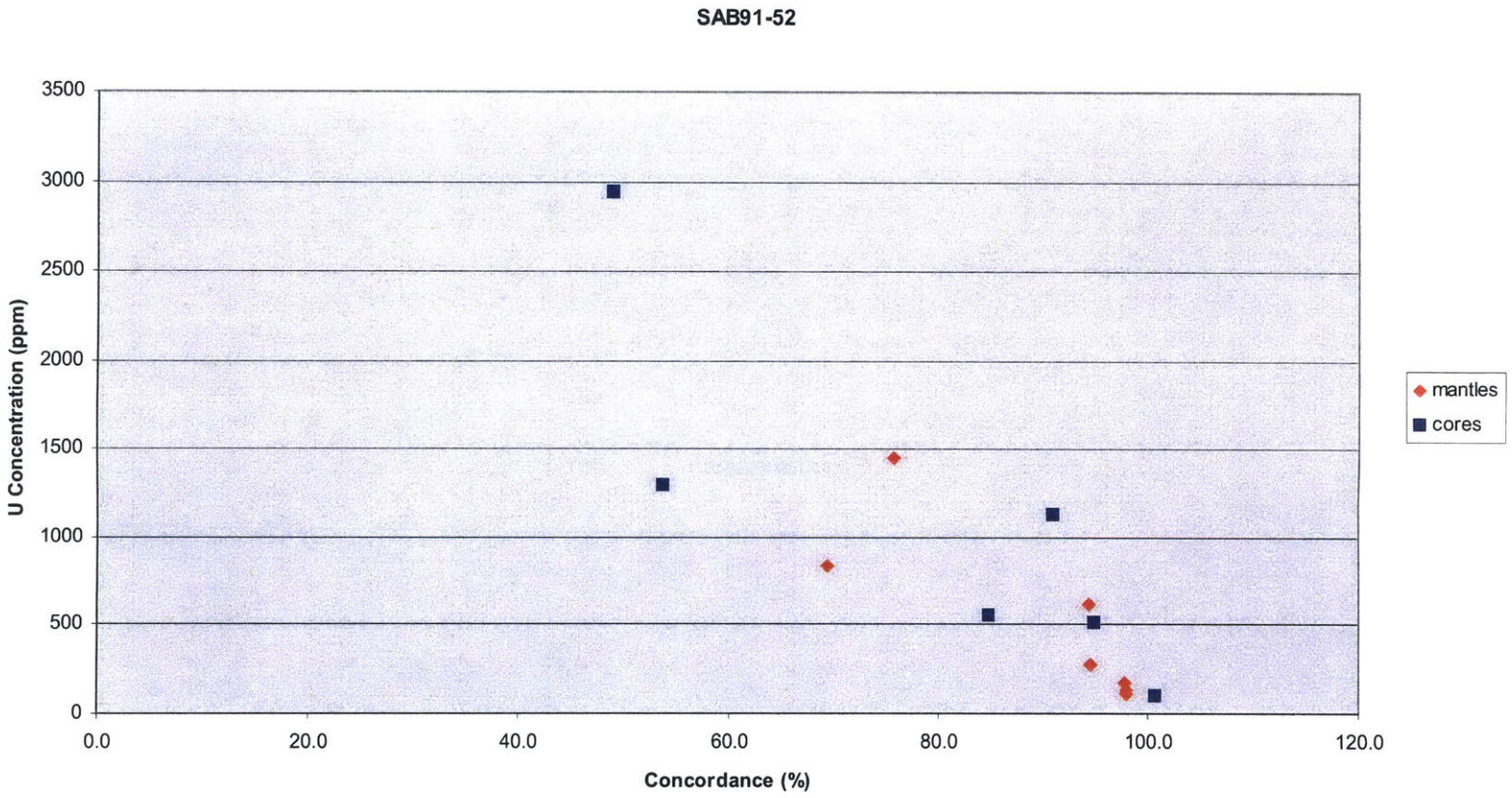
SAB91-52
3500
3000
2500
2000
1500
1000
500
0
U Concentration (ppm)
0.0
20.0
40.0
60.0
80.0
100.0
120.0
Concordance (%)
mantles
cores

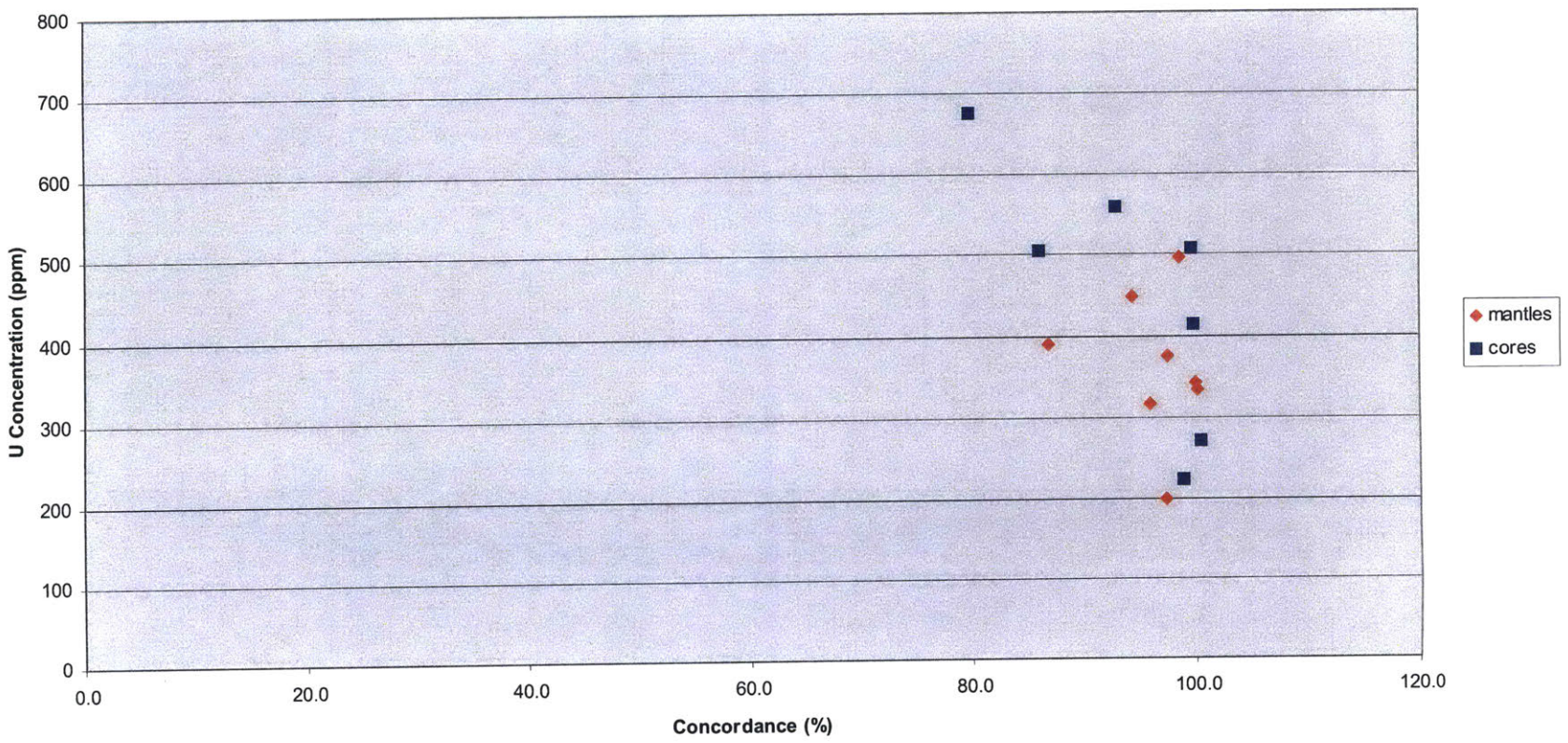
SAB91-53
800
700
600
500
400
300
200
100
0
U Concentration (ppm)
0.0
20.0
40.0
60.0
80.0
100.0
120.0
Concordance (%)
mantles
cores

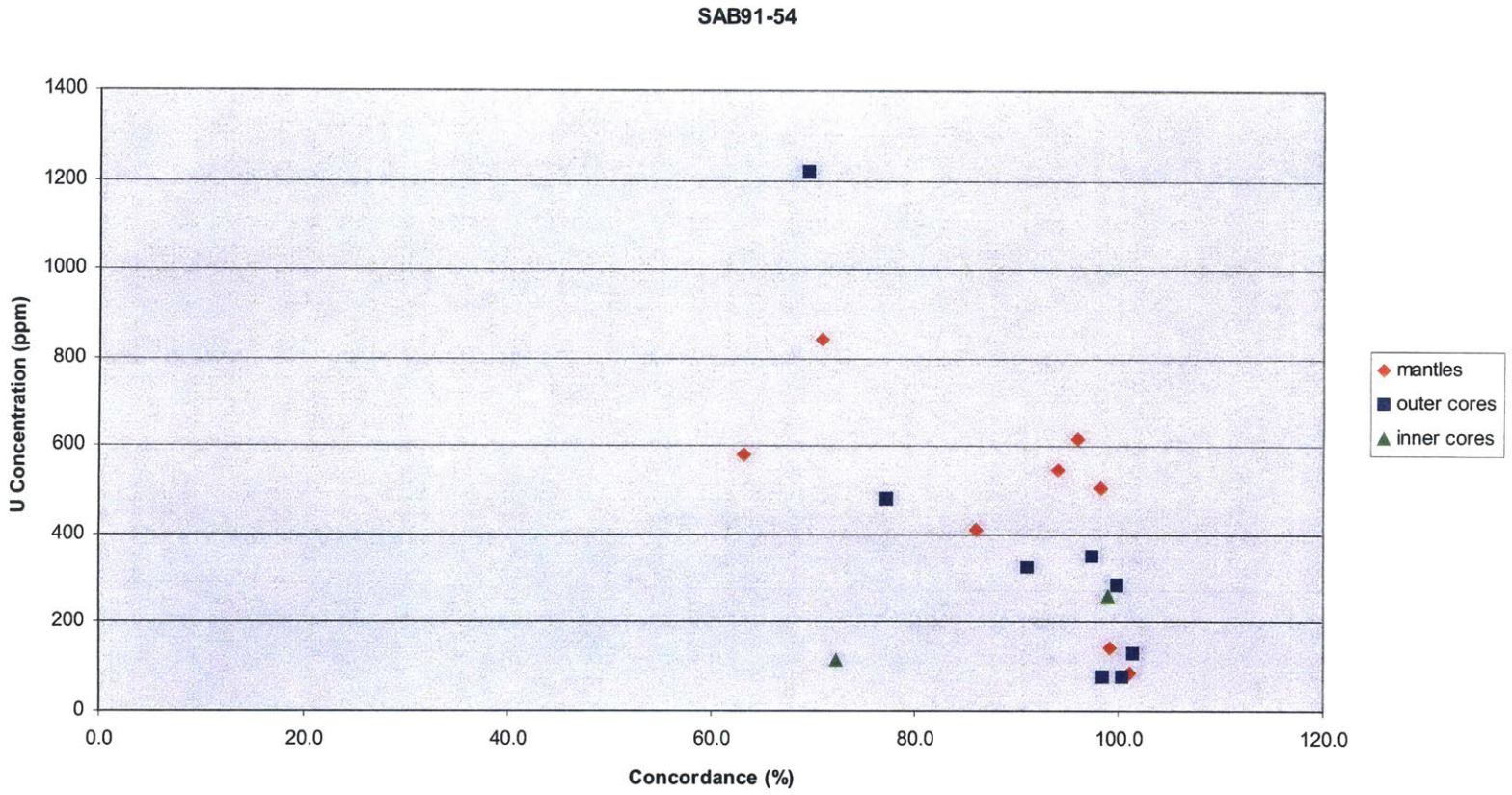
SAB91-54
U Concentration (ppm)
1400
1200
1000
800
600
400
200
0
0.0
20.0
40.0
60.0
80.0
100.0
120.0
Concordance (%)
mantles
outer cores
inner cores

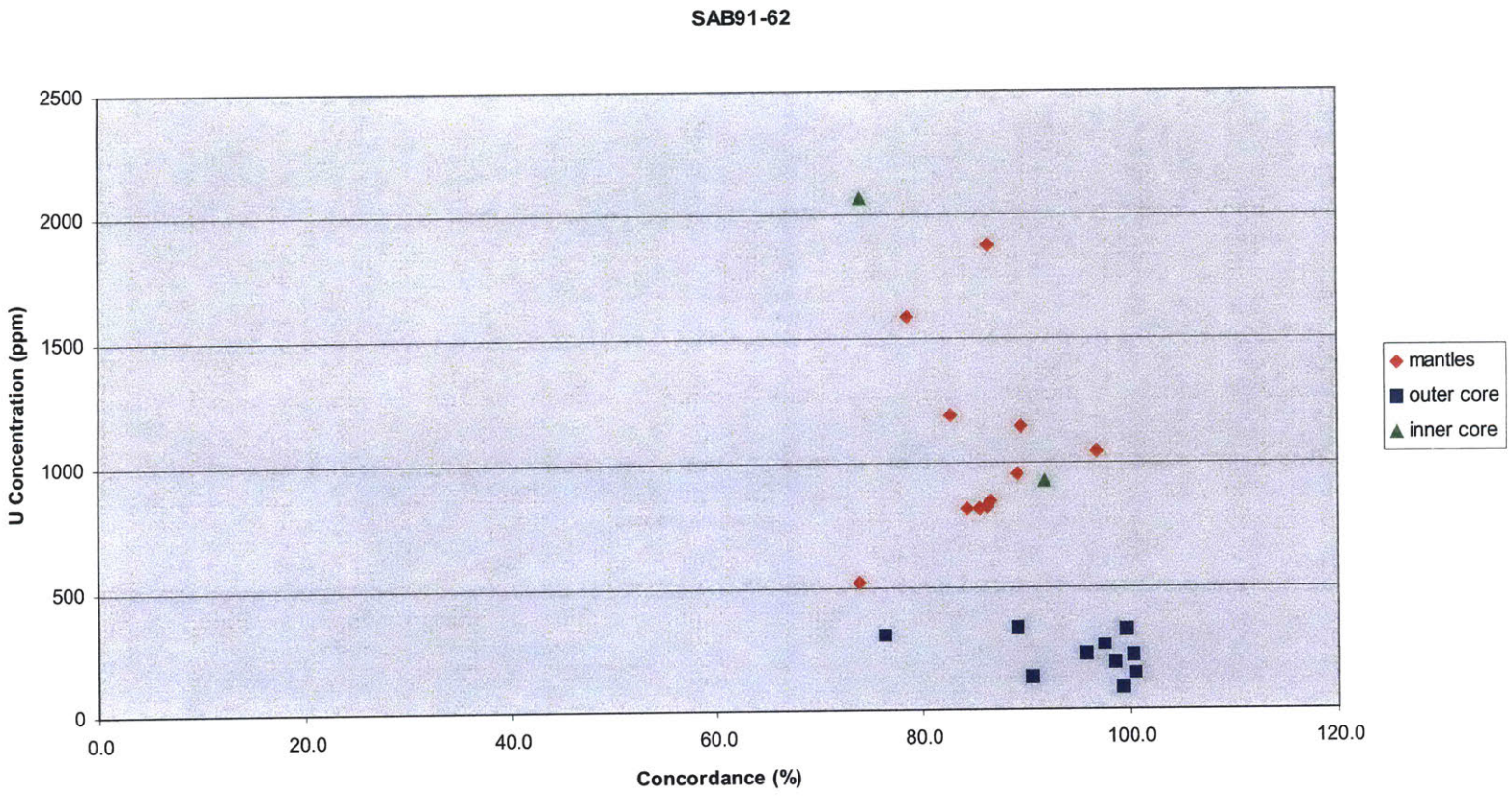
SAB91-62
2500
2000
1500
1000
500
0
U Concentration (ppm)
0.0
20.0
40.0
60.0
80.0
100.0
120.0
Concordance (%)
mantles
outer core
inner core

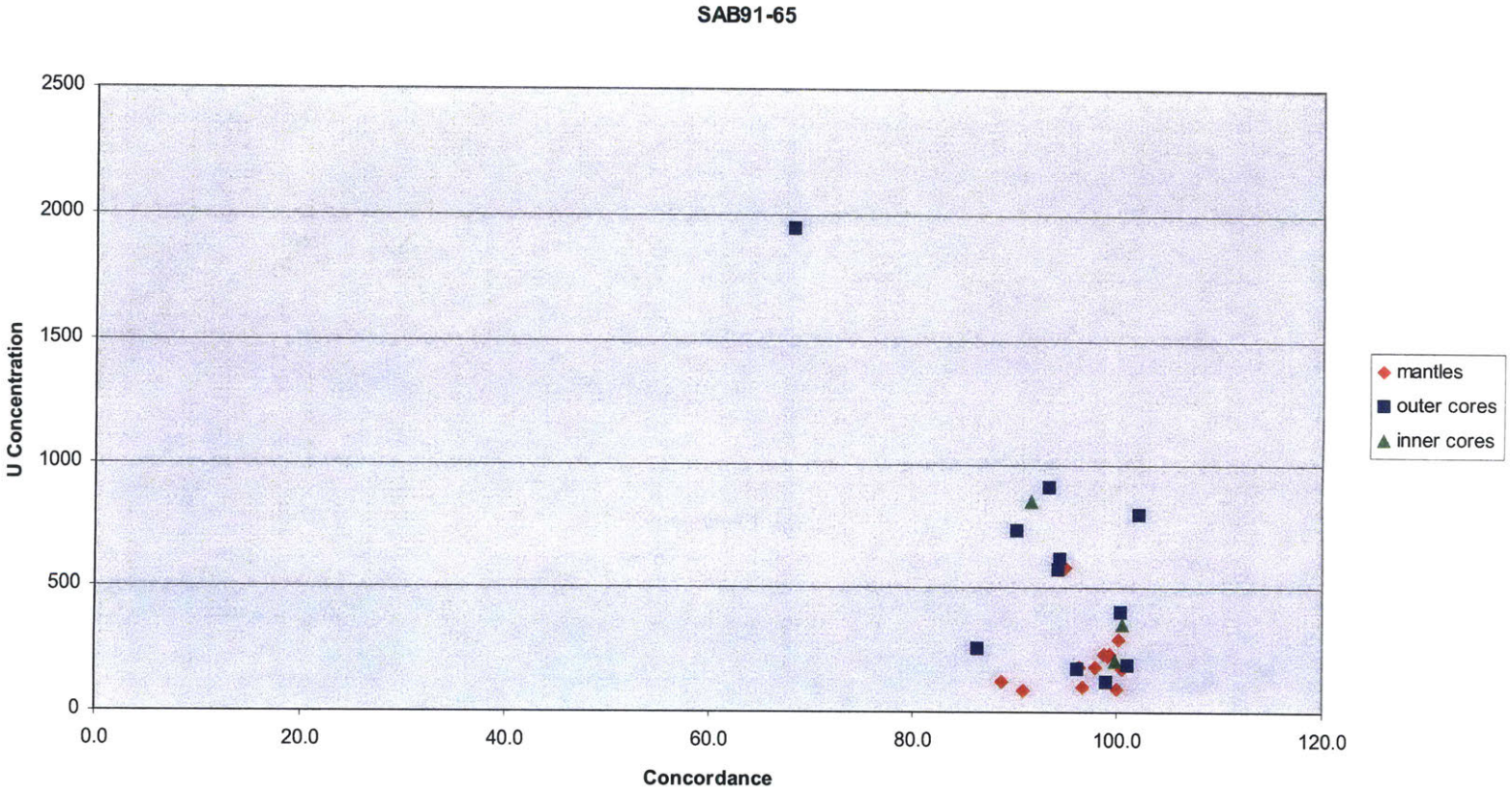
SAB91-65
2500
2000
1500
1000
500
0
U Concentration
0.0
20.0
40.0
60.0
80.0
100.0
120.0
Concordance
mantles
outer cores
inner cores

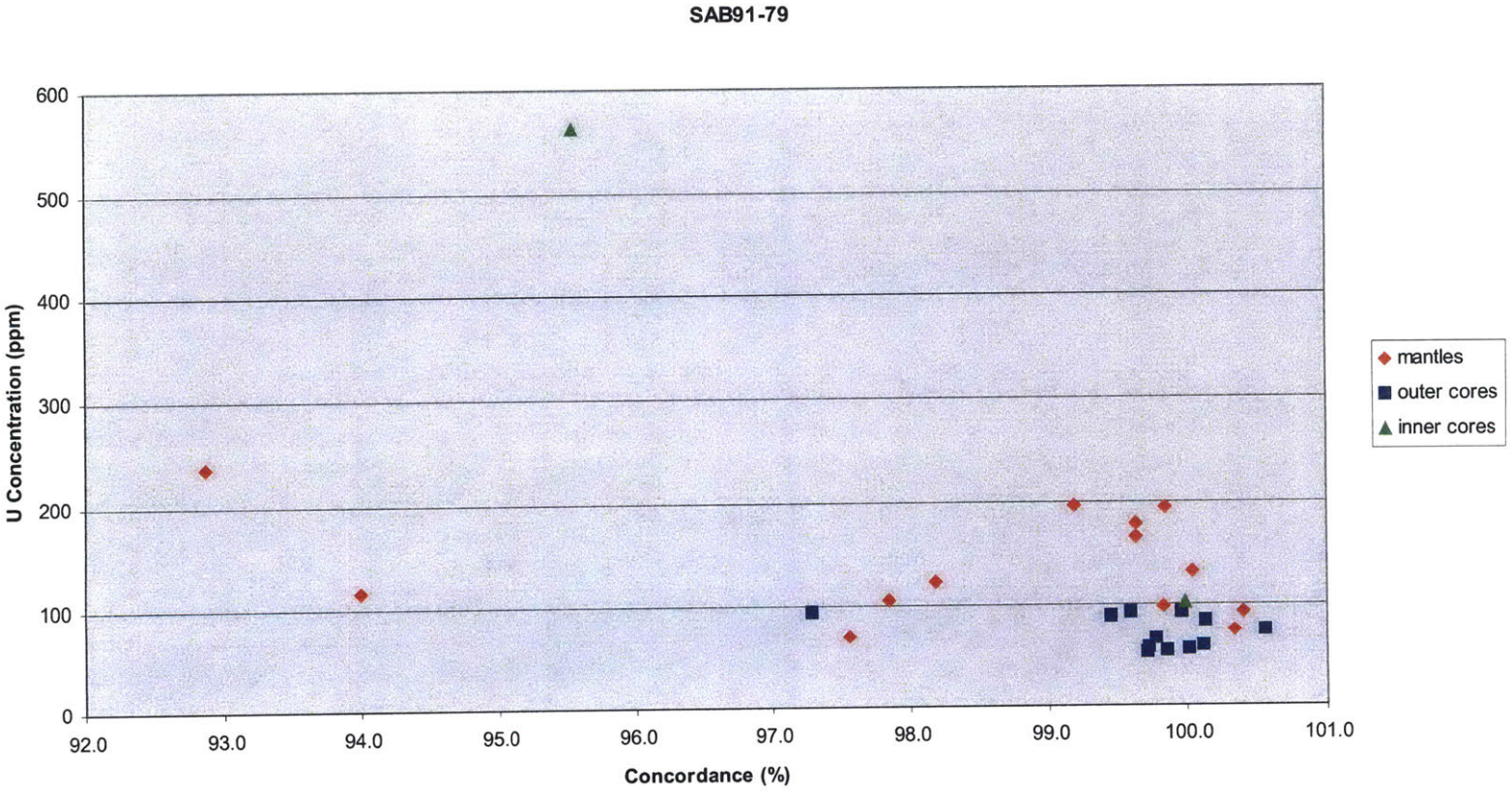
SAB91-79
600
500
400
300
200
100
0
U Concentration (ppm)
92.0
93.0
94.0
95.0
96.0
97.0
98.0
99.0
100.0
101.0
Concordance (%)
mantles
outer cores
inner cores

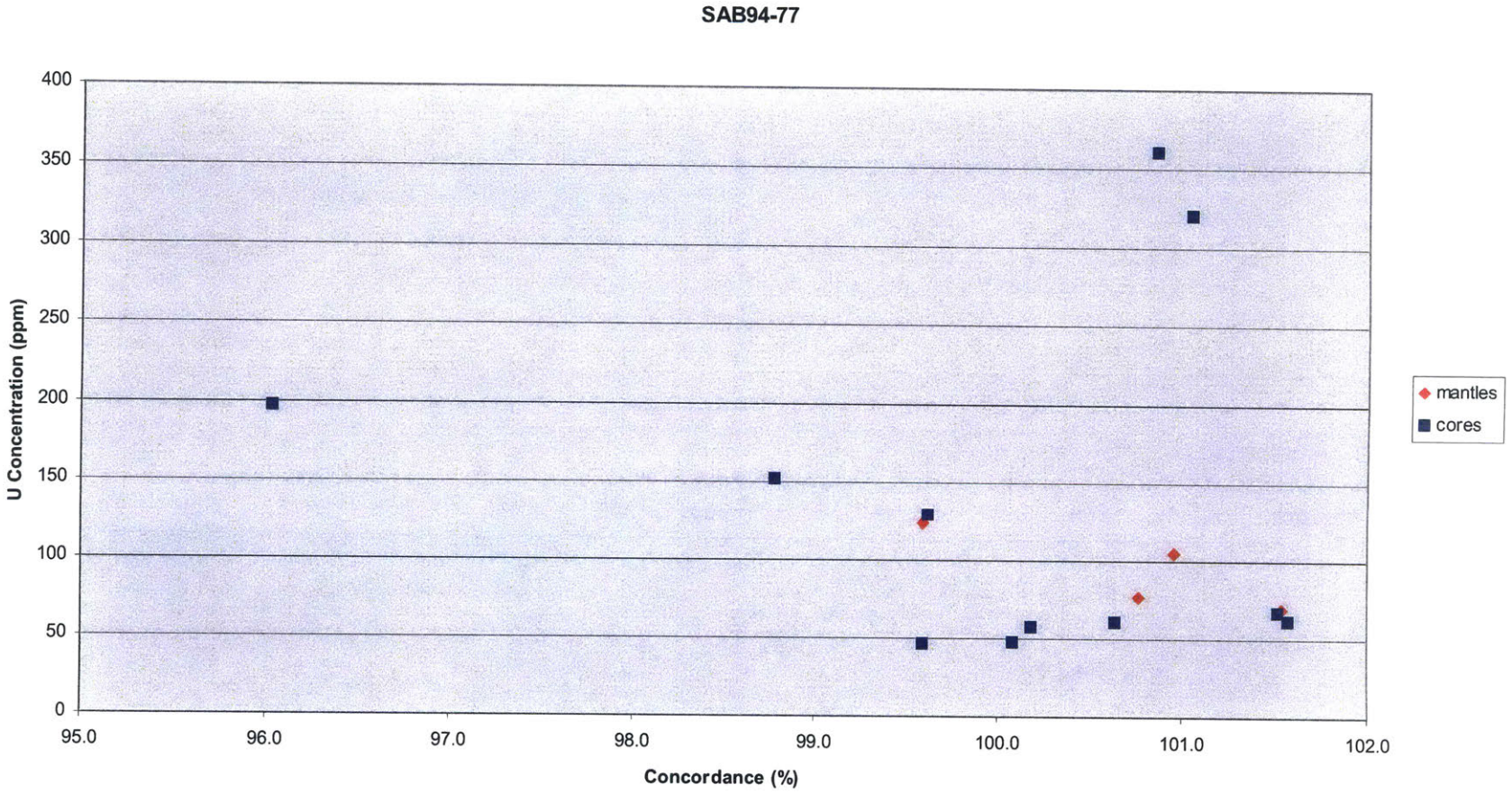
SAB94-77
U Concentration (ppm)
400
350
300
250
200
150
100
50
0
95.0
96.0
97.0
98.0
99.0
100.0
101.0
102.0
Concordance (%)
mantles
cores

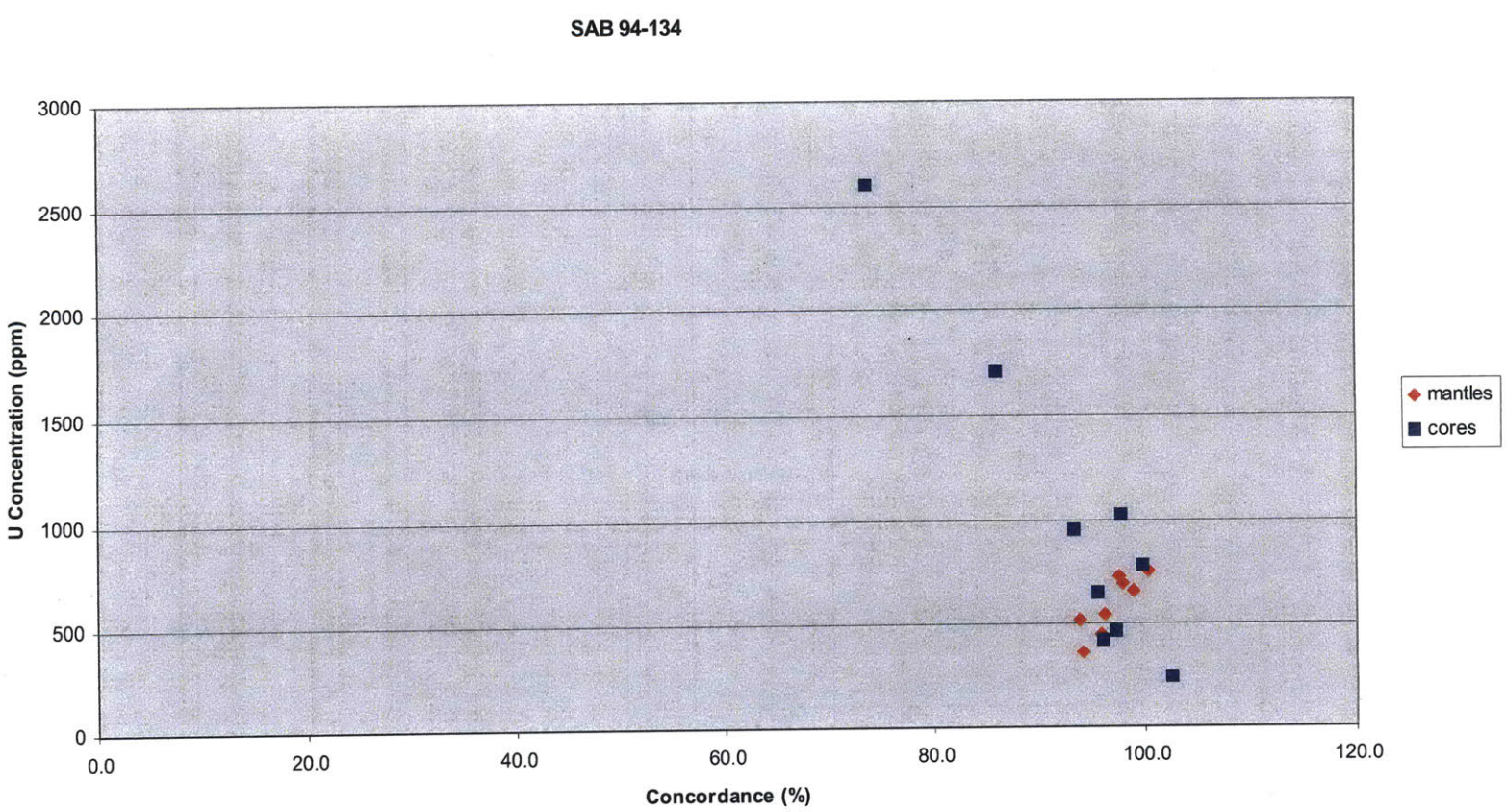
SAB 94-134
U Concentration (ppm)
3000
2500
2000
1500
1000
500
0
0.0
20.0
40.0
60.0
80.0
100.0
120.0
Concordance (%)
mantles
cores

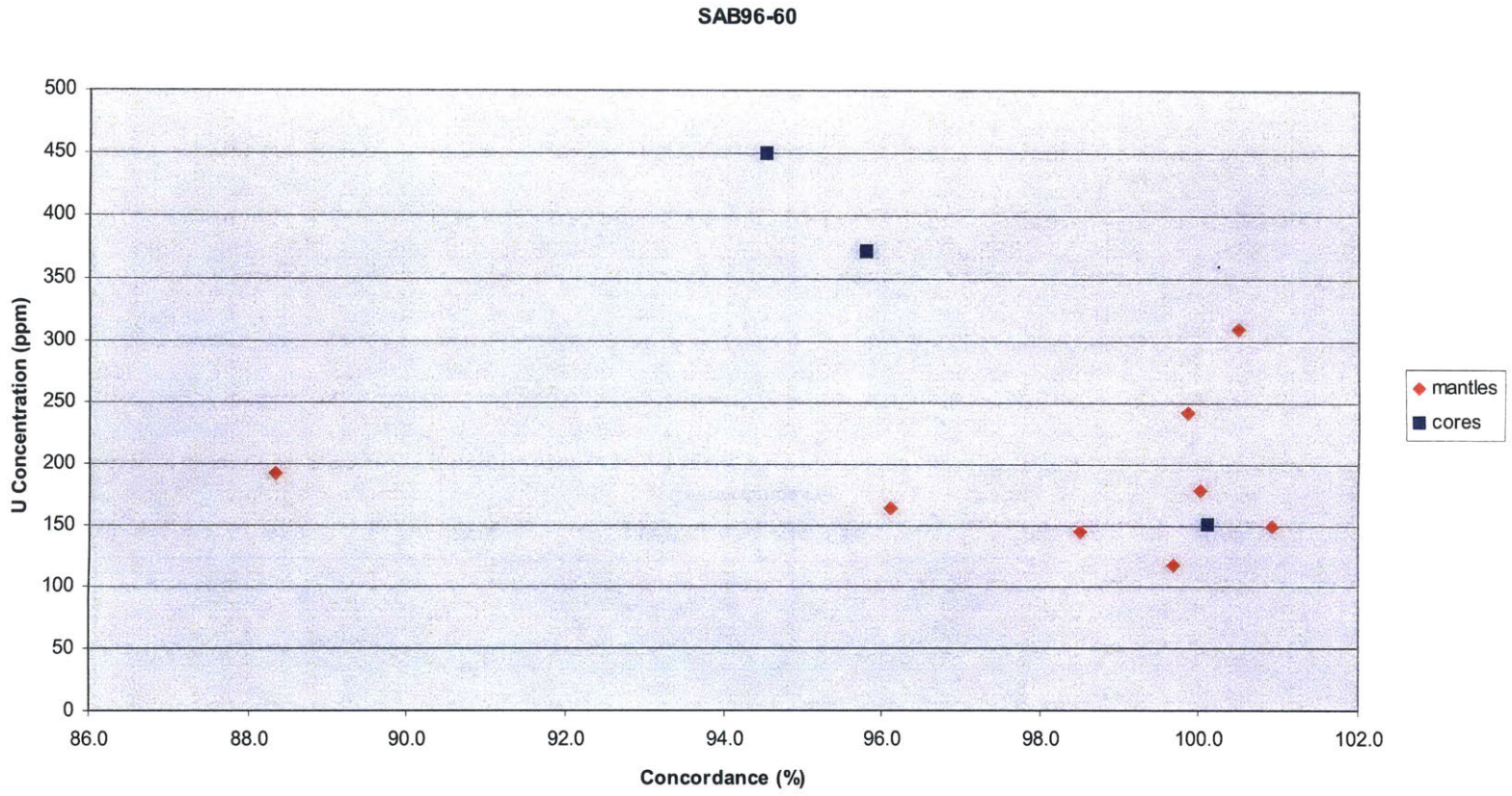
SAB96-60
U Concentration (ppm)
500
450
400
350
300
250
200
150
100
50
0
86.0
88.0
90.0
92.0
94.0
96.0
98.0
100.0
102.0
Concordance (%)
mantles
cores

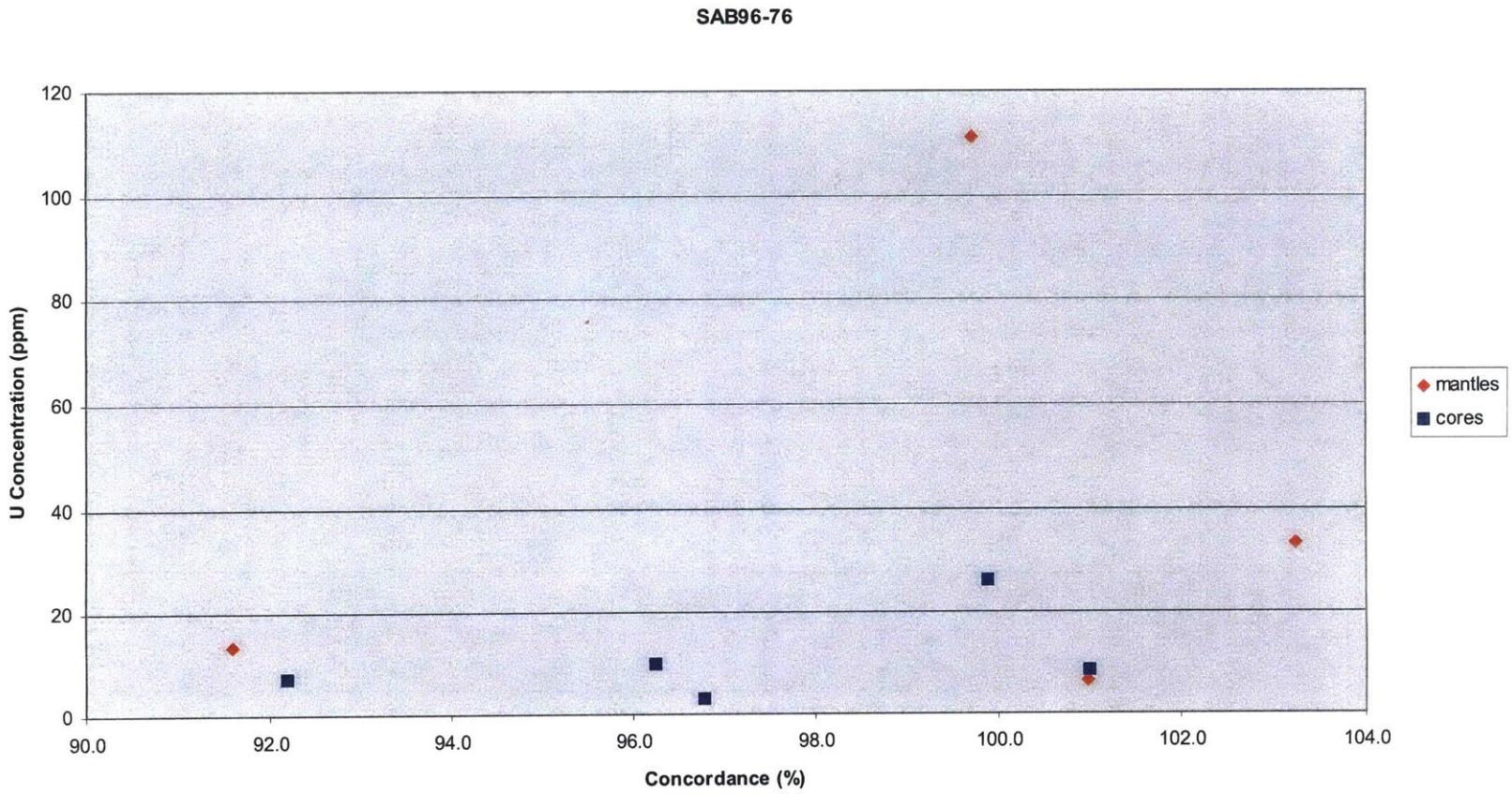
SAB96-76
120
100
80
60
40
20
0
U Concentration (ppm)
90.0
92.0
94.0
96.0
98.0
100.0
102.0
104.0
Concordance (%)
mantles
cores